Reconstruction of the hydrodynamics in a tropical estuary

Diploma Thesis

Peter Holtermann

University of Rostock
Faculty of Mathematics and Natural Science

August 12, 2007

Contents

1. Summary

The general scope of this study is to give an overview of the hydrodynamics in the Segara Anakan lagoon. This includes assembling, recording and calculating basic parameters like area, bathymetry, flushing time, main freshwater input, salinity changes and setting up a numerical computer model with the attempt to reconstruct the hydrodynamics. Hydrodynamic data in Segara Anakan is rare and only the combination of different datasets including remote sensor data and model results together with the in situ measurements create a dataset feasible to understand the hydrodynamics.

For the in situ data two field trips at different monsoon seasons were carried on. The main measurements were ADCP water volume flux transects, sea level recordings, salinity measurements as well as depth soundings. The concentration of data sampling was targeted on the western and central parts of the lagoon.

The model results show that the hydrodynamics can be modelled with GETM within acceptable limits. Despite the rather coarse information of the boundary conditions, especially weather and the freshwater input, many measured features are well reproduced. The combination of discharge measurements at key locations coupled with sea level and salinity samples turned out to be a useful validation of the model results. Especially the long time measurements in Klaces have been proven to be a valuable data set. Monsoon induced changes in the salinity and the seawater age could be reproduced with GETM. But with the small amount of salinity data during the dry season in summer 2005 differences are hard to quantify. The tidal forcing could be well represented with the tidal constituents derived from *Egbert and Erofeeva* [2002]. Due to the virtually complete absence of salinity and discharge data in the eastern part the model results of this area should be second guessed if more in situ data is available.

2. Introduction

2.1. Motivation

The Segara Anakan Lagoon is situated at the southern coast of Central Java and is one of the last large mangrove fringed estuarine systems left on Java. It is semi-enclosed by the Nusa Kambangan Island with two outlets to the Indian Ocean (figure 2.3). The city Cilacap is located in the east of Segara Anakan. It has a population of 200000 inhabitants (*www.citypopulation.de* [June 5.,2007]) and the only international harbour on the southern coast of Java. With the biggest oil refinery of Indonesia (348000 barrels per day, *American Embassy Jakarta* [2000]) and a cement factory Cilacap is a major industrial area. Several small villages are distributed throughout Segara Anakan. Fishing is the main income of the people living there. During the last 25 years the area of the lagoon as well as the land cover changed rapidly due to urbanisation, land reclamation from swamps, exploitation of the mangrove forest and silt deposition. These changes are accompanied by pollution from households and industry, an increase in the population and a decrease in fishery. The mangrove swamp area reduced from 18000 ha in 1978 to 9000 ha in 2004 (*Ardli and Wolff* [accepted]).

The hydrodynamics driving the lagoon are hardly quantified and not well understood. With its large gradients of salinity and suspended matter, its manifold influences through tide, freshwater runoff and the high biological activity Segara Anakan is a rather complex and fast changing ecosystem. Better knowledge about the physical processes is needed as it is the basis for many processes, including sedimentation, biology, pollutant and mangrove propagule propagation. This study aims to reconstruct the hydrodynamics based upon GIS data, field measurements, satellite data and a computer model of the hydrodynamics. It is part of the bilateral Indonesian-German research and education initiative SPICE[1] (Science for the Protection of Indonesian Coastal Marine Ecosystems).

2.2. Description of the Segara Anakan Lagoon

The geographical position of Segara Anakan is $108°46'E - 109°03'E, 7°35'S - 7°48'S$. Its extension is about 30 km in the east-west and 15 km in the north-south direction with an overall area of 120 km^2. 26 km^2 of the lagoon are covered by water and 94 km^2 by mangroves (table 2.1 and figure 2.3).

Mangrove estuaries are classified on local factors like shore morphology, the influences of tides, river flow and the variations in salinity and sedimentation

[1] SPICE is a project to identify and study the important issues for a sustainable management of the Indonesian coastal ecosystems.

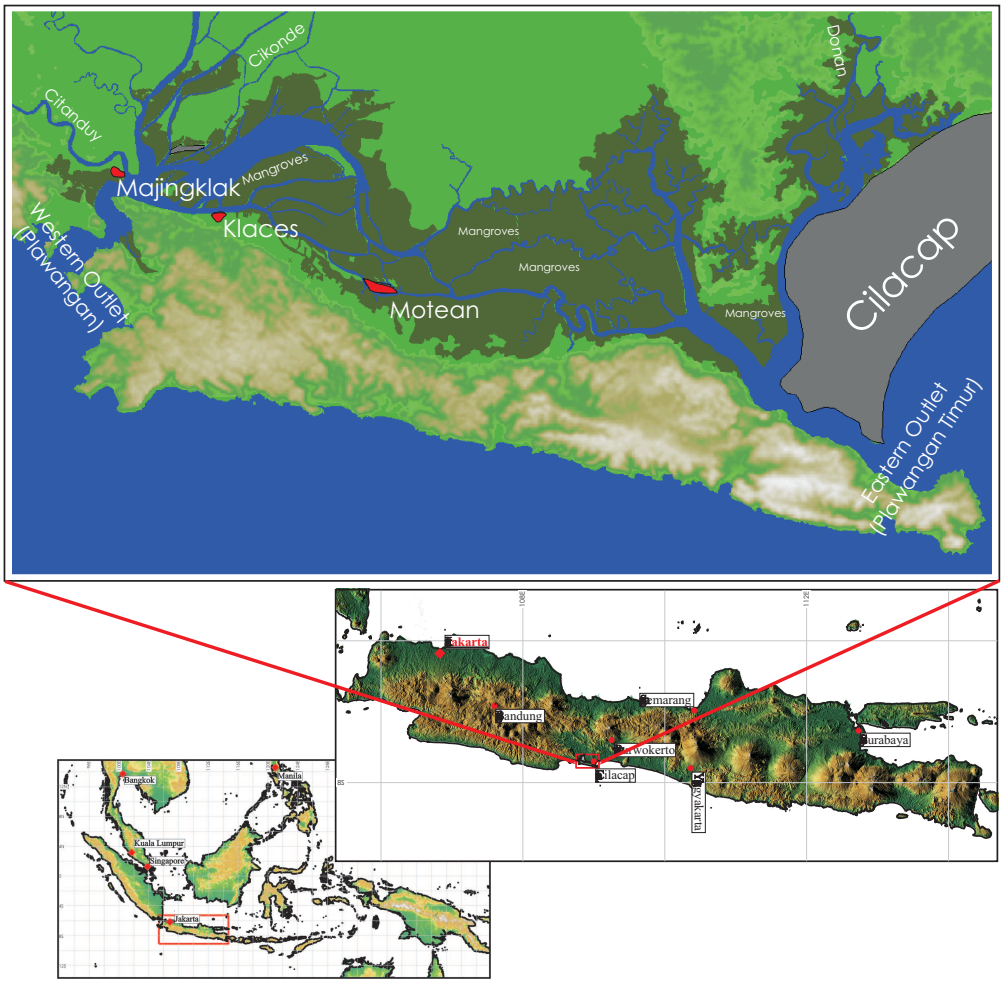

Figure 2.1: The area of this study is the mangrove fringed Segara Anakan lagoon situated in the south central part of Java, Indonesia. The lowest panel shows South-east Asia. The middle panel illustrates the Java Island and the upper panel the Segara Anakan lagoon. It is semi enclosed by the Nusa Kambangan island.

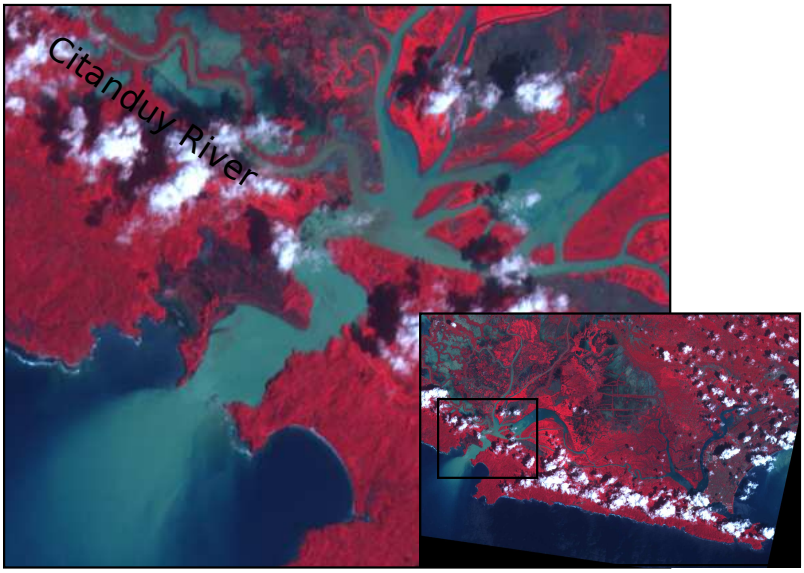

Figure 2.2: Segara Anakan SPOT scene of Dec. 30.,2004 with zoom to the Citanduy estuary. The red colors are due to the infrared channel of the satellite. The Citanduy River entering the western part of Segara Anakan has a high load of suspended matter and is the reason for the continuous siltation.

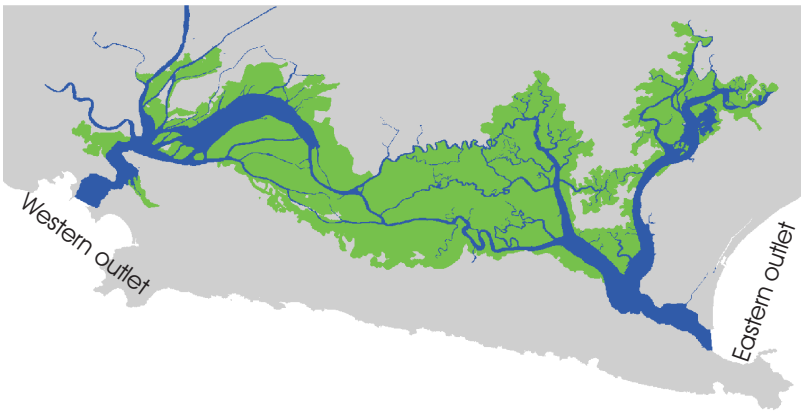

Figure 2.3: Distribution of water and mangrove areas in Segara Anakan. The green colored area are mangroves with approx. three quarters of the lagoons area, blue is the remaining one quarter and is water area (table 2.1).

area of	water	mangroves
	26 km^2	94 km^2

water volume of	water	mangroves
mean water level	0.106 km^3	0 km^3
mean high water springs (MHWS (+0.7 m))	0.130 km^3	0.048 km^3
mean low water springs (MLWS (-0.7 m))	0.082 km^3	0 km^3
mean high water neaps (MLWN (+0.2 m))	0.113 km^3	0.006 km^3
mean low water neaps (MLWN (-0.2 m))	0.0995 km^3	0 km^3
mean water volume = 0.131 $\mathbf{km^3}$		

Table 2.1: Water area and volume at different sea levels of the Segara Anakan lagoon.

(*Hogarth* [1999]). The Segara Anakan Lagoon can be categorised as basin mangroves with an area sheltered by wave action, great variety in salinity and possible hyper-saline conditions due to evapotranspiration of the mangroves. Evapotranspiration describes the freshwater demand of mangrove trees satisfied by excluding salt from saline water of the environment. The left salt causes a higher salinity. Low turbulence due to the sheltered area results in a sink for nutrients and sediment, which is being investigated in different studies (e.g. *Pohlenga* [2007]).

The main hydrodynamic force is the Indian Oceans tide and the freshwater input of numerous rivers entering the lagoon. The tide is M_2 dominated with a spring tide amplitude of 0.7 meter and a neap tide amplitude of 0.2 meter. The tide wave propagates from west to east along south Java. Calculations of the phase difference between the two outlets result in 1.7°, which is equivalent to 4 minutes time difference.

Location	neap tide	spring tide
western outlet (Plawangan)	654 m^3/s	1370 m^3/s
eastern outlet (Plawangan Timur)	1610 m^3/s	4400 m^3/s

Table 2.2: Mean amplitudes of the volume fluxes at the outlets.

Table 2.2 shows the mean ocean-lagoon volume flux amplitude during neap and spring tide [2]. The tropical humid climate in Cilacap is monsoon governed with an annual precipitation of 3540 mm . In January-February the precipitation is doubled compared to August-September. The mean wind strength and distribution for the 2 monsoon seasons is shown in Figure 2.4. The rainy season (March-November) has a north-west wind with 4 knots on average. The dry season is dominated by a north-east wind with an average of 2.6 knots.

The major freshwater input into the lagoon is the Citanduy-River in the western part of Segara Anakan. The average discharge changes annually from approximately 300 m^3/s in rainy to 100 m^3/s in dry season. The fluxes of all

[2] model results

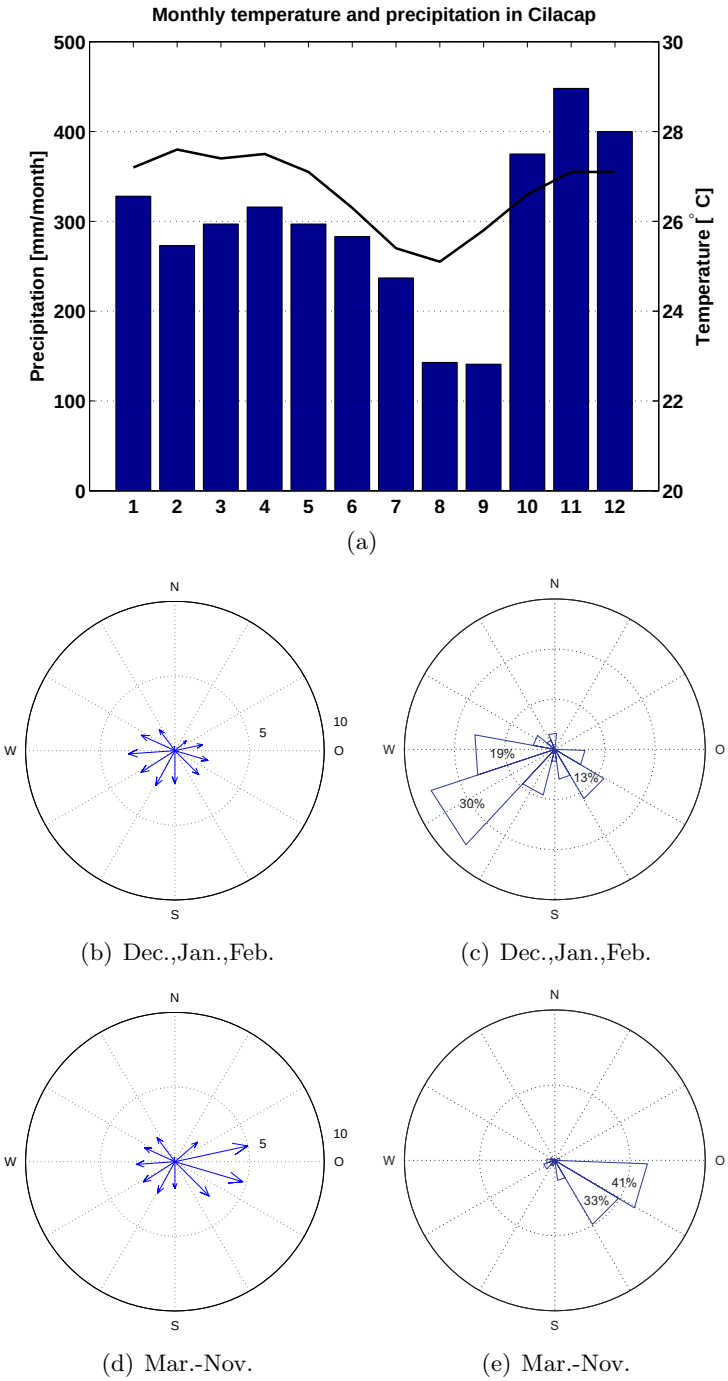

(a)

(b) Dec.,Jan.,Feb.

(c) Dec.,Jan.,Feb.

(d) Mar.-Nov.

(e) Mar.-Nov.

Figure 2.4: Panel (a): Blue bars: Monthly precipitation [mm/month] in Cilacap. Black line: Temperature [°C] in Cilacap (*White et al.* [1989]). Panels (b)-(e): Mean wind direction and strength in Cilacap between 2001-2005, wind in knots.

smaller rivers sum up to 150 m^3/s respectively 50 m^3/s (see chapter 4.7.2 for details).

The total suspended matter (TSM) of the river Citanduy is 1114.4 mg/l *Yuwono et al.* [2007] with an estimated silt transport of 3039 t/year into the lagoon *White et al.* [1989]. A major part of the TSM discharges to the Indian Ocean but some amount remains in the lagoon. The remaining matter is the reason for the siltation of Segara Anakan (Figure 2.2).

2.3. Methods of this study

The absolute amount of available bathymetry and hydrodynamic data in the Segara Anakan lagoon is small. This study combines different methods and data to understand and reconstruct the hydrodynamics:

- data from two field trips
- satellite images and remote sensing data
- meteorological data
- tidal forcing from an ocean tide model
- hydrodynamic numerical model

The collected data is processed, validated and discussed but field measurements are always limited in space and time. A computer model can help to understand the studied system and to gain information of areas not covered by field measurements. The used model is the public domain model GETM ((G)eneral (E)stuarine (T)ransport (M)odel *Burchard and Bolding* [2002]). With its drying/flooding feature and the opportunity to adapt the source code of the model to the physics of a mangrove fringed tropical estuary it is well suited for the requirements.

2.4. Structure of the work

This thesis is structured into the theoretical part discussing the mathematical background needed for the processing of ADCP data. The equations used by GETM to describe the hydrodynamics are introduced as well as the seawater age implementation. The huge amount of intertidal areas motivates a detailed description of the drying/flooding algorithm. The last part of the theory chapter deals with the spatiotemporal discretization and resulting constraints within the computer model.

The next chapter describes the field works and post processing of the measured data. The second part of this chapter is about weather data and results of remote sensing data, including catchment areas of the rivers entering Segara Anakan. Effects of wind induced water currents are investigated in the end of this chapter.

A detailed discussion of the in situ data as well as comparisons with model results are done in the subsequent chapter. With the fact in mind, that the

model results and the in situ measurements are similar within an acceptable range, results harder to verify with the existing in situ data are presented later on. Finally suggestions for further work are given in the outlook chapter.

We hope you will enjoy reading this thesis and get a good view into the complex and interesting processes of Segara Anakan.

3. Theory

3.1. Principles of water current measurement with an Acoustic Doppler Current Profiler (ADCP)

Measuring water currents can be done in different ways. An elegant solution is the usage of the Doppler shift of sound due to water movement. A class of devices using the Doppler effect are called Acoustic Doppler Current Profiler (ADCP). The principle function of the ADCP is explained in the following section. If the ADCP transmits an acoustic pulse with a well known frequency, the pulse will be reflected on small particles in the water. The device listens to the reflected pulse with its frequency, time delay and strength. The frequency of the reflected signal will be different, since the small reflecting particles have a speed relative to the beam. This is the Doppler effect. Thus an ADCP measures the relative speed of small particles in the direction of the beam. If the particles are passive and float with the water velocity, the measured speed is the water velocity. This is the key assumption of ADCP measurements. Sometimes vertical velocities of long time moorings show day/night cycles. They are caused by small organisms and their daily up/down movements in the water column (pers. comm. Thoralf Heene). These velocities are small compared to the horizontal velocities and will not disturb the measurements in Segara Anakan. The Doppler effect only occurs in the direction of the pulse. But if one wants to measure all three dimensions, three pulses in different directions are needed. In practice an ADCP has four beams with an angle of 15° or 20° degrees to the vertical (Figure 3.4(a)). Every beam measures velocities parallel to its direction $\vec{e_{b_1}}$ for the first beam, $\vec{e_{b_2}}$ for the second beam and $\vec{e_{b_3}}$ for the third beam. Thus the water velocity $\vec{V}$ can be expressed as a linear combination of the speed components in the beam directions

$$\vec{V} = v_{b_1} \cdot \vec{e_{b_1}} + v_{b_2} \cdot \vec{e_{b_2}} + v_{b_3} \cdot \vec{e_{b_3}}.$$

With triangulation the components v_{b_1}, v_{b_2}, v_{b_3} are split up into the Cartesian components u, v, w

$$\vec{V} = u \cdot \vec{e_x} + v \cdot \vec{e_y} + w \cdot \vec{e_z}.$$

The fourth beam with the component $\vec{e_{b_4}}$ is not necessary but is used for another calculation of the velocity, e.g.:

$$\vec{V'} = v'_{b_1} \cdot \vec{e_{b_1}} + v'_{b_2} \cdot \vec{e_{b_2}} + v'_{b_4} \cdot \vec{e_{b_4}}$$

and

$$\vec{V'} = u' \cdot \vec{e_x} + v' \cdot \vec{e_y} + w' \cdot \vec{e_z}.$$

Naturally the velocities $\vec{V}$ and $\vec{V'}$ differ. For instance due to random errors. This difference is used to quantify the quality of the measurement.

The acoustic pulse travels with the speed of sound, if the ADCP measures the time of the reflected signal and knows the speed of sound, it can determine the position of the back scattering (see Figure 3.1). So it is possible to split the water column into cells and measure the velocity in each cell (if there are back scatterer). A transmitted pulse is not only reflected by small particles but also from the seabed. This is the bottom velocity ($\vec{V_b}$). Again with the assumption of a fixed sea bed the bottom velocity is equivalent to the speed over ground. Moving mud layers could be an example of a moving seabed and would end up in wrong bottom velocities. The time integral of the bottom velocity is the ADCP track, which is the position of the ADCP relative to the start position. It can be used for discharge measurements of channels (Chapter 3.2). Even if the error of every measurement is negligible the integration over time accumulates errors. For tasks needing an accurate absolute position, like bathymetry, the ADCP bottom track is not usable.

Figure 3.5 shows a typical ADCP measurement done in Segara Anakan. It was taken to measure the discharge of the Plawangan outlet. The east and north velocity components of the measurements are plotted against depth and time. A depth cell size is 15 cm and the time interval is 10 seconds. Note the lowest panel in figure 3.5, where the relative echo amplitude defined as

$$20 \cdot log_{10} \cdot \frac{I_{backscatter}}{I_{transmit}}$$

is plotted. The strength of the received signal is in the range of $20 - 50 \cdot 10^{-20}$ times weaker than the transmitted signal. This shows how much accuracy and precision an ADCP needs to get good results.

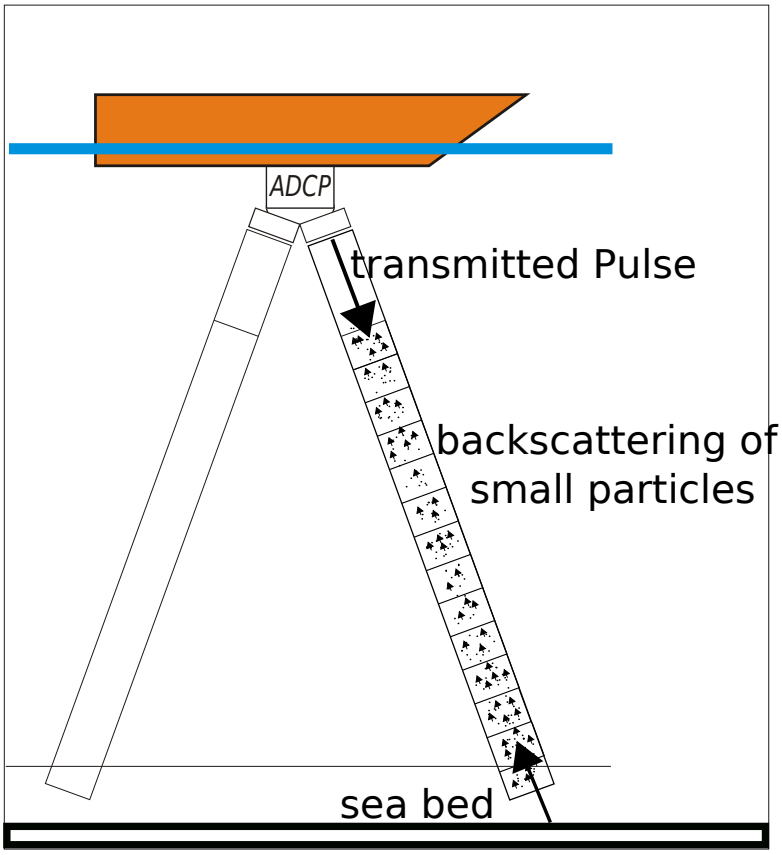

Figure 3.1: An ADCP transmits an acoustic pulse with a well known frequency and listens to the received echo with the time delay and the frequency shift. This data can be transformed into the distance and the velocity relative to the sender (Doppler effect). Small particles with a dimension around 1 mm reflect the pulse. The same happens at the sea bed but with a much stronger reflection. The reflection at the sea bed interferes with the back scatter signal close to it and prevents measurements in a 6% thick bottom layer (side lobe effect, chapter 3.2). With three beams three velocity components can be measured and transformed into Cartesian coordinates.

3.2. Determining discharge with the ADCP

3.2.1. Introduction

The majority of ADCP measurements were done to quantify the water fluxes inside the lagoon (chapter 4.5). This section describes how to calculate the discharge from ADCP raw data and to determine the error.

3.2.2. General equations and technical limitations

To quantify the flux through a surface, it is necessary to calculate the flux perpendicular to the surface and multiply it with the surface area. For a small surface element da, the normal vector $\vec{n}$ and the water velocity $\vec{V_f}$ the discharge is

$$\vec{V_f} \cdot \vec{n}\ da.$$

The discharge D through an area A

$$A = \int\int_A da$$

is the integral of the projected water velocity $\vec{V_f} \cdot \vec{n}$ over the surface A:

$$D = \int\int_A \vec{V_f} \cdot \vec{n}\ da. \tag{3.1}$$

To get the surface elements da it is needed to multiply the bottom track velocity $\vec{V_b}$ with dt to get a small track in the direction of the moving ADCP. Hence with a depth element dz a surface element is:

$$da = |\vec{V_b}|\ dz\ dt.$$

The projected velocity $\vec{V_f} \cdot \vec{n}$ can be rewritten with the sinus of the angle ω between $\vec{V_f}$ and $\vec{V_b}$ (Figure 3.2)

$$\vec{V_f} \cdot \vec{n} = |\vec{V_f}|\ sin(\omega).$$

The volume flux through the surface A is rewritten by a time integral over the transect time T and an integral over the depth $d(t)$

$$\int\int_A \vec{V_f} \cdot \vec{n}\ da = \int^T \int_0^d |\vec{V_f}||\vec{V_b}|sin(\omega)\ dz\ dt. \tag{3.2}$$

This is the z component of the cross product between the vectors $\vec{V_f}$ and $\vec{V_b}$:

$$\int\int_A \vec{V_f} \cdot \vec{n}\ da = \int^T \int_0^d (\vec{V_f} \times \vec{V_b}) \cdot \vec{e_z}\ dz\ dt. \tag{3.3}$$

(*Simpson and Oltmann* [1990], *Gordon* [1989])

The equations integrate the whole transect. Three technical limitations do not permit to measure the whole discharge area. Namely ringing, side lobe effect and shoreline:

Ringing: after a transmitted impulse some of the transmitted energy lingers. The ADCP must wait until the ringing fades away to receive the much weaker back scatter signal. The ringing time multiplied with the speed of sound is the ringing distance. According to *RD Instruments* [2002b] the ringing distance of the 1200 kHz Workhorse is 0.5 m. The first valid velocity starts 50 cm below the transducer.

The side lobe effect: Each transducer transmits besides the main pulse a side lobe pulse which is approx. 15° rotated from the main pulse. If the side lobe pulse is also reflected with significant strength and the two pulses reach the transducer at the same time, they interfere. Then it is impossible to measure water velocities. This scenario happens in a 6% thick bottom layer. Here the strong sea bed bottom echo drowns the weaker main lobe echo (Figure 3.4(a)).

The third limitation is the shore: It is not always possible to start a transect directly on the shore. The first measurement is more likely some meters away. All these missing areas have to be extrapolated (see Figure 3.3). A good approximation for the surface layer is a constant velocity, which is the velocity of the first measured ADCP cell. For simplicity a linear decrease of the velocity of the last valid cell is chosen for the bottom layer. A slightly more realistic approach would be the assumption of a logarithmic velocity distribution. Missing shore areas are extrapolated by assuming that the sea floor rises linearly and the velocity decreases linearly in direction to the shore (Figure 3.4). Figure 3.5 shows an example discharge track in Plawangan, note the missing data on the top and the bottom.

Equation 3.3 can be rewritten as

$$= D_m + D_{shore} + D_{sidelobe} + D_{ringing} \tag{3.4}$$

with the measured discharge D_m

$$D_m = \int^T \int_{d_r}^{d_s} (\vec{V_f} \times \vec{V_b} \cdot \vec{e_z}\ dz\ dt$$

and the shore, side lobe and ringing effects extrapolations

$$D_{shore} = \int_0^{X_T} \int_0^d \overrightarrow{\overrightarrow{V_1}}(x)\ dz\ dx = \frac{1}{3}\ \overrightarrow{\overrightarrow{V_1}}(x)\ X_T\ d(X_T),$$

$$d(x) = d(X_T)\frac{x}{X_T} \quad \overrightarrow{\overrightarrow{V_1}}(x) = \overrightarrow{\overrightarrow{V_1}}\frac{x}{X_T},$$

$$D_{sidelobe} = \int^T \int_{d_s}^{d} (\vec{V_f}(z,t) \times \vec{V_b}(t)) \cdot \vec{e_z}\ dz\ dt = \int^T (\vec{V_f}(d_s,t) \times \vec{V_b}(t)) \cdot \vec{e_z}\ 0.5\ (d - d_s)\ dt,$$

$$[|\vec{V_f}(z)|]_{d_s}^{d} = \left| \vec{V_f}(d_s,t))\ \left(\frac{d-z}{d-d_s}\right) \right|,$$

$$D_{ringing} = \int^T \left(\vec{V_f}(d_r,t) \times \vec{V_b}(t)\right) \cdot \vec{e_z}\ d_r\ dt.$$

3.2.3. Discretization

The ADCP measures m cells with a high of Δz and pings approximately three times a second. Usually 20-30 measurements are averaged to reduce the standard deviation. A surface element has the dimensions: $\Delta t\ \vec{V_b}$ along the ADCP track and Δz vertical. Converting the integrals into sums equation 3.2.2 becomes:

$$D_m = \sum_n \sum_m (\vec{V_f}(m,n) \times \vec{V_b}(n)) \cdot \vec{e_z}\ \Delta t \Delta z. \tag{3.5}$$

with a transect duration of $n\ \Delta t$ seconds and m vertical cells per Δt. Please note that not every depth cell of the m cells must have a valid value, since it is possible that in shallow areas the cells are below the sea floor. These cells are not taken into the sum. The same conversion for the side lobe

$$D_{sidelobe} = \sum_n (\vec{V_f}(m(d_s),n) \times \vec{V_b}(n)) \cdot \vec{e_z}\ 0.5\ (d - d_s)\ \Delta t$$

and the ringing area

$$D_{ringing} = \sum_n (\vec{V_f}(m(d_r),n) \times \vec{V_b}(n))) \cdot \vec{e_z}\ d_r\ \Delta t.$$

Where $m(d_s)$ is the cell of the last valid measurement before the side lobe effect occurs and $m(d_r)$ is the first cell below the ringing distance.

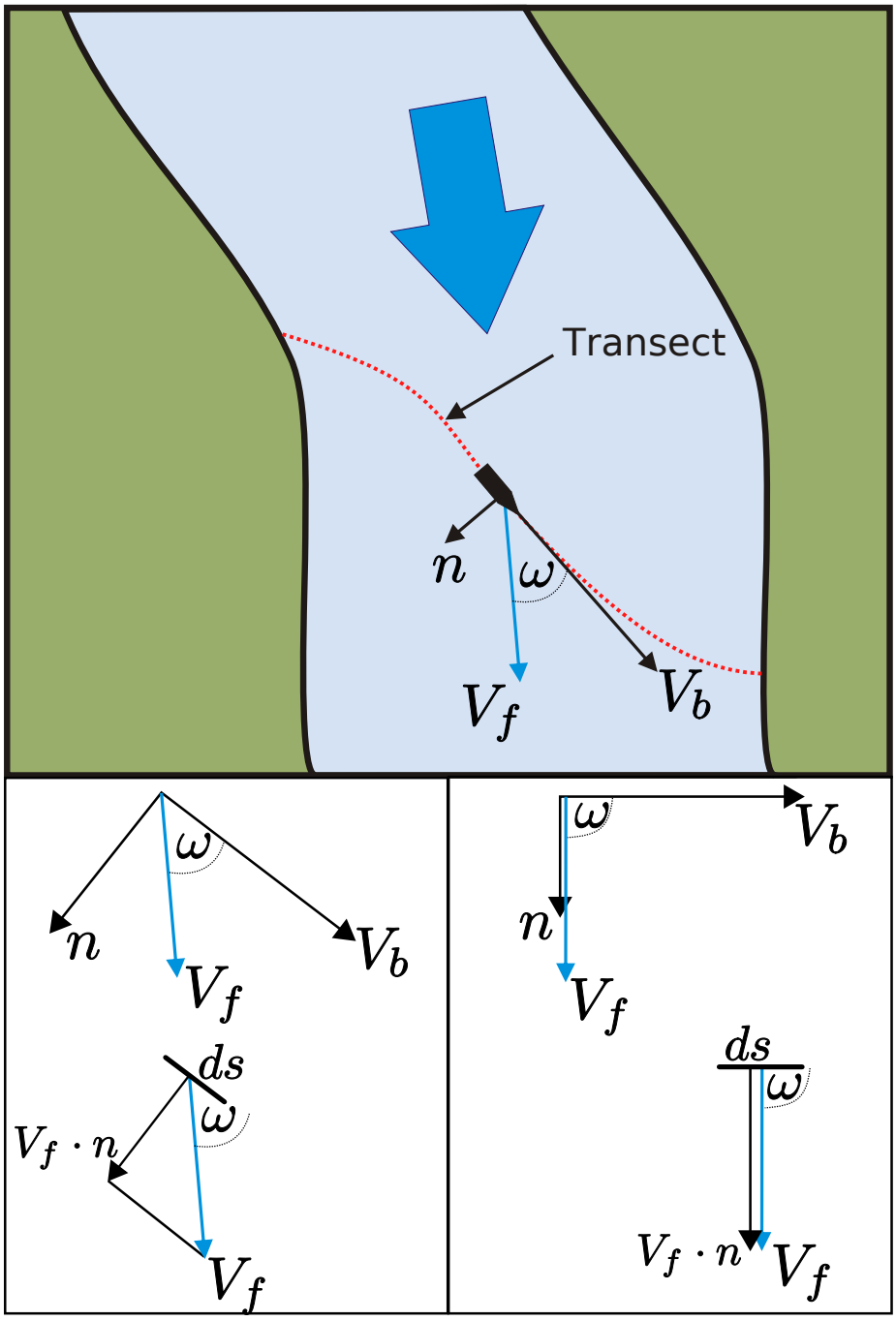

Figure 3.2: Vectors for ADCP discharge calculation, the transect across a river is not always perpendicular to the water velocity. To determine the river discharge the projected water velocity $\vec{V_f} \cdot \vec{n}$ is integrated over the transect area of the river $A = \int \int_A da$. Where da is the ADCP speed multiplied with dt: $da = |\vec{V_b}|\ dt\ dz$. To project the water velocity onto da the sine of the angle ω between $\vec{V_f}$ and $\vec{V_b}$ is multiplied with $|\vec{V_f}|$. If ω is 90° $\vec{V_f} \cdot \vec{n} = |V_f|$, the ADCP moves perpendicular to the water velocity. If ω is 0° the ADCP will move with or against the water velocity and no discharge will be measured since $\vec{V_f} \cdot \vec{n} = 0$.

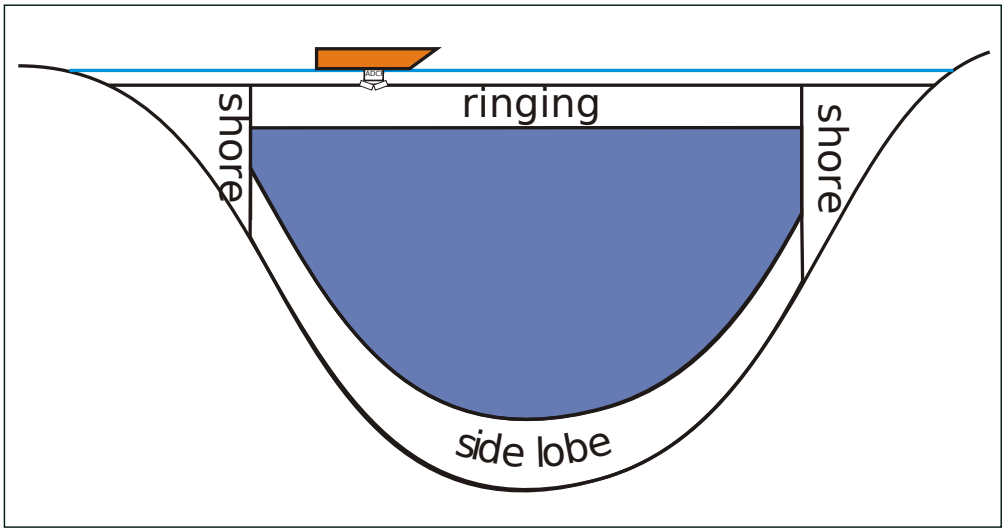

Figure 3.3: Shore, ringing and side lobe areas which cannot be measured within an ADCP discharge transect.

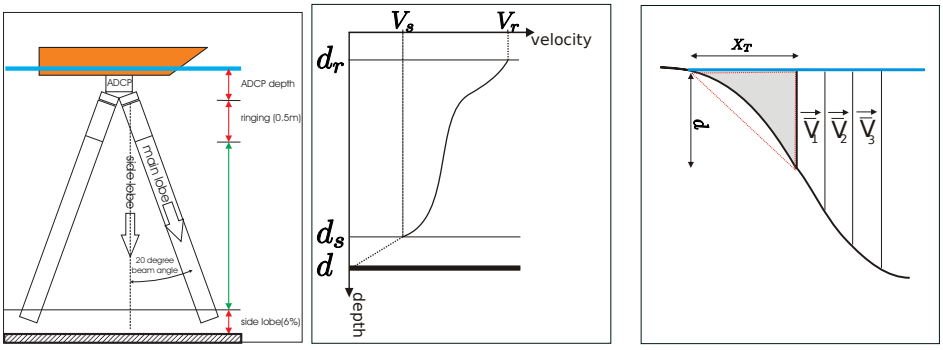

(a) (b) (c)

Figure 3.4: Panel (a): Due to the side lobe effect 94% of the water column can be measured. The ringing forbids to measure closer than 0.5 meters to the transducers. Panel (b): the ringing area is extrapolated by using the first valid velocity for the complete upper ringing area (constant velocity approach). The side lobe area is extrapolated by assuming a linear decrease of the velocity with no velocity at the bottom. Panel (c): the area to the shore is extrapolated by using a linear decrease of the first/last valid mean velocity to zero at the shore and a linear depth decrease of the first/last valid velocity.

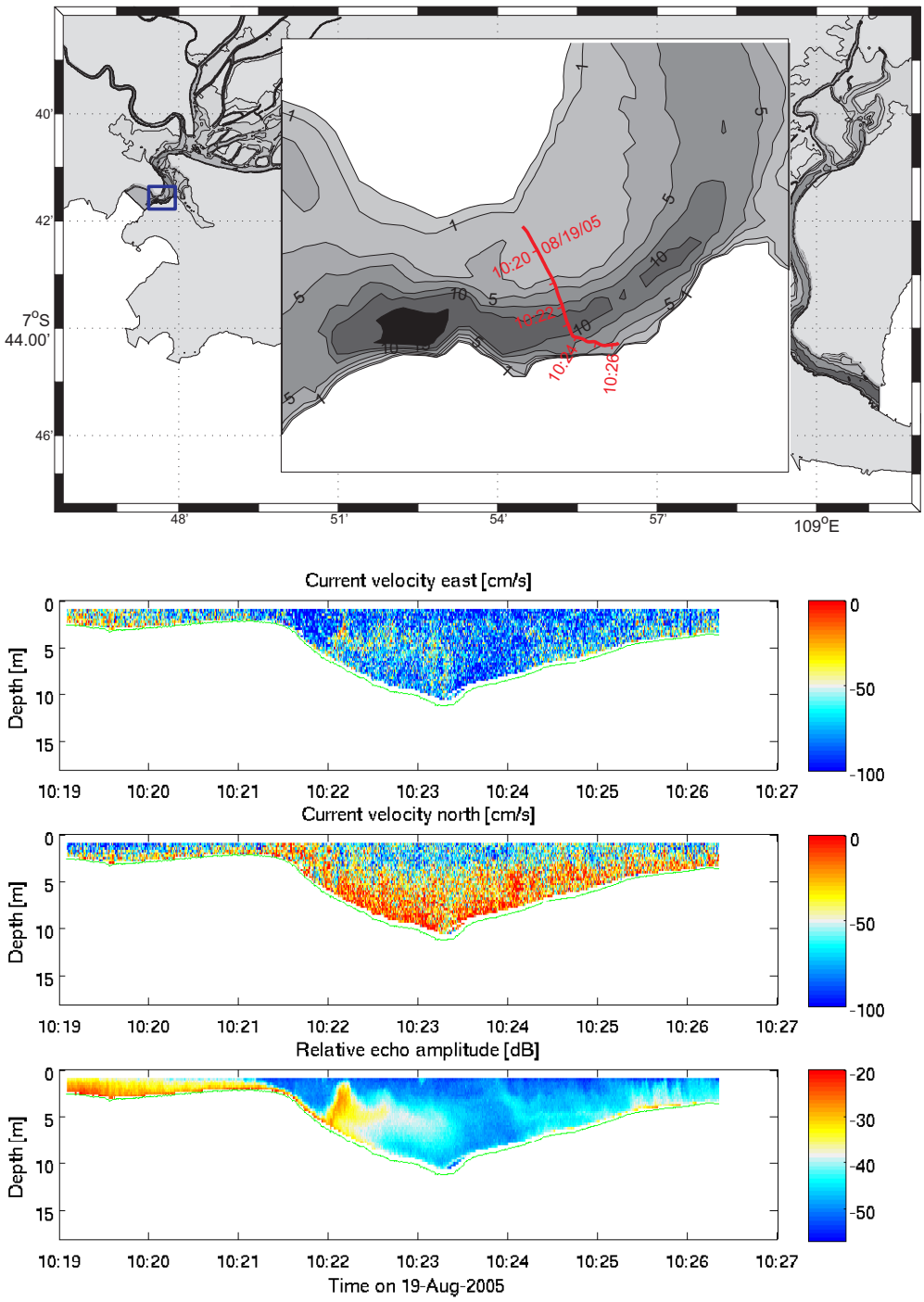

Figure 3.5: ADCP discharge measurement in Plawangan, the western outlet of Segara Anakan. Highest plot: current in north direction; middle plot: current in east direction; lowest plot: back scatter strength in dB. The high back scatter signal in direction to the shore is probably due to a mud plume.

3.2.4. Uncertainty of the discharge measurement

The error of the ADCP measurement consists of the random error and the bias. The mean value is shifted from the real value by the bias. The n measurements are distributed as a Gauss function around the mean value. The mean and the standard deviation define the shape of the Gauss function.

The bias is typically less than 10 mm/s and is neglected through all following considerations, since *RD Instruments* [2002b] state that it is not possible to measure the ADCP bias and to calibrate or remove it in post processing.

The standard deviation of typical ADCP Setups is shown in table 3.1. To

Vertical Resolution [m]	Range [m]	Std. dev. [mm/s]
0.25	11	182
0.5	12	66
1	14	30
2	15	18

Table 3.1: RDI Sentinel-Workhorse ADCP standard deviation of a single ping (*RD Instruments* [2002a]).

calculate the standard deviation from an ensemble of velocities *RD Instruments* [2002b] recommends to compute the standard deviation of the error velocities. This is because the random errors are independent from beam to beam and the ADCP scales the error velocity to give a correct magnitude for the horizontal-velocity errors.

The error of the measured discharge is:

$$D_{m_u} = \frac{\partial D_m}{\partial V_f} u_{V_f} + \frac{\partial D_m}{\partial V_b} u_{V_b} \tag{3.6}$$

$$D_{m_u} = \left(\frac{\partial (\int^T \int_{d_r}^{d_s} |V_f||V_b| sin(\omega)\ dz\ dt)}{\partial V_f} \right) u_{V_f} + \left(\frac{\partial (\int^T \int_{d_r}^{d_s} |V_f||V_b| sin(\omega) dz dt)}{\partial V_b} \right) u_{V_b}$$

$$= \left(\int^T \int_{d_r}^{d_s} |V_b| sin(\omega)\ dz\ dt \right)\ u_{V_f} + \left(\int^T \int_{d_r}^{d_s} |V_f| sin(\omega)\ dz\ dt \right)\ u_{V_b}$$

where u_{V_f} is the standard deviation of the water current error velocities and u_{V_b} the standard deviation of the bottom track error velocities.

The discharges of the side lobe, ringing and near shore areas are extrapolated, with an unknown error. To estimate the error of the whole discharge the relative error of the measured area is taken as the relative error for the whole discharge.

The error of a discharge measurement is:

$$D_u = D\ \frac{D_{m_u}}{D_m}. \tag{3.7}$$

3.3. Hydrodynamics in mangrove estuaries

Figure 3.6: An Avicennia mangrove tree. Note the pneumatophores above the soil.

3.3.1. Introduction to Mangroves

Mangrove forests are considered as among the biologically most active environments besides rain forest and coral reefs. They are trees and shrubs that live in intertidal coastal habitats (*Hogarth* [1999]). Mangroves developed various adaptations to survive huge saline gradients, anoxia and inundation. The mangrove group is taxonomic divers. This means that the adaptations evolved independently on several locations within different species in different families. These adaptations are necessary but expensive. Most mangroves are able to survive in freshwater environments but cannot compete with freshwater adapted plants.

Mangroves grow in areas where the annual mean temperature does not drop below 20 °C. They can survive air temperatures as low as 5 °C but are intolerant to frost. These conditions limit the distribution to tropical and subtropical areas and the number of species tends to decrease when the temperature limit approaches. The worldwide mangrove area is estimated to be 180000 km^2. Salt adaptation is not limited to tropical and subtropical areas. In temperate latitudes salt adapted ecosystems like salt marshes exist but the additional costs in growing and operating as a tree seem not to be feasible to latitudes, where low temperature and a short day for photosynthesis occur for much of the year.

Many different animal species live in mangroves. The most abundant are mollusks and crabs.

3.3.2. Water volume in mangrove swamps

The anoxic sediment forced mangroves to develop techniques to absorb oxygen in different ways. All mangrove species developed air roots located above the sediment. Different mangrove species have very differently shaped roots. The relative root mass in the mangrove group is higher than in other plants. This is due to the satisfaction of the water demand in saline environments. These roots and the rest of the mangroves need a volume V_M inside a volume V. Hence the "free" water volume in a box with the volume of V is $V - V_M$. The roots are a resistance for the water currents entering the swamp. The ratio V_M/V can reach up to 0.45 for the Bruguierra Gymnorrhiza (*Mazda et al.* [1997]).

3.3.3. Evapotranspiration

The evapotranspiration is the sum of transpiration and evaporation. Transpiration is the evaporation of water through leaves and stems of plants. Mangroves satisfy their demand of freshwater by excluding salt from the water taken by the roots. The demand of water has been estimated between 4 mm/day and up to 7 mm/day *Wolanski and Gardiner* [1981] and *Stieglitz* [2002]. This is in the same range of the mean precipitation during the field trips (4.7mm/day July-August 2005; 8.1 mm/day February-March 2006). With an area of 96 km^2 the freshwater demand of the mangroves lies between 4.5 m^3/s and 8 m^3/s. With an average of 10 ppt and a sea water density of 1011 kg/m^3 the mangroves leave 40-90 kg salt per second. This amount is small compared to the 5500 kg salt per second entering the Lagoon through Plawangan but can increase the salinity in regions far away from the outlets and cause hyper-saline environments in areas which are flooded only at spring tide.

The separated salt can cause "self inflicted" ecological stress. The low water velocity in mangrove swamps due to the high resistance of the aerial roots can be too small to flush the hyper-saline water. Crustaceans living on the soil with their burrows help to create a more efficient water exchange and help as "bio-engineers" to remove the salinity stress due to hyper-saline conditions.

3.4. Seawater age

The age of seawater is the time elapsed since a water particle left the region where it is set to zero. It is a characteristic that every particle carries with itself. In a Lagrangian model it would be easy to attach an age-clock to every particle. An Eulerian model, as GETM is, has to describe the age in a different way. How to define the water age in a bucket which was mixed from a bucket with "zero" age water and another bucket with 1000 year old water? *Deleersnijder et al.* [2001] developed the theory of the age of seawater as a passive tracer similar to the salinity tracer but with a source term of one. Every time step the tracer will become "older". The age can mix like every other tracer. The differential equation of the age a is

$$\frac{Da}{Dt} = 1. \tag{3.8}$$

With an implemented age tracer a zero age region has to be defined, otherwise the water would simply become older. An example of a region with zero age could be the water surface. All water particles touching the surface become "young". Descending water becomes older. This allows to calculate the age of deep sea water. To calculate the residence time of water in an estuary the zero region definition has to be chosen differently. Water shall age inside the lagoon but is exchanged by young water through the boundaries. Hence the age is set to zero at the open boundaries. Incoming Ocean water, river input and precipitation are water masses with zero age and mix with the older water inside. Chapter 6.9 shows the results of an age tracer application with zero age at the boundaries.

3.5. Hydrodynamic Model

3.5.1. Introduction

GETM (**G**eneral **E**stuarine **T**ransport **M**odel, www.getm.eu, *Burchard and Bolding* [2002]) is a 3D numerical model simulating the most important hydrodynamic and thermodynamic processes in natural waters. The open source model includes a drying/flooding of intertidal flats. GETM uses general vertical coordinates with surface and bottom defining the uppermost and lowermost levels respectively. In contrast to z-level coordinates with a predefined vertical layer thickness, general coordinates are predefined in the sense of the number of layers. Each water column has, regardless of the actual depth, the same number of vertical layers. This helps to resolve stratification in shallow areas.

3.5.2. Equations behind GETM

The hydrodynamics in GETM are described by the hydrostatic equations of motion in the flux form with the Boussinesq approximation and the Eddy viscosity assumption:

$$\begin{aligned}
&\partial_t u + \partial_z(uw) - \partial_z\left((\nu_t+\nu)\partial_z u\right)\\
&\quad +\alpha\Big(\partial_x(u^2) + \partial_y(uv) - \partial_x\left(2A_h^M\partial_x u\right) - \partial_y\left(A_h^M(\partial_y u + \partial_x v)\right)\\
&\quad -fv - \int_z^\zeta \partial_x b\, dz'\Big) = -g\partial_x\zeta,
\end{aligned} \tag{3.9}$$

$$\begin{aligned}
&\partial_t v + \partial_z(vw) - \partial_z\left((\nu_t+\nu)\partial_z v\right)\\
&\quad +\alpha\Big(\partial_x(vu) + \partial_y(v^2) - \partial_y\left(2A_h^M\partial_y v\right) - \partial_x\left(A_h^M(\partial_y u + \partial_x v)\right)\\
&\quad +fu - \int_z^\zeta \partial_x b\, dz'\Big) = -g\partial_y\zeta.
\end{aligned} \tag{3.10}$$

With u, v and w the velocities in Cartesian coordinates x, y, and z. The buoyancy b defined as

$$b = -g\frac{\rho-\rho_0}{\rho_0}. \tag{3.11}$$

g is the gravitational acceleration, ρ the density of the water and ρ_0 the reference density. A_h^M is the horizontal molecular diffusivity and is set to zero in this study. The vertical kinematic viscosity ν and the vertical Eddy viscosity ν_t. The vertical velocity w is calculated with respect to the incompressibility condition:

$$\partial_x u + \partial_y v + \partial_z w = 0. \tag{3.12}$$

For drying/flooding the parameter α is incorporated, so that in shallow waters (defined with the variables D_{min}, D_{crit}) the physics are simplified to a balance of tendency, friction and external pressure gradient

$$\alpha = \min\left\{1, \frac{D - D_{min}}{D_{crit} - D_{min}}\right\}. \tag{3.13}$$

The details of the drying/flooding procedure are explained in Chapter 3.5.5.

Due to equation (3.12) mass conservation is guaranteed and the surface elevation ζ can be obtained with

$$\partial_t \zeta = -\partial_x U - \partial_y V, \tag{3.14}$$

where U,V are the vertical integrated velocities of u and v

$$U = \int_{-H}^{\zeta} u \, dz \quad V = \int_{-H}^{\zeta} v \, dz. \tag{3.15}$$

3.5.3. Tracer equations

Tracers can e.g. be temperature, salinity, nutrients, phytoplankton, suspended matter and seawater age. The two most important tracers, potential temperature and salinity are implemented within GETM:

$$\begin{aligned} &\partial_t \theta + \partial_x(u\theta) + \partial_y(v\theta) + \partial_z(w\theta) - \partial_z(\nu_t' \partial_z \theta) \\ &-\partial_x(A_h^\theta \partial_x \theta) - \partial_y(A_h^\theta \partial_y \theta) = \frac{\partial_z I}{c_p' \rho_0}, \end{aligned} \tag{3.16}$$

$$\begin{aligned} &\partial_t S + \partial_x(uS) + \partial_y(vS) + \partial_z(wS) - \partial_z(\nu_t' \partial_z S) \\ &-\partial_x(A_h^S \partial_x S) - \partial_y(A_h^S \partial_y S) = 0. \end{aligned} \tag{3.17}$$

Where ν_t' is the Eddy diffusity and A_h^S, A_h^θ the horizontal diffusivities for salinity and potential temperature. The diffusivities are set to zero. On the right hand side of the equations are the source terms. It is zero for salinity and the absorption of solar radiation for the temperature. The water column absorbs the incoming radiation I_0. GETM uses a modified exponential law to describe the absorption described by *Paulson and Simpson* [1977]

$$I(z) = I_0 \left(a e^{-\eta_1 z} + (1-a) e^{-\eta_2 z}\right). \tag{3.18}$$

Where I_0 is the incoming albedo corrected radiation normal to the sea surface. The parameters a, η_1 and η_2 depend on the turbidity of the water.

The boundary conditions for the surface fluxes of the temperature are the sensible heat flux Q_s, the latent heat flux Q_l and the long wave back radiation Q_b

$$\nu_t' \partial_z T = \frac{Q_s + Q_l + Q_b}{c_p' \rho_0}, \qquad \text{for } z = \zeta. \tag{3.19}$$

The *Kondo* [1975] bulk formulae are used for calculation of the momentum and temperature surface fluxes due to air-sea interactions. For more details refer to *Burchard and Bolding* [2002].

3.5.4. Turbulence model

The vertical Eddy viscosity ν_t refers to the Eddy viscosity principle which is the assumption that the Reynolds stress may be modelled in the same way as the viscous stress ν. The stress caused by the Eddy viscosity can be explained as the internal stress due to turbulent water flow. The same is valid for the Eddy diffusity ν_t'. Calculations of the Eddy viscosity/diffusity is done via GOTM calls (General Ocean Turbulence Model, www.gotm.net, *Umlauf et al.* [2005]) inside the momentum/tracer routines.

3.5.5. Drying and flooding

Three quarters of the Segara Anakan lagoon are intertidal mangroves (tabular 2.1). These areas are flooded twice a day. The water volume of the intertidal areas changes the hydrodynamics significantly (see chapter 6.2.2). Thus intertidal flats have to be reproduced within the model. GETM has a built in drying/flooding algorithm. It is implemented with an α factor (equation 3.13) to slowly shut down all physical effects except tendency, friction and external pressure gradient. Furthermore a virtual water level is implemented to prevent the water level falling below a predefined constant (figure 3.7). The advantage of this approach is the integration of drying/flooding into the differential equations without the need for special case routines controlling the behaviour of the model during drying/flooding situations. The sea level and α factor computation is done during the barotropic mode. Here the vertically integrated velocities U and V are computed:

$$\begin{aligned}\partial_t U + \frac{R}{D^2}U\sqrt{U^2+V^2} + \alpha\Big(& S_F^x + \partial_x\left(\frac{U^2}{D}\right) + \partial_y\left(\frac{UV}{D}\right) \\ & -\tau_s^x - \partial_x\left(2A_h^M D\partial_x\left(\frac{U}{D}\right)\right) - \partial_y\left(A_h^M D\left(\partial_y\left(\frac{U}{D}\right) + \partial_x\left(\frac{V}{D}\right)\right)\right) \\ & -fV + S_A^x - S_D^x + S_B^x\Big) = -gD\partial_x\zeta\end{aligned} \tag{3.20}$$

and

$$\begin{aligned}\partial_t V + \frac{R}{D^2}V\sqrt{U^2+V^2} + \alpha\Big(& + S_F^y\partial_x\frac{UV}{D} + \partial_y\frac{V^2}{D} \\ & -\tau_s^y - \partial_x\left(A_h^M D\left(\partial_y\left(\frac{U}{D}\right) + \partial_x\left(\frac{V}{D}\right)\right)\right) - \partial_y\left(2A_h^M D\partial_y\left(\frac{V}{D}\right)\right) \\ & +fU + S_A^y - S_D^y + S_B^y\Big) = -gD\partial_y\zeta.\end{aligned} \tag{3.21}$$

with α as in equation 3.13 and the bottom resistance term:

$$R = \left(\frac{\kappa}{\ln\left(\frac{z+z_0}{z_0}\right)} \right)^2 . \tag{3.22}$$

The Karman constant $\kappa = 0.41$, the distance from the sea bed z and z_0 the bottom roughness in meter. The terms $S_A^y\ S_D^y\ S_B^y$ and $S_A^y\ S_D^y\ S_B^y$ are interaction terms between the barocline and barotrop mode (see chapter 3.5.6 and *Burchard and Bolding* [2002] for details)

A water depth above D_{crit} results in $\alpha = 1$ and the differential equations are solved in their full appearance. If the depth D reaches D_{crit} α decreases linearly towards zero. α becomes zero when $D = D_{min}$ and the equations 3.20 and 3.21 reduce to:

$$\partial_t U + \frac{R}{D^2} U \sqrt{U^2 + V^2} = -gD\partial_x \zeta \tag{3.23}$$

and

$$\partial_t V + \frac{R}{D^2} V \sqrt{U^2 + V^2} = -gD\partial_y \zeta. \tag{3.24}$$

This is the balance between tendency, friction and external pressure gradient. To prevent cells to fall below D_{min} the virtual water level is established. If the depth D_{min} is reached, and adjacent cells have a sea level lower of the dried cell it is set to the sea level of the dry cell. The sea level gradients $-gD\partial_x\zeta$, $-gD\partial_y\zeta$ become zero and consequently the velocities u and v are zero (see figure 3.7).

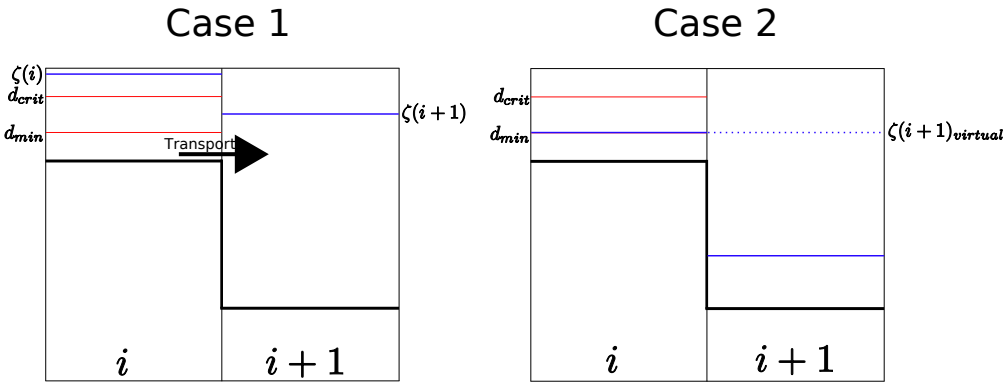

Figure 3.7: The virtual water level prevents the sea level of a dried cell to fall below the seabed. The left panel shows an external pressure gradient $-gD\partial_x\zeta > 0$ between boxes i and i+1. A transport lets the water level sink in box i. In the right panel the water level is at d_{min} and is per definition dried out but has still a gradient $-gD\partial_x\zeta > 0$. Without the virtual water level $\zeta_{virtual}$ in box i+1 the sea level in box i could even fall below the seabed.

The algorithm for drying/flooding has been proven to work, (*Burchard et al.* [2007], *Stanev et al.* [2003]) but becomes unstable in bathymetries with high bathymetry gradients between cells which can fall dry and cells with water. Unstabilities are water depths below the sea floor (negative water depths).

The mangrove areas in Segara Anakan are intertidal. Through the mangroves swamps are running relatively deep channels of up to seven meters. These conditions can be considered as a bathymetry with high gradients.

During model runs of the lagoon negative water depths occurred and caused the model to crash. To cope with these extreme conditions an emergency break was built into the GETM code. If the sea level falls below the minimum depth, all transports of the affected box are set to zero and the sea level is calculated again. As the stopped transports can cause adjacent boxes to fall dry, the check must done iteratively to test if adjacent boxes fall dry due to the changed transports. The test costs some computational time but is necessary to model the Segara Anakan lagoon with GETM.

3.5.6. Discretization and mode splitting

For the discretization of the infinitesimal values dx, dy, dz, dt to Δx, Δy, Δz and Δt some constraints have to be fulfilled. If the spatial resolution is defined and the free surface is numerically treated in an explicit way a strict constraint for Δt depending on Δx, Δy evolves:

$$\Delta t < \left[\frac{1}{2}\left(\frac{1}{\Delta x} + \frac{1}{\Delta y}\right)\sqrt{2gD}\right]^{-1}. \tag{3.25}$$

The idea behind this constraint is that the propagation of information in the grid boxes must not be faster as $\frac{\Delta x}{\Delta t}$. If it were faster it would skip an adjacent cell and produce substantial instabilities. Shallow water surface waves with a propagation speed of $\sqrt{2gD}$ are the fastest information and the inequation is set to fulfill this constraint. This is the stability criterion for shallow water waves. In contrast to that, the stability criterion for advection is

$$\Delta t < \min\left\{\frac{\Delta x}{u_{\max}}, \frac{\Delta y}{v_{\max}}\right\}, \tag{3.26}$$

and is a much weaker constraint in typical environments. Because the Δt of the constraints differ so much it is advantageous to split the model into 2 modes, the first is the external mode (or barotrop mode) with high resolution micro time steps Δt_m. The second is the internal mode with macro time steps Δt. The external mode is limited by (3.25), the internal mode by (3.26).

The barotrop mode solves equation 3.20 and 3.21 to get the sea level and the vertical integrated velocities U and V. The computational more expensive barocline mode is computed at the macro time steps. Within GETM the factor n has to be set. It defines the splitting of the barotrop and barocline mode. The macro time step is n times the micro time step. This is every nth micro time step and is in typically in the range of $n = 10 - 30$. The disadvantage are interaction terms between the external and the internal mode.

4. Field trips and remote sensing data

4.1. Introduction

The first part of this chapter is about the field measurements in Segara Anakan and the post processing of the in situ data as it is needed for the setup of the computer model. The second part describes how the remote sensing data is used to quantify freshwater fluxes into Segara Anakan. It also estimates the effect of wind induced sea level changes inside the lagoon and their effect on the hydrodynamics.

Two field trips were carried on in Segara Anakan. The measuring dates were chosen to obtain data at different monsoon seasons.

- August-September 2005 (dry season)
- February-March 2006 (rainy season)

Our team formed during the first field trip and did not change on the second field trip. It consisted of Alo a student of marine biology and translator, Andrew the captain of the hired boat Miund and myself. In both field trips bathymetry, tide, water fluxes, salinity and temperature were measured. The kernel was always the RDI Workhorse-Sentinel 1200 kHz ADCP. The main focus of the first field trip were depth soundings for a bathymetry of Segara Anakan. A look e.g. at figure 4.17 shows denser measurements during the second field trip. The experiences and contacts of the first field trip helped a lot to increase the amount of recorded data during the second field trip (see section 4.2). The original data of the measurements is stored in different ways and medias. To build a database for easy and fast processing all measurements and results are converted into a format readable by the MATLAB (R14, August 2005) software.

4.2. Geographical and socio-cultural constraints

Measuring hydrodynamic data is not a trivial task. To get the desired information weather, infrastructure, technical problems and other obstacles have to be mastered. On a modern scientific vessel most of the problems are minimized and the attention can be targeted to the scientific problem. The situation is different in Segara Anakan. After searching for almost a week it was clear that a lot of the wanted and needed informations had to be measured by ourselves. No continuous tide levels were recorded, except the navigation channels of the harbour, the bathymetry of the lagoon was unknown and the weather data was restricted to monthly averages of temperature, precipitation and wind. All measurements were done by using local facilities (ships, ferries) and with great

help of the Indonesian partners. Some measurements were done by local villagers like reading the tide gauges or taking water samples. This was a nice way to save time needed for further ADCP measurements and to get in touch with the local people, their lifestyle, culture, knowledge and problems with Segara Anakan. We experienced many specific problems like the omnipresent fishing nets at spring tide, which made measurements impossible or very expensive (paying the fishing nets cut by our propeller became a fix part in the budget) or the experience not to tow a device with a visible rope. The rope was precious enough to be taken by someone, although its value is only a negligible fraction of the measuring device. Due to this, we lost the only pressure sensor to automatically measure the sea level. Heavy thunder and monsoons rainstorms often hindered us to measure; especially during the night. Even at rising tide the depth soundings were often joined with groundings since nobody really knew where the lagoon became too shallow for the ships draught. Freeing the grounded ship by pushing became our sport and two pairs of trousers were self-evident. Nevertheless the acquiring of data was fun and we learned a lot about Segara Anakan. The results are promising that even in difficult environments good scientific data can be obtained.

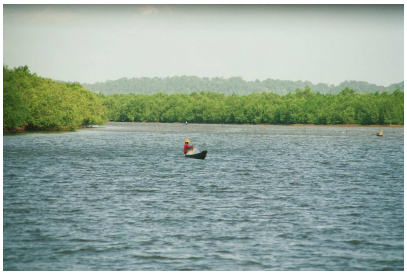

(a) View into a channel.

(b) Omnipresent nets during spring tide.

(c) Tide gauge installation in Seleko.

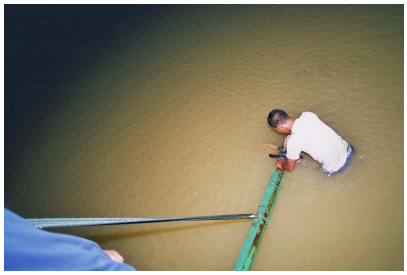

(d) During a night measurement trapped fishing net is cut by Andrew.

(e) Local fisherman.

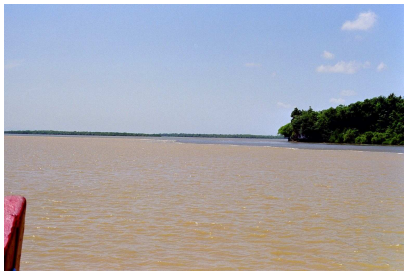

(f) Waterfront of Citanduy water plume (front) and sea water (back).

Figure 4.1: Some photos from Segara Anakan and the field work.

4.3. Tide

The tide is the main forcing of the hydrodynamics and it is essential to have information about water level changes in tidal scales. During the field trips two permanent tide gauges had been installed. In the first field trip a third gauge was installed in the middle of the lagoon (Motean village). But the maintenance of three gauge stations is time expensive and the number was reduced to two stations in the 2006 trip. The tide stations were manually read every hour for 13 hours a day by local villagers (for positions and operation see figure 4.2 and Table 4.1). Unfortunately it was not possible to install another tide gauge at the Indian Oceans shore to record the tide at the outlets. Instead, the tidal constituents from *Egbert and Erofeeva* [2002] were taken. The measured water levels can be seen in Figure 4.3. The lowest of the plots is always the Indian Oceans tide from *Egbert and Erofeeva* [2002].

Station Name	Data Quality 7-8.2005	Data Quality 2-3.2006
Seleko	good	good
Motean	good	N.A.
Klaces	bad	good

Table 4.1: Tidestation operation and data quality during the field trips (see figure 4.3).

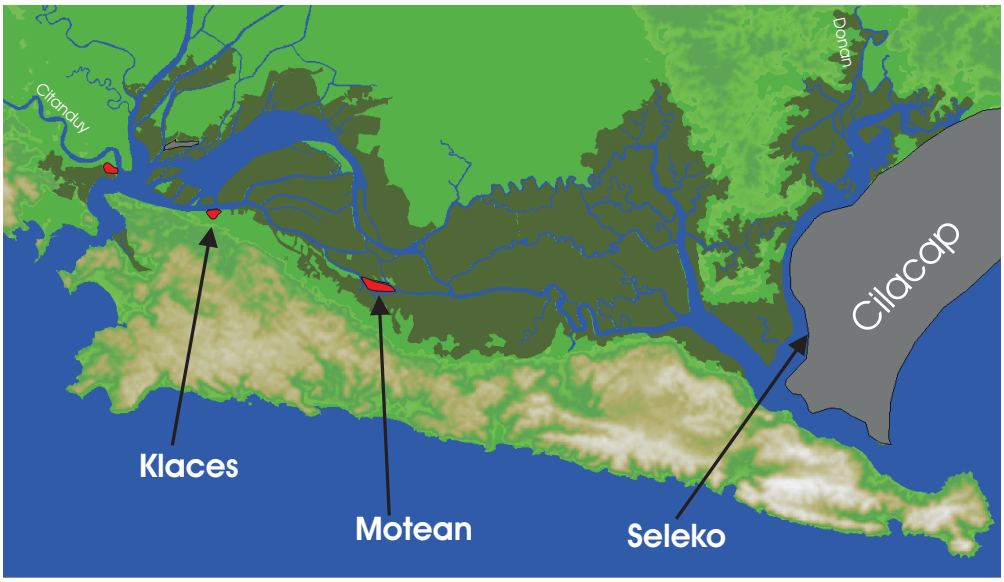

Figure 4.2: Position of permanent tide gauges during the field trips.

4.4. Bathymetry

The bathymetry is essential for the understanding of the hydrodynamics and the quantification of fluxes only makes sense if the water volume is known. A lot of time was spent to do depth soundings combined with GPS positions. The depth soundings had to be corrected as the measurements were done on different tide phases. The corrected depth data has to be referenced to a sea level datum. Sea charts usually refer to the lowest astronomical tide (LAT), which is the lowest low water under normal circumstances. For practical reasons the bathymetry is referenced to the mean sea level. This makes a GETM setup easier. The complete bathymetry consists of the depth sounding data, shorelines from satellite images, a sea chart and bathymetry data of the mangrove area.

The detailed steps to set up the bathymetry are:

- extraction of shorelines from a SPOT satellite picture (section 4.4.1)

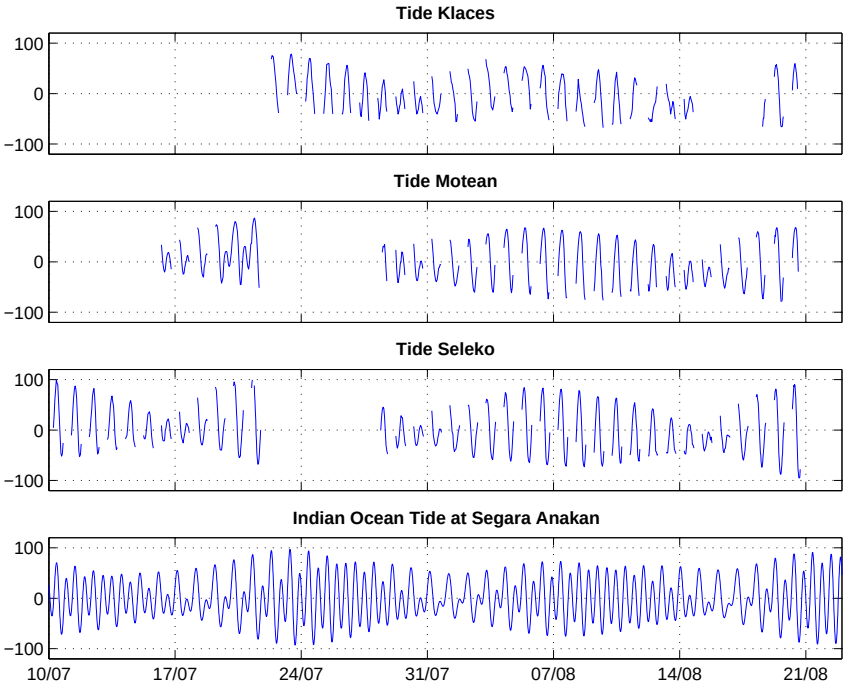

(a) Tide 2005

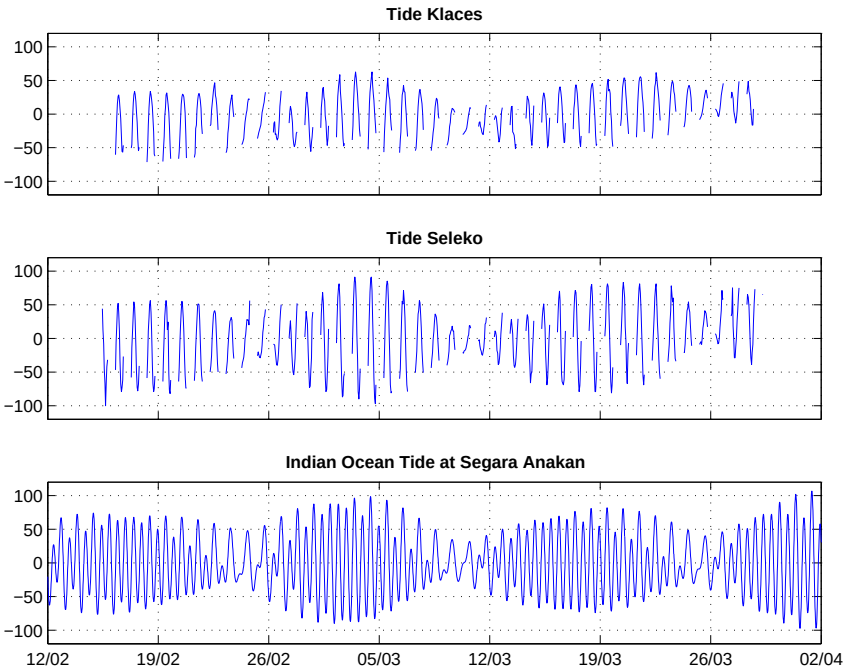

(b) Tide 2006

Figure 4.3: Tide measurements in Segara Anakan. Upper panel: 3 tide gauges were installed in the 2005 field trip with good quality of the Motean and Seleko stations. Lower panel sea levels during the 2006 field trips: Two stations were installed in Klaces and Motean, both with good data quality.

- referencing of the depth soundings to the mean tide level (section 4.4.2)
- using a sea chart of the Cilacap-harbour for additional bathymetry (*Hydrographic Office* [1994]) (section 4.4.3)
- bathymetry assumptions in the mangrove-areas (section 4.4.4)
- rastering the spatially unstructured data into a regular grid and interpolating a surface (section 4.4.5)

4.4.1. Shorelines

To extract the shorelines, 3 SPOT Scenes of Segara Anakan were used. The images were saved in the geotiff format. Which is a tiff image with an extra header containing the position of the image on the earth. To test if the georeference is correct it is visually checked by a comparisons of known GPS positions on the image. We for example walked along some shorelines with a recording GPS. Superposing of the track with the SPOT scene should give the shorelines. This was not the case for the scene on Dec. 30.,2004. The georeference was shifted around 500 meter from the correct position (figure 4.4). A freely available geotiff manipulation package (libgeotiff, remotesensing.org/geotiff/geotiff.html) was used to change the georeference header and visually check the results until the positions agreed. The first approach to extract the shorelines and to differentiate between water, mangroves and land was done by a semiautomatic area classification of the GRASS GIS program (*GRASS Development Team* [2007]). Well known test areas are defined and set to an area type. GRASS analyzes the color spectrum of the test areas and classifies the rest of the scene with respect to the color spectra of the test areas. The process worked quite well but could not resolve the fine channel structures of the inner mangroves. Finally the land-water mask was hand-made with an ordinary image manipulating program (GIMP, www.gimp.org).

4.4.2. Depth soundings

The ADCP bottom tracking signal combined with GPS positions are the depth soundings. Most of the measurements were made by hauling a float with the installed ADCP and transfer the data directly to a laptop on board (Figure 4.14). In some areas the water was not deep enough for the draught of a ship capable to carry a laptop. Here the ADCP float was hauled with a log boat and rowed or driven with a small outboard motor to the areas. Parallel a GPS with a clock referenced to the ADCP clock had been put onto the ADCP float (figure 8.1(b)). The two data sets were combined in post processing. The focus of the depths soundings was the western part of the lagoon (compare the coarse resolution in the eastern part with the numerous measurements in the western part on figure 4.11). The small channels running through the mangrove forest had to be skipped due to time reasons and the fact that most of the channels are shallow and fall dry during low tide. Their influence on the hydrodynamic is unknown but they are probably not important.

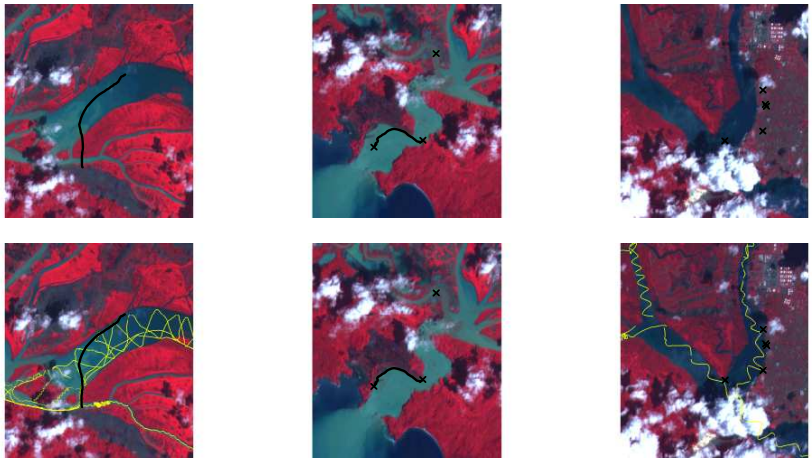

Figure 4.4: Some SPOT scenes had to be georeference again. Upper panels: original georeference with an approx. error of 500m. Lower panels: re-referenced SPOT image with depth soundings (yellow), GPS Tracks (black) and points directly on the shore (black crosses).

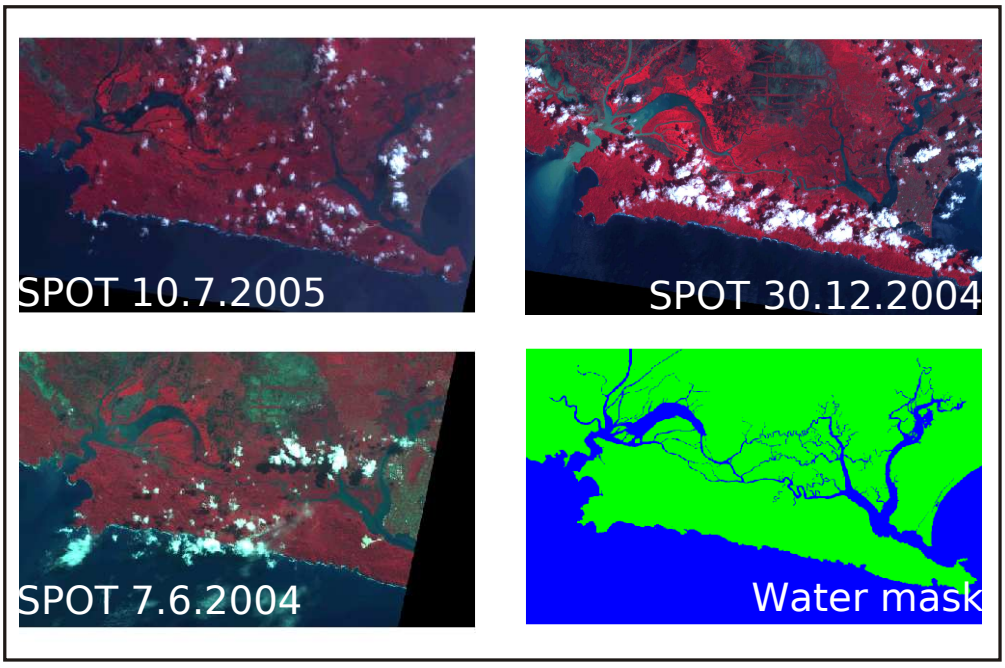

Figure 4.5: Water mask derived from SPOT scenes.

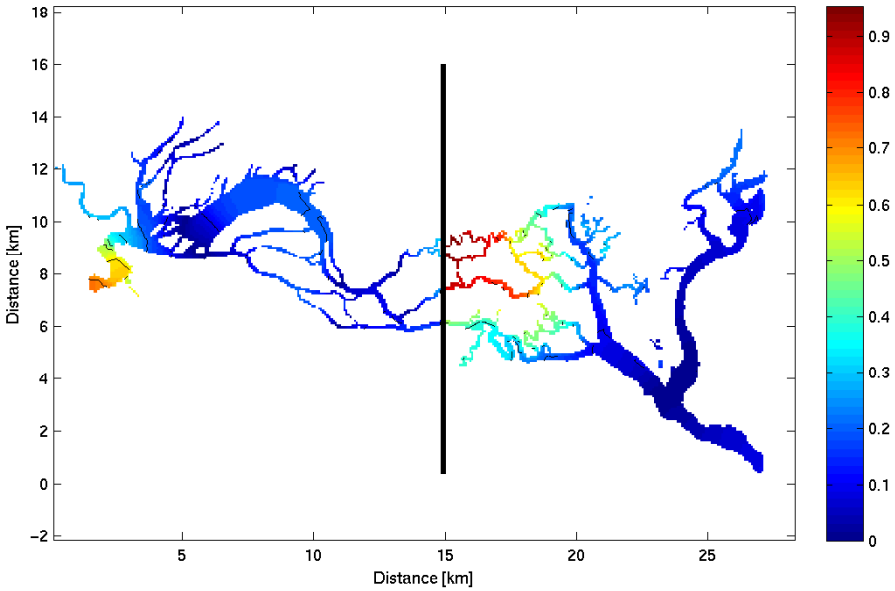

Figure 4.6: Maximum error of the bathymetry due to the tidal correction of the depth soundings. Colorbar: Bathymetry error in meter. Black Isolines are plotted with distance of 0.10 meter error. Western part: Tidal correction with Klaces tide gauge. Eastern part: Tidal correction with Seleko tide gauge.

Mean sea level referencing

The sea surface elevation due to tide can change the measured depth at the same location at different times up to 1.4 meter. To reference the depth to the mean sea level all depth soundings have to be tide corrected. The sea level was recorded in Klaces and Seleko. For the correction of the western part depth soundings the Klaces Tide was subtracted. Seleko Tide was subtracted from the eastern lagoons measurements.

The tidal wave entering Segara Anakan propagates with a certain speed and needs some time to reach every location in the lagoon. The time is approx. 1-2 hours for the middle of Segara Anakan (see chapter 6.4.2).

The referencing is correct in the very near of a tide gauge, but becomes wronger with a growing distance. For instance the tidal correction in the middle of the lagoon is done with a sea level of approx. 2 hours difference. Figure 6.16(b) shows the M_2 phase delay inside Segara Anakan. With this delay the bathymetry error due to the sea level referencing can be estimated. The phase delay of Klaces (Seleko) is defined as zero. Every location has a phase delay relative to Klaces (Seleko). This phase delay can be expressed in minutes. To get the maximal error due to mean sea level referencing we multiply the time delay in minutes with the maximum change of the sea level (which is obviously during spring tide) $max(\frac{d\zeta}{dt}) = 50$ cm/h. Figure 4.6 shows the maximum error due to tidal corrections. It is divided into the western part where the Klaces tide gauge is used for the correction and the eastern part with the Seleko tide gauge.

Figure 4.7: Scanned and georectified sea chart of Cilacap *Hydrographic Office* [1994].

4.4.3. Sea chart

A sea chart (*Hydrographic Office* [1994]) of the eastern part is available because the city Cilacap has an international harbour and an oil refinery. The sea chart was scanned and georectified with GRASS (figure 4.7). The isolines and depth points were saved in a MATLAB readable format. The depth datum of the sea chart is the lowest spring tide level. To translate the datum to the GETM environment, which uses the mean water level 1.1 meter have to be added to the depth data.

4.4.4. Mangroves

The total mangrove area of Segara Anakan has been estimated to 96 km^2 (*Ardli and Wolff* [accepted]). This is three quarters of the overall area. It contributes to the water volume and influences the hydrodynamics (see chapter 6.2.2) but cannot be measured with depth soundings. A measurement of the height is difficult. The aerial roots of neighboring trees often cross and result in an impenetrable tangle. A 100 meter dash through a mangrove swamp can take up to 22 minutes (*Hogarth* [1999]). Another way to estimate the water volume and bathymetry of the mangrove swamps had to be developed. Mangroves adapted their metabolism to survive in saline environments. As mentioned in Chapter 3.3.1 these adaptations are expensive. They could survive in freshwater

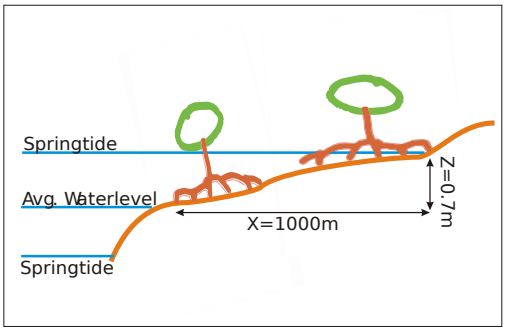

Figure 4.8: Assumption for the volume calculation of the mangrove swamps. Mangroves habitats are inter tidal. Therefore they do not grow above spring tide water level.

environments but cannot compete with pure freshwater flora. This reduces the habitat to saline environments. The mangrove areas are simultaneously a brackish or saline environment and are flushed with saline water. Our main assumption is that mangroves are at least reached by the average spring tide water level (figure 4.8). That means that all mangroves are at least flushed twice a month with salt water. The spatial mangrove distribution from *Ardli and Wolff* [accepted] is used to calculate the distance of every mangrove to water (figure 4.9). The area is integrated over the distance. The lower panel of figure 4.10 shows that 98% of the whole mangrove area reside closer than 1000 meter to water. With an average spring tide amplitude of 0.7 meter the spatial gradient rectangular to the shore is 7/1000 (figure 4.8).

4.4.5. Rastering and interpolation of the spatial unstructured data

The gathered topographic data is spatially unstructured and partly incomplete. Figure 4.11 shows the bathymetry data of the water areas. Note the blue dots, indicating missing data but manually added bathymetry to get smoother gradients and to include the not measured smaller channels. All channels were set to a depth of 50 cm. It is obvious that the depth soundings should be distinguished as a beginning and being far away from a complete and dense depth sounding of Segara Anakan. The same is true for the mangrove bathymetry. It is based on assumptions without a single measurement. But despite of these weak points the model results have the right order of magnitude and justify the extrapolations and assumptions.

The structuring begins with defining a grid. We choose a (20x20) meter grid resolution. This is the resolution of the SPOT scenes and is 4 times finer than the final resolution used in GETM. The grid is filled with the shorelines. In the next step a search algorithm finds for every depth sounding data the corresponding cell of the grid and fills the cell with the depth data. If two or more measurements fall into the same cell, the average of the measurements will be taken. The filled grid has still many missing cells (white cells in figure 4.12(a)). These cells are interpolated using a Delaunay triangulation algorithm implemented in MATLAB (*Barber et al.* [1996]). The result can be seen in

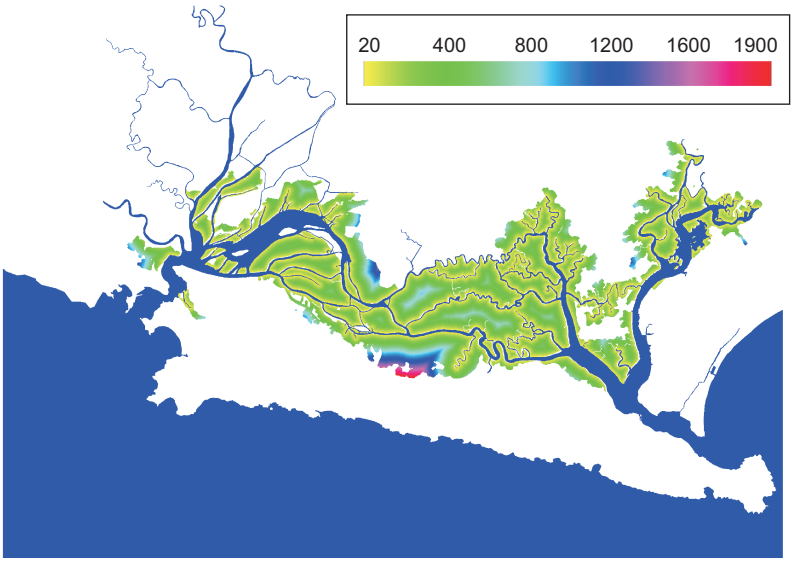

Figure 4.9: To estimate the water volume of the mangrove areas the distance of the mangroves from water is calculated; Legend: Distance [m].

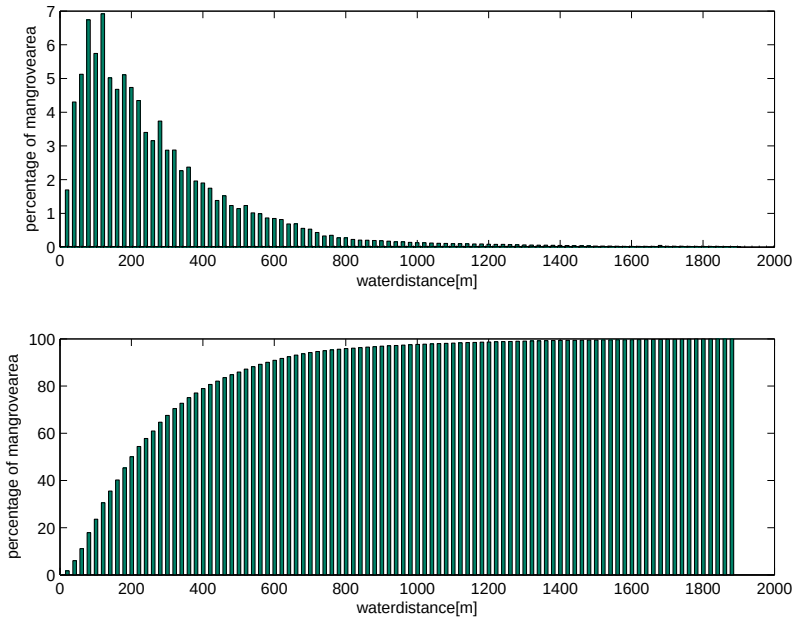

Figure 4.10: Distribution function of the mangroves. Upper panel: percent of mangroves in layers of 20 meter distance. Lower panel: Integration of the mangrove distribution. Percent of mangrove area vs. distance from water.

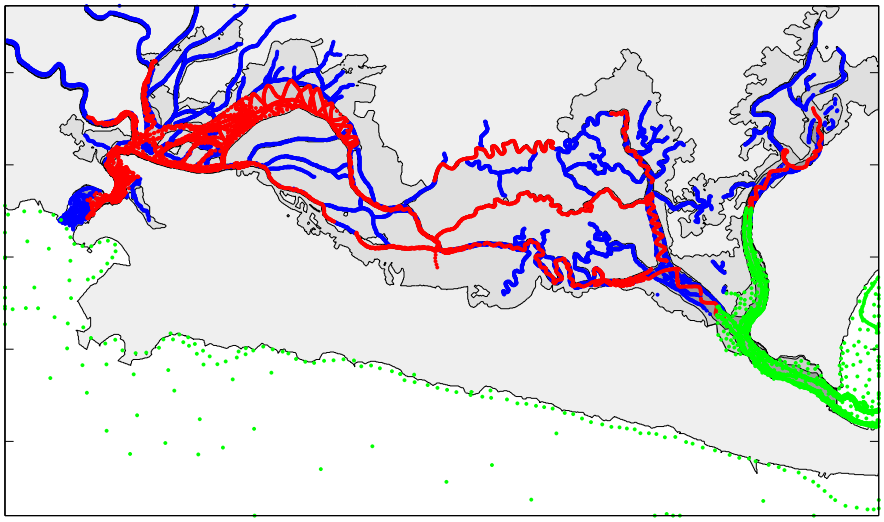

Figure 4.11: Bathymetry data of the water areas. Red: depth soundings; blue: extrapolation and guessing; green: sea chart. The light gray area are mangrove trees and are described with a depth depending on the distance to the water.

Figure 4.12(b). The bathymetry outside Segara Anakan contains some obvious artifacts. For this study it is an aesthetically flaw and does not disturb the results since no computations are done outside the lagoon.

4.5. Discharge measurements

To quantify the water fluxes in the lagoon, discharge measurements at key locations had been done. The main focus of the discharge measurements was the western part with the Citanduy river, the outlet and the biggest channel between the eastern and the western part. Two devices were available, the ADCP and a SD-6000 current meter. It measures water current with a rotor. The initial plan was a SD-6000 mooring in the Citanduy river. The velocity should be calibrated with ADCP transects. With this method a complete discharge time series of the Citanduy would be available. The SD-6000 was set out for a two day test mooring. But the recovered data showed zero velocities 3 hours after the release. An analysis of the device displayed a jammed rotor. Fine black sediment contaminated the bearings and made the resistance too high for rotation. It pointed out that the sediment was attracted by the static magnet used as the transducer of the rotation. Hereon the use of the SD-6000 was discontinued and the Citanduy discharge had to be measured with the ADCP.

For the discharge measurements the ADCP was installed on a float and hauled over the channels. The ADCP configuration was done with the WinRiver and PlanADCP Software provided by RD Instruments. Important configuration factors are the data storage, standard deviation, depth cell size and time taken for one measurement. The first decision is the way of the data storage (see Appendix B). The internal storage method was used when the float was installed

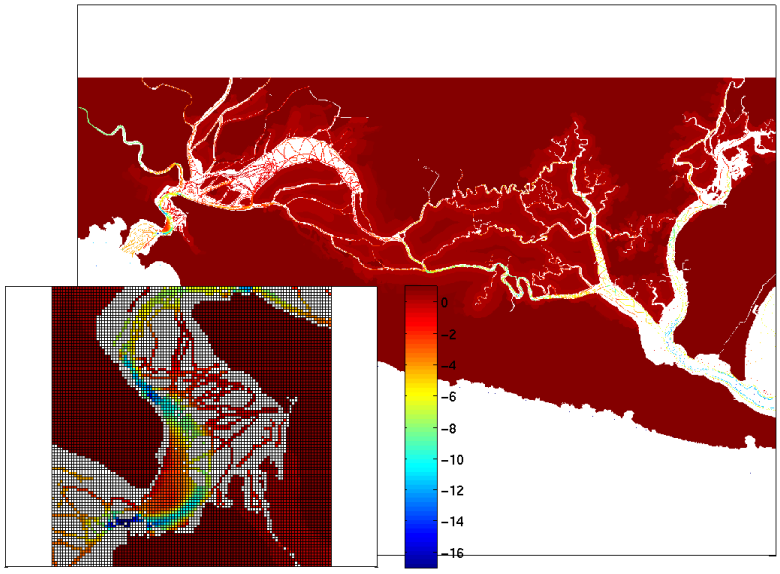

(a)

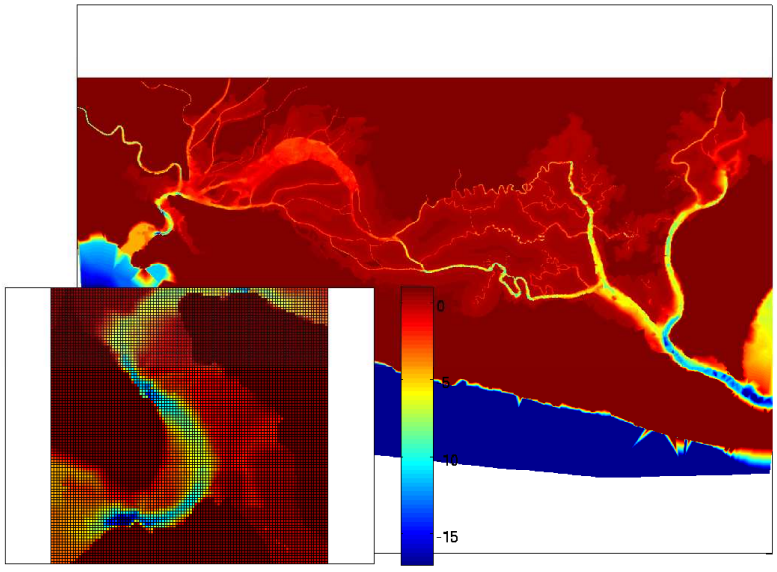

(b)

Figure 4.12: Panel (a): The unstructured depth soundings are rastered into a regular grid with a resolution of (20x20) meter. The small panel shows the Plawangan outlet. Colored cells have at least one depth information, white cells are empty and need to be interpolated. Panel (b): The interpolated bathymetry created with a surface fitting algorithm implemented in MATLAB.

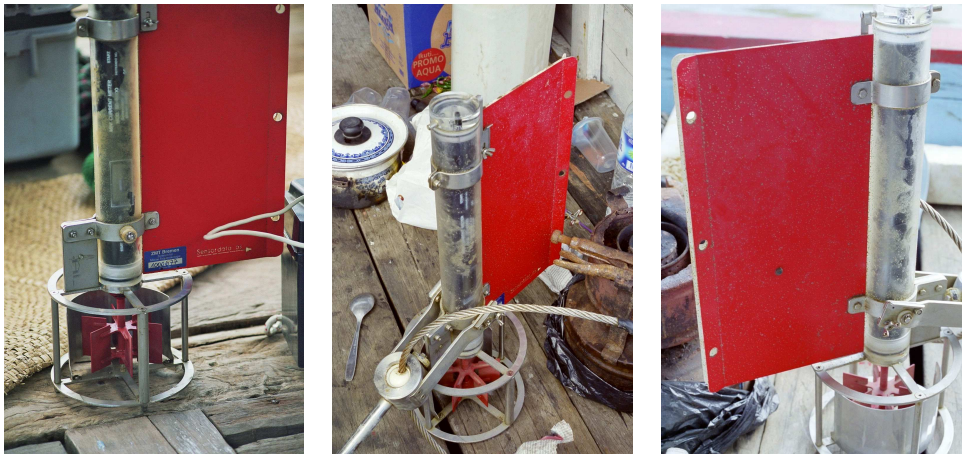

(a) (b) (c)

Figure 4.13: The SD-6000 mini current meter. The device was colonised by organisms after a three day mooring in a calm environment at the Motean village. A mooring in the Citanduy rivers had to be stopped, since the bearings were jammed with magnetic sediment attracted by the static magnet in the rotor.

on log boats for rowing over small channels and shallow areas (e.g. figure 4.14a). The version with a laptop and GPS connection was used when the depth was big enough for the draught and the channel wide enough for manoeuvres of a bigger boat. This was almost only the case in Plawangan. Figure 4.14b shows the working place with a laptop, external power supply through a car battery and a GPS to the left of the laptop. An external GPS antenna was installed on the roof.

The time interval for a measurement depends on the data storage method. The internal mode is limited by the installed data capacity and the relative time consuming download process. Thus if the internal storage mode was chosen, an ADCP internal data averaging was enabled. 20-30 pings were averaged into one ensemble. This reduces the standard deviation and download time, but increases the time interval of one measurement, which is typically 10 seconds for this setup.

The external mode has the advantage of parallel GPS position saving and higher time resolution (1 measurement per second), but needs a bigger boat for the overhead of a laptop and is more power consuming. In Plawangan, this setup was used in approx. 1/3 of all measurements.

The depth cell size was in general 20 cm and bottom tracking mode was always enabled.

An overall number of 1279 ADCP transects were taken during the field trips from which 869 transects were done in Plawangan, Citanduy and East-west water-exchange. This shows the emphasis on the western part.

The volume transport is calculated by using the formulae of chapter 3.2. The speed over ground can be taken either from the bottom tracking signal or (if available) from the GPS data. All calculations were done with the bottom

(a) (b)

(c) (d)

Figure 4.14: ADCP and measuring float pictures.

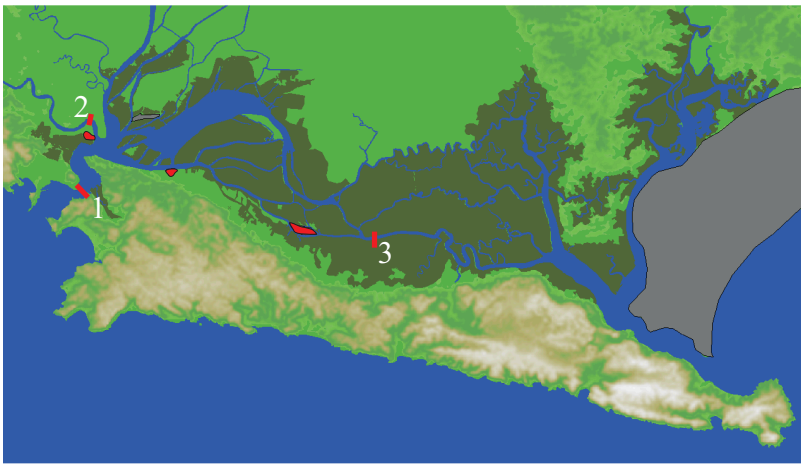

Figure 4.15: Main volume flux transects 1: Plawangan 2: Citanduy 3: East-west channel.

tracking signal.

Figures 4.16, 4.17, 4.18 show the ADCP transects of the Citanduy, Plawangan and the water-exchange channel. The upper panel shows the measurements in 2005, the middle panel the 2006 measurements and the lower panel shows the quotient of the calculated error and the overall volume flux. For small volume fluxes the quotient is greater than 1. This means that the error is bigger than the measurement. This can be understood, since the standard deviation is approx. 0.18 m/s for the external and $0.18/\sqrt{20}m/s \approx 0.04$ m/s for the internal storage setup (table 3.1). If the mean velocity is in the same order of magnitude, error and volume transport have similar quantities.

4.6. Salinity measurements

In an estuary with ocean and freshwater inflow, the time and spatial salinity gradients range from $0-35$. Therefore salinity measurements are necessary and important. Salinity measurements were done with different kinds of devices. Main positions for salinity measurements are shown in figure 4.20.

During the summer 2005 field trip a refractometer and a WTW "MultiLine P4" multimeter (figure 4.19(b)) were used. Because of the manual operation only single samples and no long time measurements were taken. In the winter 2006 field trip a Seabird SBE16 (figure 4.19(a)) was additionally available. It is capable to measure conductivity and temperature automatically in time intervals of up to 5 seconds. Long time measurements were much easier to record and had been done in Klaces and Motean villages. The SBE16 was calibrated in the laboratories of physical oceanography at the IOW, Warnemünde. It has an accuracy of at least a tenth ppt. This is sufficient for the demands in Segara

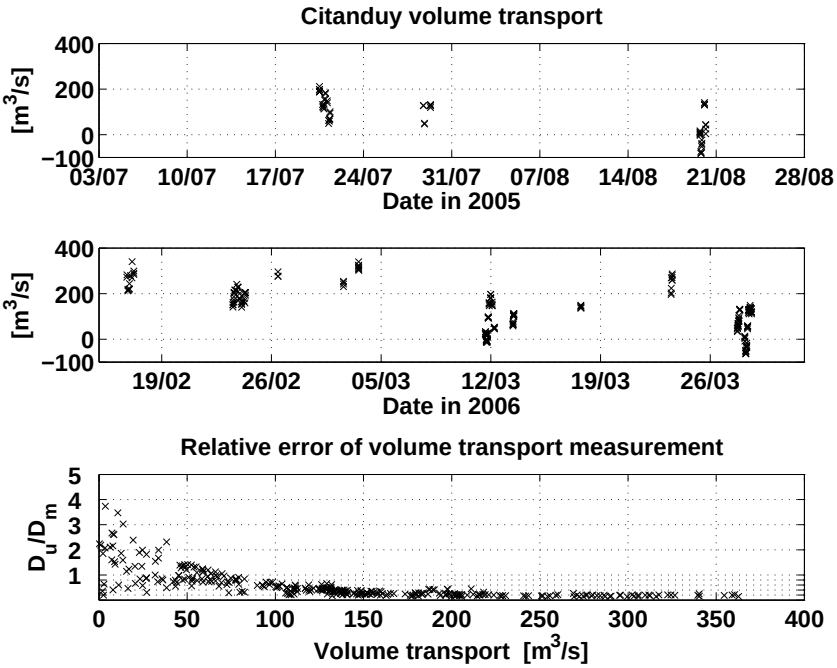

Figure 4.16: Citanduy discharge measurements during the 2005 field trip (upper panel) and 2006 field trip (middle panel) and the relative error (lower panel), positive discharge: into lagoon.

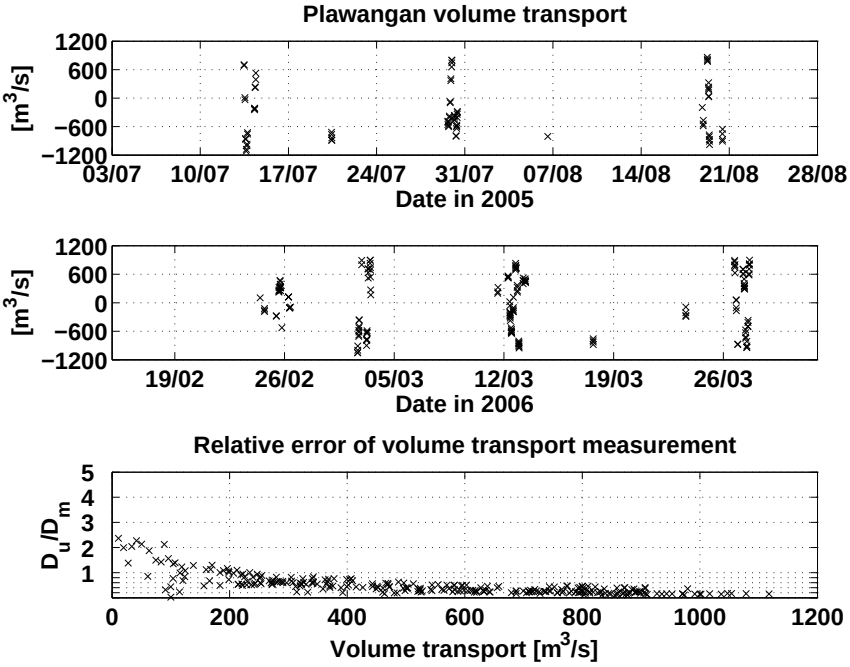

Figure 4.17: Plawangan ADCP volume flux measurements during the 2005 field trip (upper panel) and 2006 field trip (middle panel) and the relative error (lower panel), positive discharge: into lagoon.

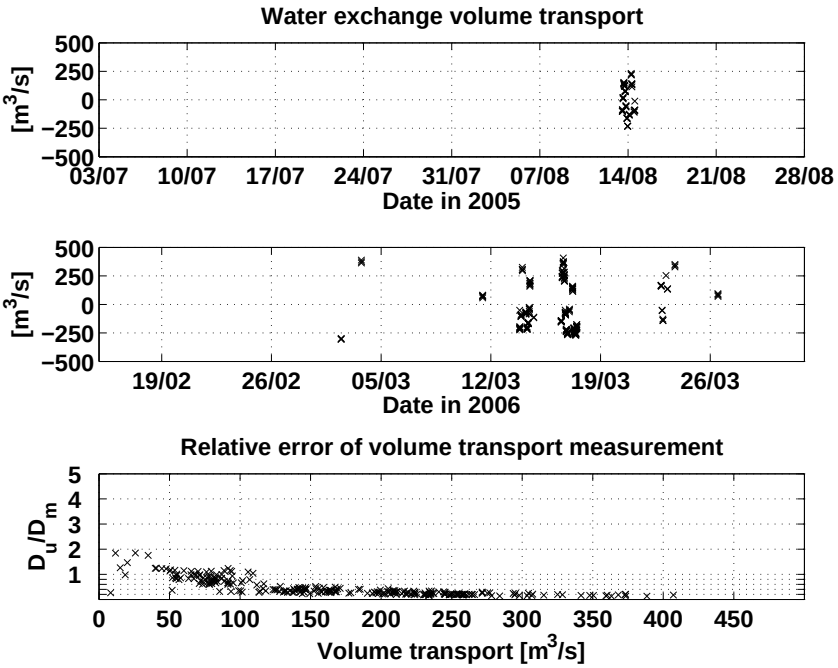

Figure 4.18: Water exchange ADCP volume flux measurements during the 2005 field trip (upper panel) and 2006 field trip (middle panel) and the relative error (lower panel), positive discharge: from west to east.

Anakan. The WTW "MultiLine P4" was calibrated weekly with calibration solutions provided by the manufacturer. The accuracy is also a tenth of a ppt. Before every measurement the refractometer was blind checked with destillated water. The accuracy is ±2 ppt. Figures 4.21 and 4.22 show all salinity measurements taken during the two field trips on the base stations.

The salinity at the Klaces village is influenced by the Citanduy and the Oceans water plume as well as the mixed water of the central part. These effects and the ability of the sensors supervision by a villager made the location valuable for a long time mooring. The most complete long time data set of the field trips were recorded in Klaces with a tide gauge as well as salinity and temperature.

(a) Seabird SBE16 CT-recorder (www.seabird.com).

(b) WTW Multi-Line P4 Multimeter (www.wtw.com).

Figure 4.19

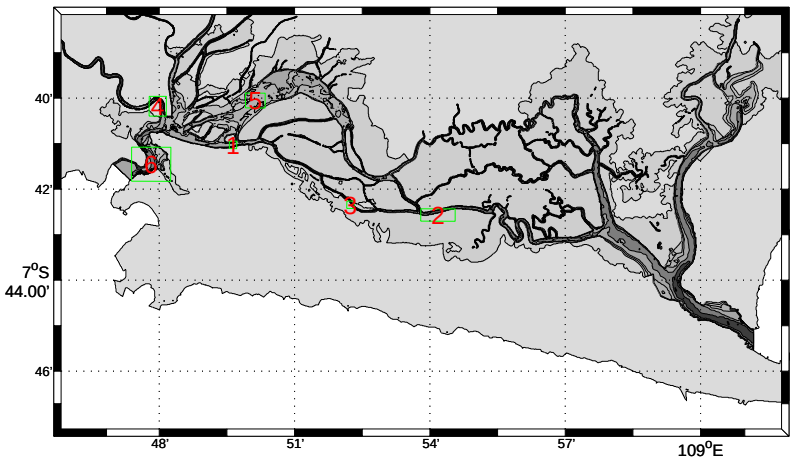

Figure 4.20: Salinity measurements: 1. Klaces 2. Water Exchange 3. Motean 4. Citanduy 5. Central Lagoon 6. Plawangan.

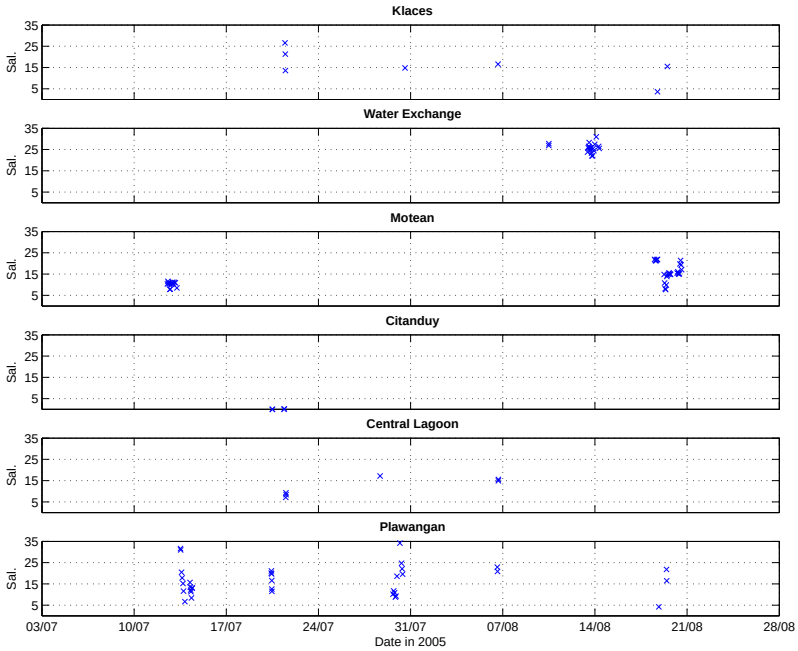

Figure 4.21: Salinity measurements August - September 2005.

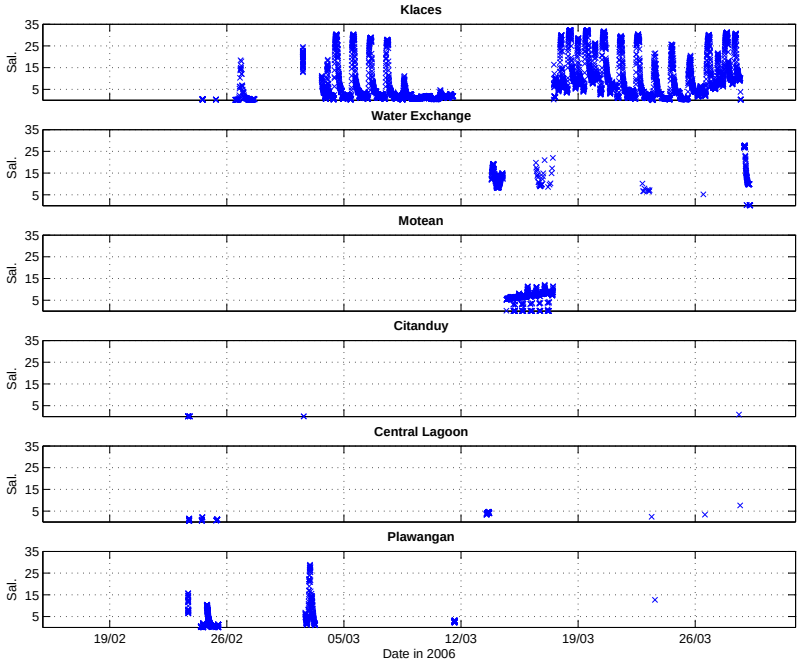

Figure 4.22: Salinity measurements February - March 2006.

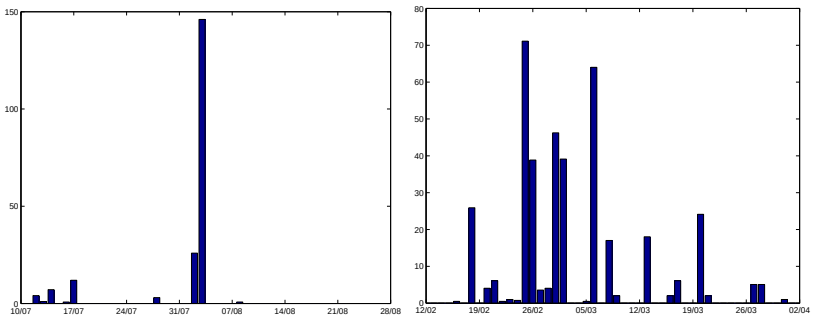

(a) 2005 (b) 2006

Figure 4.23: Daily precipitation [mm/day] in Cilacap.

4.7. Freshwater input and wind effects

4.7.1. Precipitation

The precipitation data was taken from the Utah State University Climate Center and is a Global Surface Summary of Day (GSOD) of the Cilacap weather station. This data set has daily data of temperature and precipitation.

With an drainage area of 130 km^2 and an average precipitation of 4.7 mm/day during the 2005 field trip and 8.1 mm/day during the 2006 field trip the freshwater input due to precipitation ranges between zero and 225 m^3/s. Figure 4.23 shows the daily precipitation during the two field trips.

4.7.2. Rivers

The salinity of the lagoon is determined by the ocean salt water and the freshwater input (precipitation and river input). The biggest single freshwater inflow is the Citanduy River with an annual average of approx. 150 m^3/s. There are numerous smaller rivers with an unknown discharge. To get an idea of their order of magnitude the catchment areas are calculated by processing the freely available SRTM (http://www2.jpl.nasa.gov/srtm, DEM with an horizontal resolution of (90x90)m) digital elevation map with GRASS.

River	drainage area A^d	quotient $Q^d = A^d/A^d_{Citanduy}$
Citanduy	3520 km^2	1
Kayu Mati	32 km^2	0.0091
Cibeureum	318 km^2	0.0904
Cikando	292 km^2	0.0832
Donan	88 km^2	0.025
Mainland	122 km^2	0.0347
Nusa Kambangan	52 km^2	0.0148

Table 4.2: Drainage area of rivers entering Segara Anakan.

Table 4.2 shows the drainage area of all rivers entering the lagoon and figure

4.24 the rivers and their catchment area of south-central Java. Figure 4.25 shows a detailed view of the Segara Anakan surroundings. Note the blue rivers of the bathymetry derived from satellite images and the green rivers calculated from the elevation map data. The paths of the rivers do not correlate exactly. This is due to the vertical resolution of the SRTM data. It has an accuracy of 16 meter absolute and 10 meter relative. The hinterland of Segara Anakan is quite flat with an light positive gradient towards north. The flat area is scanned with an error of 10 meter and the river paths are erroneous here. Nevertheless the calculated rivers could be identified and are listed in Figure 4.25, the orange and red areas are areas which do not belong to big rivers. They discharge directly through small streams into the lagoon and are named Nusa Kambangan for the catchment area on the Nusa Kambangan island and mainland for the catchment area on the mainland.

Despite the Citanduy there is no further discharge information available. Precipitation of the catchment areas may be available and a hydrological model could be applied but this not the cope of this work. As a work around the most simple assumption of the discharge behaviour was made. All smaller rivers behave like the Citanduy but with a discharge proportional to their catchment area. If the discharge of the Citanduy is $D_{Citanduy}$ the discharge of the smaller rivers is $D_{Citanduy} \cdot Q^d$ (Q^d is listed in table 5.1 and is the ratio of the actual river catchment area to the Citanduy catchment area). During the rainy season the Citanduy discharge is around 300 m^3/s. The total sum of all rivers is therefore 364 m^3/s. During dry season the Citanduy discharge is 100 m^3/s, which is 121 m^3/s for all rivers. This shows the importance of the Citanduy-river with approximately 80% of the rivers freshwater input.

4.7.3. Wind

The influence of wind to the hydrodynamics is due to the drag force and the resulting sea level gradient. This section analyses whether the drag force of the local wind has an significant effect on the sea level in Segara Anakan.

The one-dimensional Reynolds-averaged Navier-Stokes equation with the Boussinesq assumption, wind forcing and no diffusion is:

$$\frac{Du}{Dt} = -\frac{1}{\rho_0}\frac{\partial p}{\partial x} + \frac{1}{\rho_0}\frac{\partial \tau_x}{\partial z}. \tag{4.1}$$

The hydrostatic equilibrium with constant density ρ_0 is formulated as:

$$-g\rho_0 = -\frac{\partial p}{\partial z},$$

integrating in z direction:

$$g\rho_0(\zeta - z) = -p(\zeta) + p(z).$$

deriving in x direction:

$$g\rho_0\frac{\partial \zeta}{\partial x} = -\frac{\partial p(\zeta)}{\partial x} + \frac{\partial p(z)}{\partial x}.$$

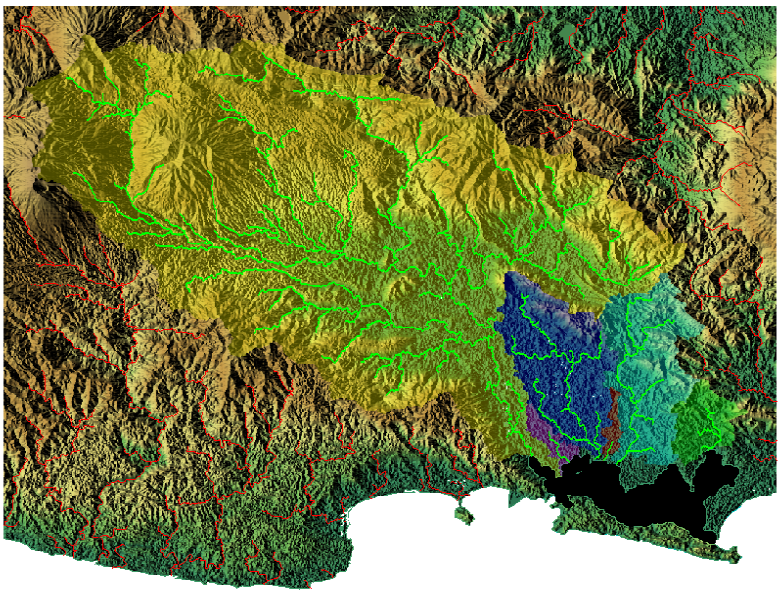

Figure 4.24: Rivers and their catchment areas of South-Central Java. The green rivers enter Segara Anakan lagoon. The biggest is the Citanduy (catchment area in light yellow), Cibeureum (dark blue), Cikando (light blue), Donan (green), Kayu Mati (violet).

The first term on the right hand side is the atmospheric pressure gradient and is in our case zero. Therefore the equation reduces to

$$g\rho_0 \frac{\partial \zeta}{\partial x} = \frac{\partial p}{\partial x}. \tag{4.2}$$

With the hydrostatic assumption and splitting the depth h into mean water level h_0 and sea level elevation ζ equation 4.1 becomes

$$\frac{Du}{Dt} = -\frac{g\rho_0}{\rho_0}\frac{\partial \zeta}{\partial x} + \frac{1}{\rho_0}\frac{\partial \tau_x}{\partial z}. \tag{4.3}$$

The linearized equation is

$$0 = -g\frac{\partial \zeta}{\partial x} + \frac{1}{\rho_0}\frac{\partial \tau_x}{\partial z}.$$

integrated over the whole water column:

$$0 = -gh\frac{\partial \zeta}{\partial x} + \frac{1}{\rho_0}(\tau_s - \tau_b).$$

With τ_b the shear Reynolds stress at the bottom and τ_s the shear Reynolds stress on the surface. Setting $\tau_b = 0$ a balance between the sea level gradient and wind drag force emerge (*Monismith* [1986])

$$\frac{\partial \zeta}{\partial x} = \frac{\tau_s}{gh\rho_0}. \tag{4.4}$$

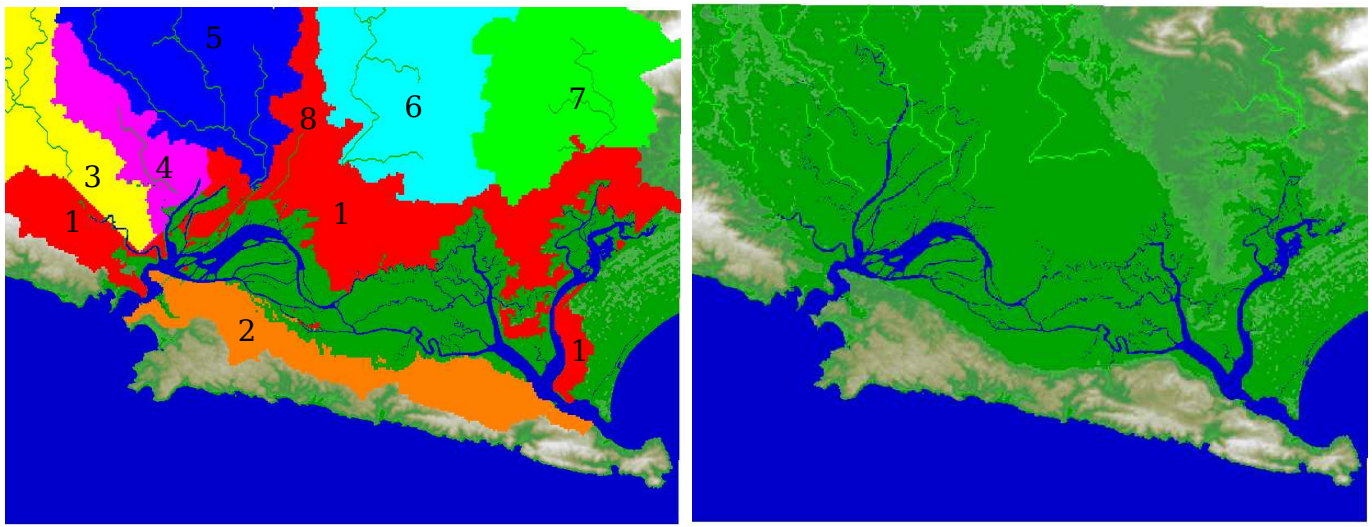

Figure 4.25: left panel: Rivers and catchment areas (1:mainland; 2:Nusa Kambangan; 3:Citanduy; 4:Kayu Mati; 5:Cibeureum; 6:Cikando; 7:Donan; 8:unknown. Right panel: The river paths in the flat hinterland of Segara Anakan are unprecise due to the SRTM measurement error of 16 meter.

The simple relation between surface stress and wind speed (*Wang* [1995]):

$$\tau_s = \rho_{air}\, C_{drag}\, V^2$$

gives a relation of the sea surface deflection and the wind speed. Where V is the wind speed in ms^{-1}, ρ_{air} the density of air and C_{drag} the drag force coefficient.

Calculating the sea level difference with the scales of Segara Anakan: Average depth 5 m, maximum wind fetch 30 km, $\rho_{air} = 1.225$ kgm^{-3}, $\rho_{water} = 1000$ kgm^{-3}, $C_{drag} = 0.0009$ (*Blake* [1991]) and the average wind $V \approx 2$ ms^{-1}:

$$\Delta\zeta = -\frac{\tau}{gh\rho_0}\Delta x = -0.0027\ m.$$

This is a sea level difference of 2.7 mm. A current forced by 2.7 mm sea level difference on 30 km is negligible and therefore wind forcing is not further considered.

5. Model setup

The model setup can be done gradually from very simple to more and more realistic setups. It always begins with a bathymetry. Followed by the open boundaries to the Indian Ocean with a prescription of the sea levels and salinities at the eastern and western outlets. Freshwater fluxes due to rivers and rain are included afterwards. Further adjustments are the changes of the water type and the mangrove areas bottom roughness. In the end a water age tracer is included to quantify the residence time of water inside the lagoon.

For the model setup of the Segara Anakan lagoon GETM version 1.5.1 compiled with the IFORT 9.1(20060816) compiler is used. Different modules of the source code were changed and added. The details of the changes are listed in appendix C.

5.1. Bathymetry

The bathymetry data is gridded with a resolution of 20 meters. This is a grid of 1500x870 points. On a 1.80Ghz Xeon workstation a setup with a horizontal resolution of 80 m and 10 equidistant depth layers has been proven to calculate in a acceptable time. This is a grid with 374x217 points. The downscaling was done by taking the mean of 4x4 clusters. If land points are inside a cluster they are sorted out and the average of the remaining points is used. The lagoon has been cut off directly at the outlets. The barotropic time step Δt_m has been set to 3 seconds. This is only slightly below the CFL constraint with 3.04 seconds. The barocline to barotropic split factor n is set to $n = 5$.

5.2. Boundary conditions, tide

The sea surface elevation at the open boundaries is prescribed by the tidal constituents of Cilacap derived from *Egbert and Erofeeva* [2002]. A 4 minute time difference between the two outlets was neglected, they would result in a maximum sea level difference of 3 cm. The salinity is set to 35 ppt at the outlets. The initial conditions are a salinity of 35 ppt over the entire model area.

5.3. Rivers

The main rivers are included with a direct correlation to the Citanduy discharge (see section 4.7.2). 20 rivers are additionally included to simulate the rainfall in the adjacent areas (areas Mainland and Nusa Kambangan in Figure 4.25a). Their discharge is the drainage area multiplied with the daily precipitation

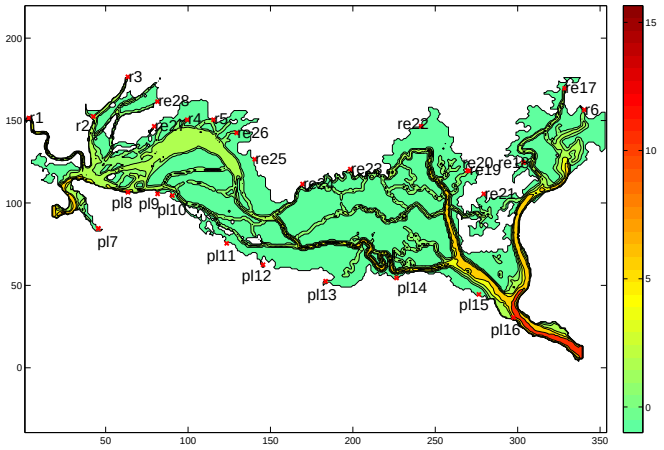

Figure 5.1: Rivers entering the Segara Anakan lagoon model setup (see table 5.1 for discharge details).

plus the discharge of the Citanduy multiplied with the catchment area quotient (table 4.2).

River	GETM Code	discharge 2005	discharge 2006
Citanduy	r1	100 m^3/s	300 m^3/s
Kayu Mati	r2	2 m^3/s	5.5 m^3/s
Cibeureum	r3	18 m^3/s	54.3 m^3/s
unknown	r4	1 m^3/s	3 m^3/s
Cikando	r5	1.7 m^3/s	5 m^3/s
Donan	r6	5 m^3/s	15 m^3/s
Mainland	r17-r28	0.86 m^3/s	1.76 m^3/s
Nusa Kambangan	pl7-pl16	0.44 m^3/s	0.89 m^3/s
Precipitation	prec	0.0049 m^3/s	0.0076 m^3/s

Table 5.1: Rivers entering the model setup of Segara Anakan, the discharges for Mainland and Nusa Kambangan are the discharges of the single rivers and mean values as the precipitation is included into the discharge calculation.

5.4. Wind

Chapter 4.7.3 shows, that wind will not have an influence on the hydrodynamics, hence wind forcing has been neglected.

5.5. Precipitation

The precipitation is taken from the daily values (see figure 4.23) and is treated as a river entering the uppermost layer of every grid box.

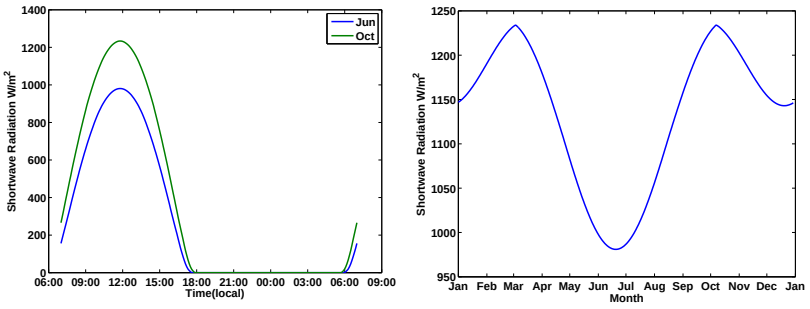

(a) (b)

Figure 5.2: Daily progress of radiation (left) and maximum radiation during the year in Segara Anakan (right) calculated with the shortwave radiation routine implemented in GETM.

5.6. Radiation

A water column is heated by the incoming radiation and looses energy due to the surface heat flux. GETM computes the daily radiation as a function of the day of the year, the time, latitude, longitude and the total cloud cover. A daily progress of the calculated radiation as well as the maximum radiation during a day in Segara Anakan is shown in figure 5.2.

The parametrisation of the temperature absorption was according to *Paulson and Simpson* [1977] (see chapter 3.5.3 equation 3.18)

$$I(z) = I_0 \left(a e^{-\eta_1 z} + (1-a) e^{-\eta_2 z} \right). \tag{5.1}$$

The parameters a, η_1 and η_2, depend on the turbidity of the water. *Paulson and Simpson* [1977] quantified the parameters for six water types defined in *Jerlov* [1968]. The standard setup is sea water Type I with $a = 0.58$, $\eta_1 = 0.35$ and $\eta_2 = 23.0$. The concentration of suspended matter in Segara Anakan is high enough, to choose the water type with the highest turbidity (Type III). The parameters are $a = 0.78$, $\eta_1 = 1.4$ and $\eta_2 = 7.9$. Figure 5.3 shows the relative absorption of the open sea water Type I and the water Type III.

The meteorological information during the field trips are limited to the air temperature and precipitation. There is no information of the total cloud cover. Thus it is defined that the total cloud cover is always 0 over the water areas and always 1 over the mangrove areas. This shall represent the mangrove canopy and helps to prevent the mangrove areas from overheating. The cloud cover of 0 is a crude assumption. A better assumption could be a relation of the cloud cover and the precipitation. This was not done in this study and is postponed to further studies. The air-sea heat flux is set to zero.

5.7. Bottom roughness

The resistance is calculated with respect to formula 3.22. It depends on the water level and the bottom roughness z_0^{const}. Mangrove areas have a much

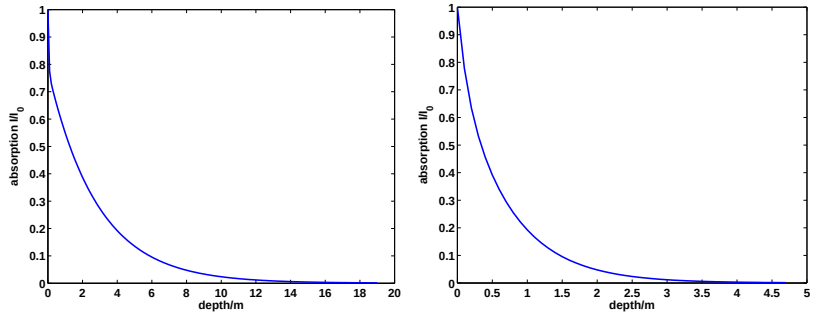

(a) Type I (b) Type III

Figure 5.3: Relative absorption of light in the water column. a: open sea water b: water with high turbidity.

bigger resistance than channels and open water. A common bottom roughness for open water is $z_0^{const} = 0.001$ meter and is used in the Segara Anakan setup. The mangroves are defined with a bottom roughness of $z_0^{const} = 0.005$ meter. As the used GETM version does not has the ability of a variable bottom roughness a hard coded routine is implemented to set the bottom roughness z_0^{const} of the mangrove swamps and the open water.

5.8. Seawater age

The seawater age introduced in chapter 3.4 is a passive tracer which can be directly implemented in an Eulerian model. The seawater age equation is of the following form:

$$\begin{aligned} &\partial_t T_{age} + \partial_x(uT_{age}) + \partial_y(vT_{age}) + \partial_z(wT_{age}) - \partial_z(\nu_t' \partial_z T_{age}) \\ &\quad = 1. \end{aligned} \tag{5.2}$$

The zero age regions are defined the way that water entering or leaving the lagoon through the open boundaries has the age of zero. Hence all the water entering through the outlets, rivers or precipitation is “zero”age water and becomes older in the lagoon.

6. Results and discussion

6.1. Introduction

The GETM model computes amongst others water velocities and tracer distributions. To test if the model results are realistic we compare them with in situ measurements on well distributed positions and times. If the differences are in an acceptable range, we assume that the model results are also correct within a similar range in not monitored areas. This feature makes computer models so valuable. But the quality of the model results depends among other things on the boundary conditions: Mainly tidal forcing, freshwater discharge and precipitation. As mentioned in chapter 4.7.2 discharge was measured for the Citanduy but is unknown for all other rivers entering Segara Anakan. It is defined as a relation to the Citanduy discharge and the catchment area of the rivers. Tidal forcing at the outlets is prescribed with tidal constituents from *Egbert and Erofeeva* [2002]. If the boundary conditions are justifiable and the model calculations agree with the in situ measurements in an acceptable range is topic of the model verification.

Chapter 6.4.3 shows a consistency between the tidal forcing and measured sea levels in Seleko. The validation of the water fluxes is primarily done via the ADCP discharge measurements and can be seen in chapter 6.3.2. Chapter 6.5 compares the long time salinity and sea level measurements in Klaces. In Chapter 6.6 the time series of salinity and sea level measurements in the Motean village and salinity of the water exchange channel are validated.

After having verified the model, spatial averages of salinity are computed and changes between the monsoon season are discussed. The seawater age of the 2006 dry season is discussed in chapter 6.9 as well as changes between the seasons. An outlook is given in chapter 7 with ideas for future studies of this kind in the Segara Anakan lagoon.

6.2. Steady state of the model and mangrove area experiments

6.2.1. Steady state of the model

Initial salinity is 35 throughout the whole lagoon. After about 14 tidal periods, the influence of this initial salinity distribution has vanished, see figure 6.22. This is consistent with the calculated flushing time at spring time, see section 6.9.

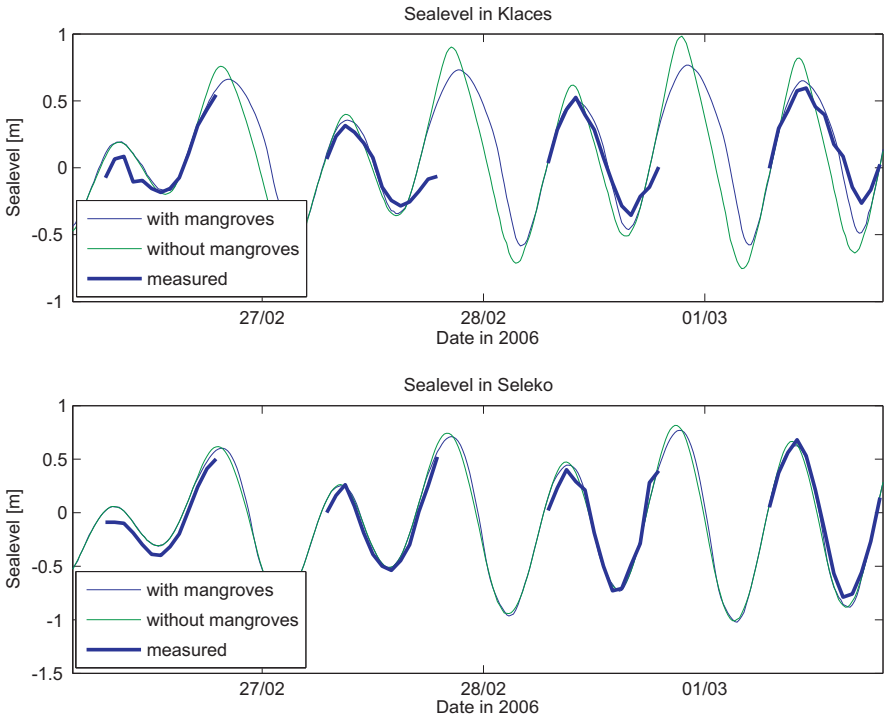

Figure 6.1: GETM sea level computations with and without mangroves compared with the measured sea level; upper panel: Klaces sea level; lower panel: Seleko sea level; measured (thick blue), with mangroves (blue), without mangroves (green).

6.2.2. Model results of Segara Anakan without mangroves

A lot of time has been spent to adapt the model to the mangrove areas and to create a bathymetry of them. Are the mangrove areas hydrodynamically important? To check this, a simulation without mangroves was done for the February 2006 period. The resulting sea levels are compared with a simulation including mangroves (Figure 6.1). The Seleko sea level is not affected too much by the removed mangroves. This agrees with the results made in chapter 6.4.3: The Seleko tide is a little modulated Indian Oceans tide. The sea level in the Klaces village gives a different picture, the tidal range is reduced by the mangroves. The tidal range of the in situ measurements is obviously even lower. Does this mean that the mangrove water volume is underestimated here? This would be worth of further investigations. Mangroves produce a delay in the draining off and the sea level becomes asymmetric with a longer draining off. This is not a mangrove specific behaviour but of mud flats in general. This asymmetry can be seen in figure 6.1: The upper panel shows a delayed low tide in Seleko (blue line). The last printed in situ measurement (thick blue line) of the upper panel in figure 6.1 shows an even longer delay. The question of an underestimated mangrove water volume arises again.

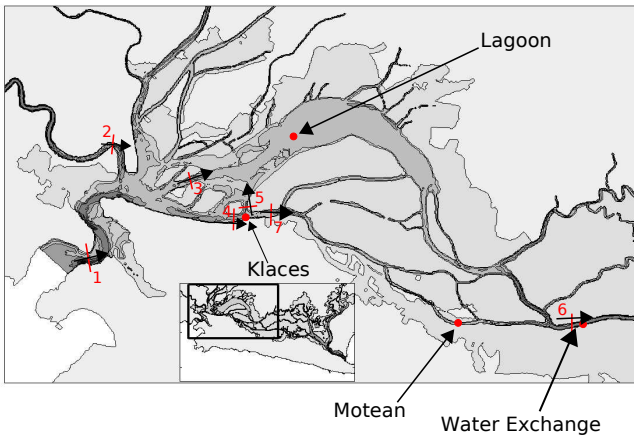

Figure 6.2: Salinity measurements (red points) and discharge transects for comparisons of measured and calculated fluxes 1: Plawangan; 2: Citanduy; 3: Lagoon channel 2 ; 4: Klaces channel ; 5: Klaces channel lagoon; 6: Water Exchange; 7: Klaces channel east. The small arrows perpendicular to the transects indicate the direction of a positive discharge.

6.3. Discharge data

Various discharge transects have been measured during the field trips (chapter 4.5). The measurements are the main data set to verify the model results. The figures of section 6.3.2 compare the measured (blue) and the computed discharges (red). All figures have an upper panel giving an overview of all measured volume transports and the order of magnitude of the fluxes. The lower panels are detailed plots of the available measurements and the corresponding model computations. The measured discharges are computed as it is described in section 3.2. For every ADCP transect the water volume flux and the error is calculated. The blue bars are the discharges plotted together with the error. The bars are centered around the calculated discharge and have the length of the estimated error. Section 6.3.1 discusses the discharge measurements of the Citanduy and a possible relation to the precipitation and monsoon seasons. The tidal time scale discharge ranges in the Citanduy and the absence of these ranges in the model results are also discussed in section 6.3.1.

6.3.1. Discussion of the Citanduy discharge

Beside the ocean tide the Citanduy river has the strongest influence on the hydrodynamics of the western and central part of Segara Anakan. Therefore many discharge transects were taken in this area. The volume transport of the Citanduy during a tidal period depends on the freshwater discharge and the sea level and can have a range of up to 250 m^3/s during one tidal period (figure 6.3). The freshwater discharge is between 50 and 350 m^3/s in dry respectively rainy season. The average discharge varied during the 2006 field trip between 70-300

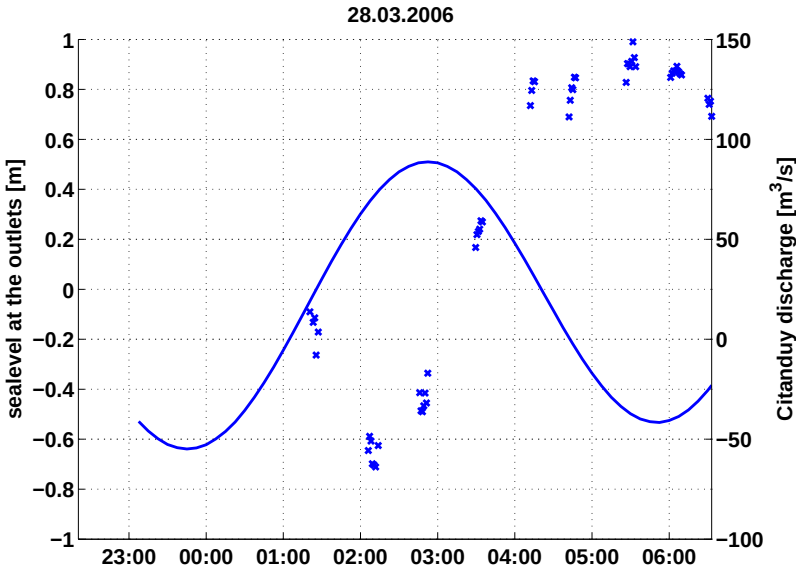

Figure 6.3: Citanduy discharge variations in tidal time scales measured on Mar. 28.,2006 at location 2 (figure 6.2). Blue line: sea level at the outlets; blue crosses: Citanduy discharge.

m^3/s with a decreasing trend towards the end of March (figure 6.4). The decrease relates to the decreasing precipitation in Cilacap. But if the precipitation in Cilacap is a valid indication for the precipitation of the drainage area has to be studied in more detail. The discharge response to a changing precipitation is probably within the time scale of days to weeks. The decreasing trend is most likely due to the change between the seasons which seems to happen in the end of March. Further information about the precipitation in the drainage area could give a closer relation between discharge and precipitation. The modelled discharge compared with the measurements is plotted in figure 6.5. The predefined discharge fluctuates around the mean of 300 m^3/s. The overall discharge is overestimated and the range in tidal scales is underestimated. This is due to the bathymetry of the river bed. It was cut off close to the estuary. The lack of the Citanduy River water volume results in a more continuous discharge. In contrast to the pulsed flow caused by the accumulation of river water during rising tide. It is unknown if the pulsed Citanduy discharge affects the salinity distribution. This will be investigated in further studies.

6.3.2. Comparison of computed and measured discharges during the field trips

The 2005 discharge data set is smaller compared with 2006 as a lot of time was spent for the bathymetry measurements. Nevertheless figures 6.6-6.8 compare the measured and computed discharge data. Figures 6.9, 6.10, 6.11, 6.12, 6.13 show the measured compared to the computed discharges of the main channels in the western part during February and March 2006. Most of the measurements

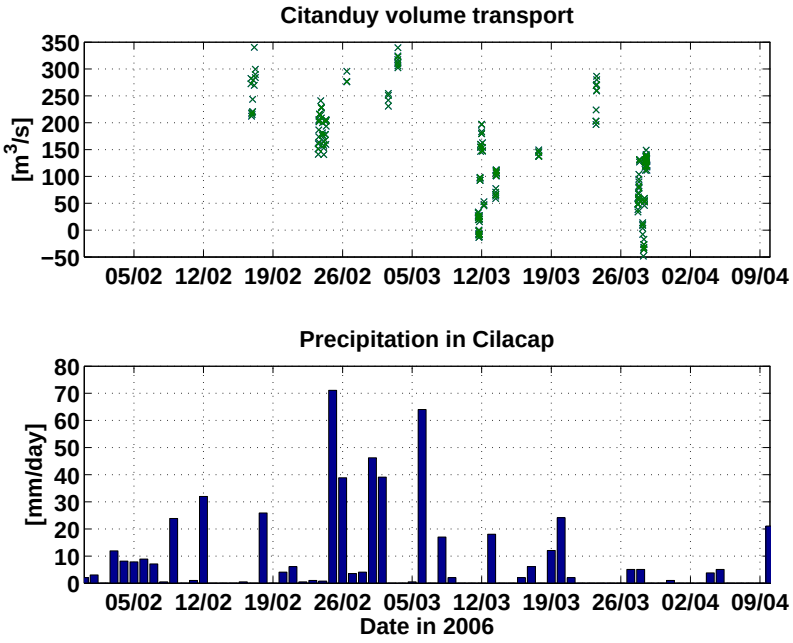

Figure 6.4: Upper panel: Citanduy discharge measurements during the 2006 field trip. Lower panel: Precipitation in Cilacap.

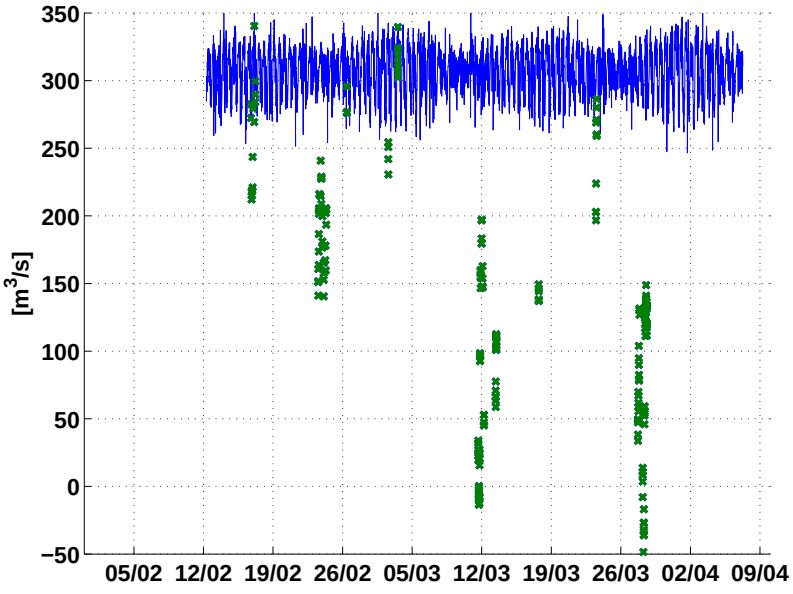

Figure 6.5: Measured (green crosses) and modelled discharge of the Citanduy. The assumption of a constant discharge during the rainy season is not correct. The modelled discharge range in tidal time scales is underestimated due to a too small river volume.

show a fair agreement with the model results. The exchange of water masses between east and west is mainly done via the water exchange channel. It seems that GETM overestimates the westerly transports (figures 6.8 and 6.12). The in situ discharge measurements are too coarse to calculate mean volume flux amplitudes of the transects. Because of the general agreements between the model results and the measurements, mean amplitudes of the main transects are calculated by using model results. Table 6.1 shows the mean volume flux amplitudes for neap time and spring time cycles. Since the fluxes of the water exchange are overestimated it is assumed that the volume flux amplitudes of this transect are also overestimated.

Location	neap tide	spring tide
western outlet (Plawangan)	654 m^3/s	1370 m^3/s
eastern outlet (Plawangan Timur)	1610 m^3/s	4400 m^3/s
Water exchange	210 m^3/s	552 m^3/s
Lagoon channel 2	158 m^3/s	362 m^3/s
Klaces channel lagoon	67 m^3/s	145 m^3/s
Klaces channel east	109 m^3/s	237 m^3/s

Table 6.1: Mean amplitudes of the volume fluxes at the main transects and the eastern outlet.

6.4. Tide

6.4.1. Tidal delay in Klaces, Seleko and Motean villages

The tidal wave needs some time to propagate from the outlets into Segara Anakan. This is represented in a delay of the recorded sea levels compared to the Indian Ocean tide. GETM should reproduce a similar delay for the same positions. The recorded sea levels of the three tide gauges in Klaces, Seleko and Motean as well as the computed sea levels are compared to the forcing tide. The average time delay between the highest daily sea level and the outlets is shown in table 6.2. Salinity in Segara Anakan is fresh to brackish. The ocean tide pumps saline water into the lagoon. Time delay of high water at the outlet and maximum salinity in Klaces is in the same order of magnitude as the sea level time delay. It is 01:47±00:42 [hh:mm] (Figure 6.15). The appearance and absence of salinity peaks is discussed in section 6.5.

6.4.2. Tidal wave propagation in Segara Anakan

The propagating tidal wave looses energy due to bottom friction and experiences a phase shift. Tidal constituents of the water body are derived from the model sea level time series. Because the forcing tide of Segara Anakan is M_2 dominated figure 6.16(a) and 6.16(b) plot the M_2 amplitude in meter and the M_2 phase in degrees. In the shallow central lagoon, the amplitude decreases to 35 cm. The narrow and shallow channels in the north have an even lower amplitude of about 20 cm. M_2 amplitudes in the eastern part with its wide and deep channels are

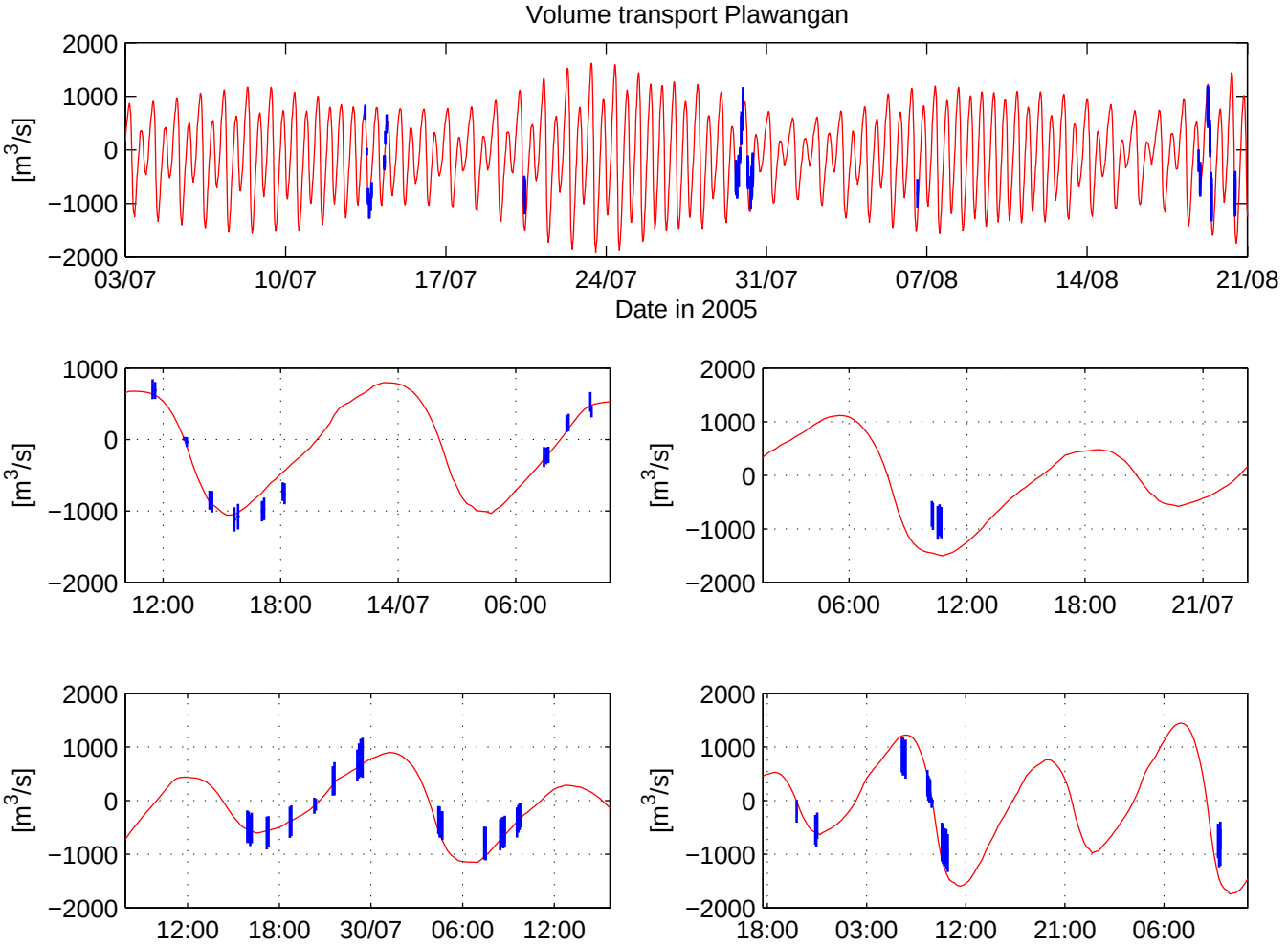

Figure 6.6: Plawangan measured (blue) and computed discharge (red).

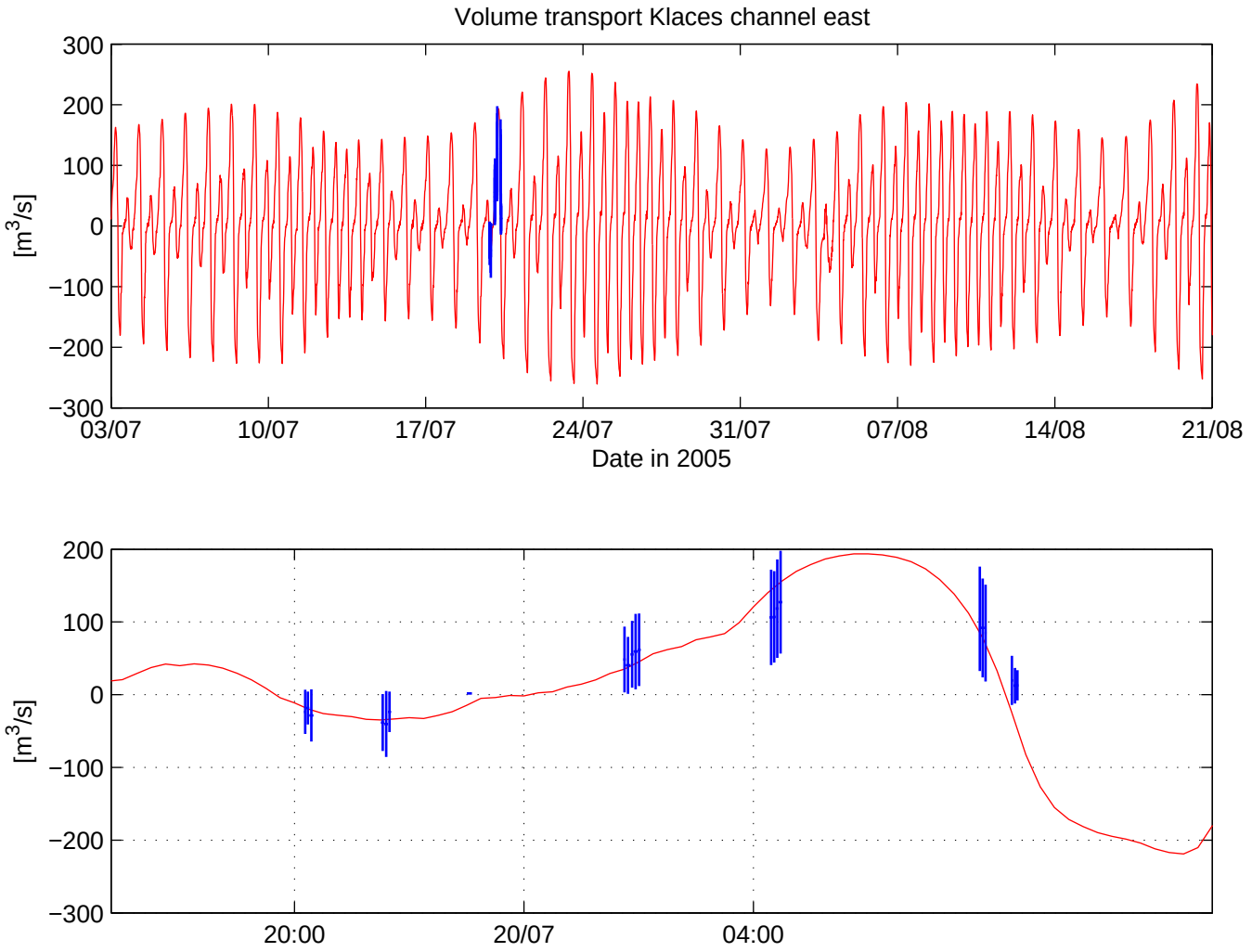

Figure 6.7: Klaces channel east measured (blue) and computed discharge (red).

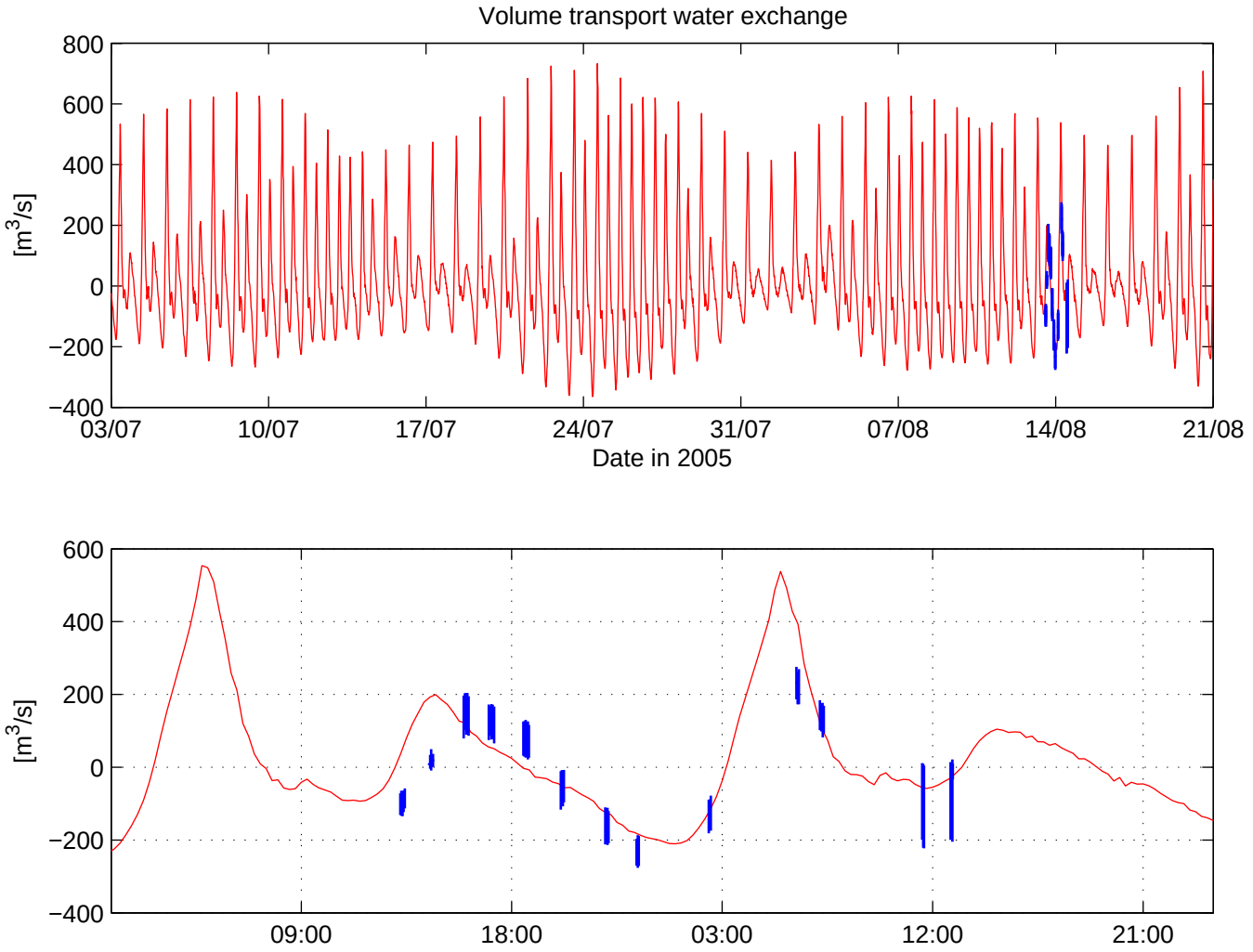

Figure 6.8: Water Exchange measured (blue) and computed discharge (red).

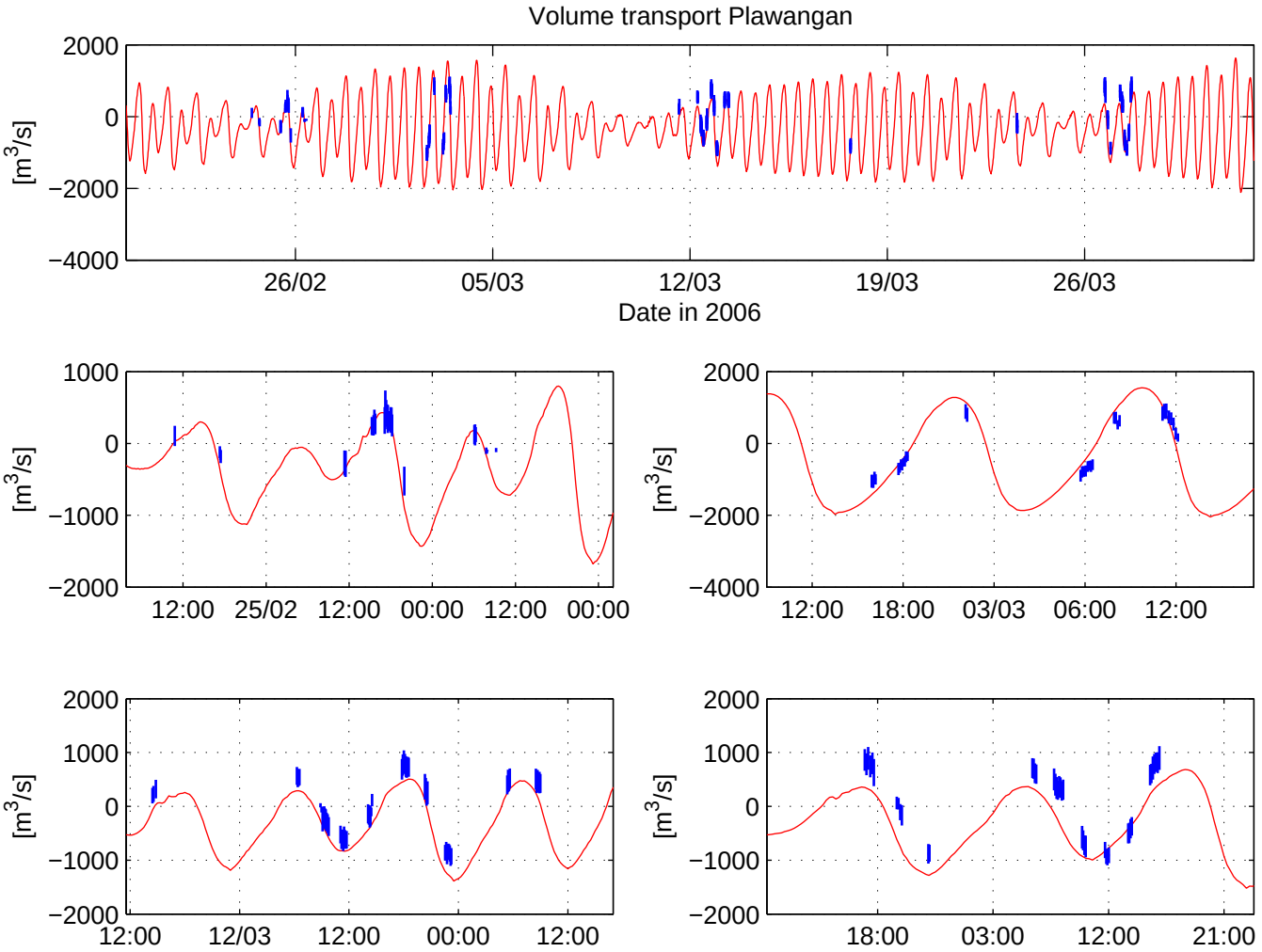

Figure 6.9: Plawangan measured (blue) and computed discharge (red).

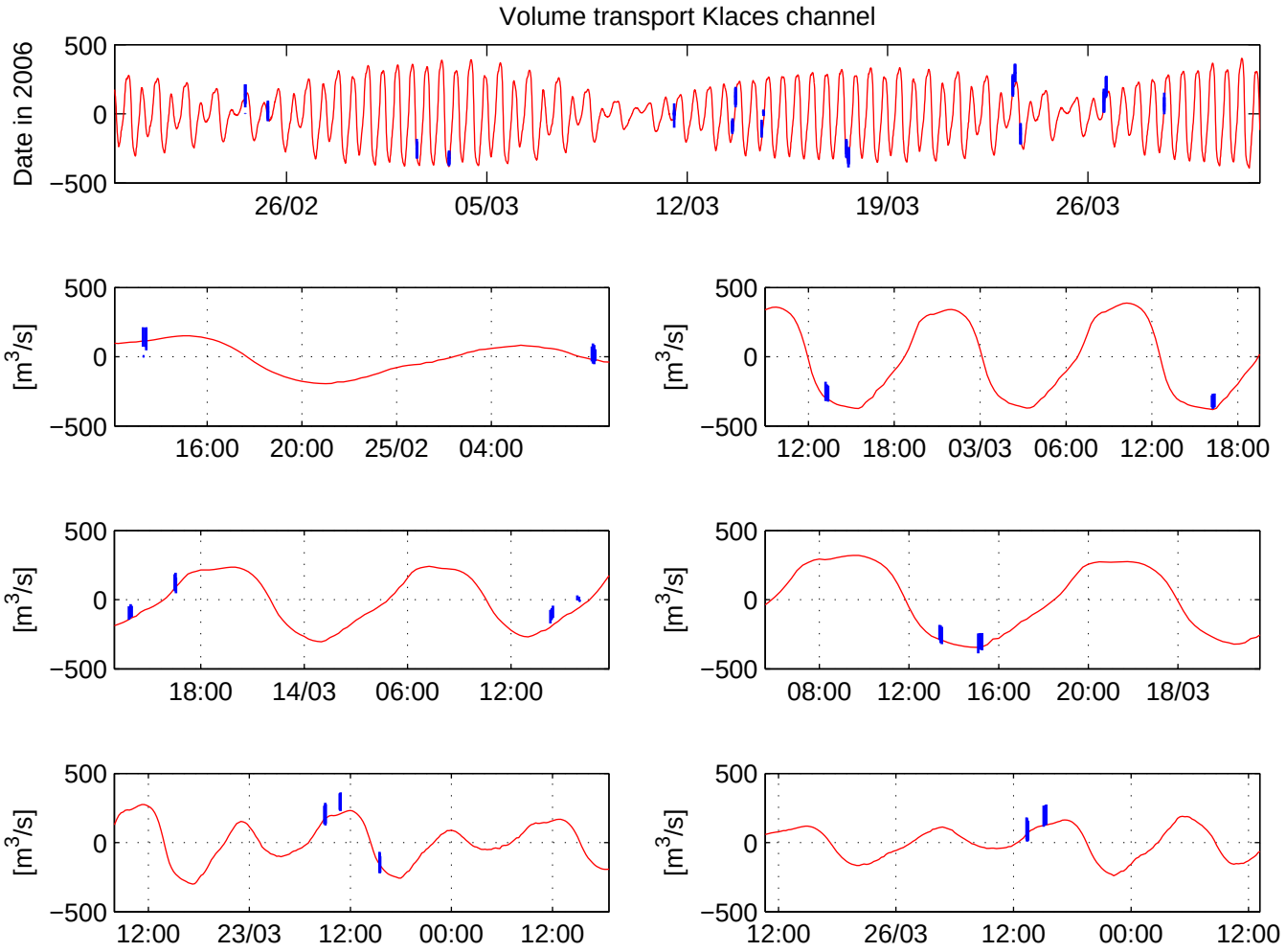

Figure 6.10: Klaces channel measured (blue) and computed discharge (red).

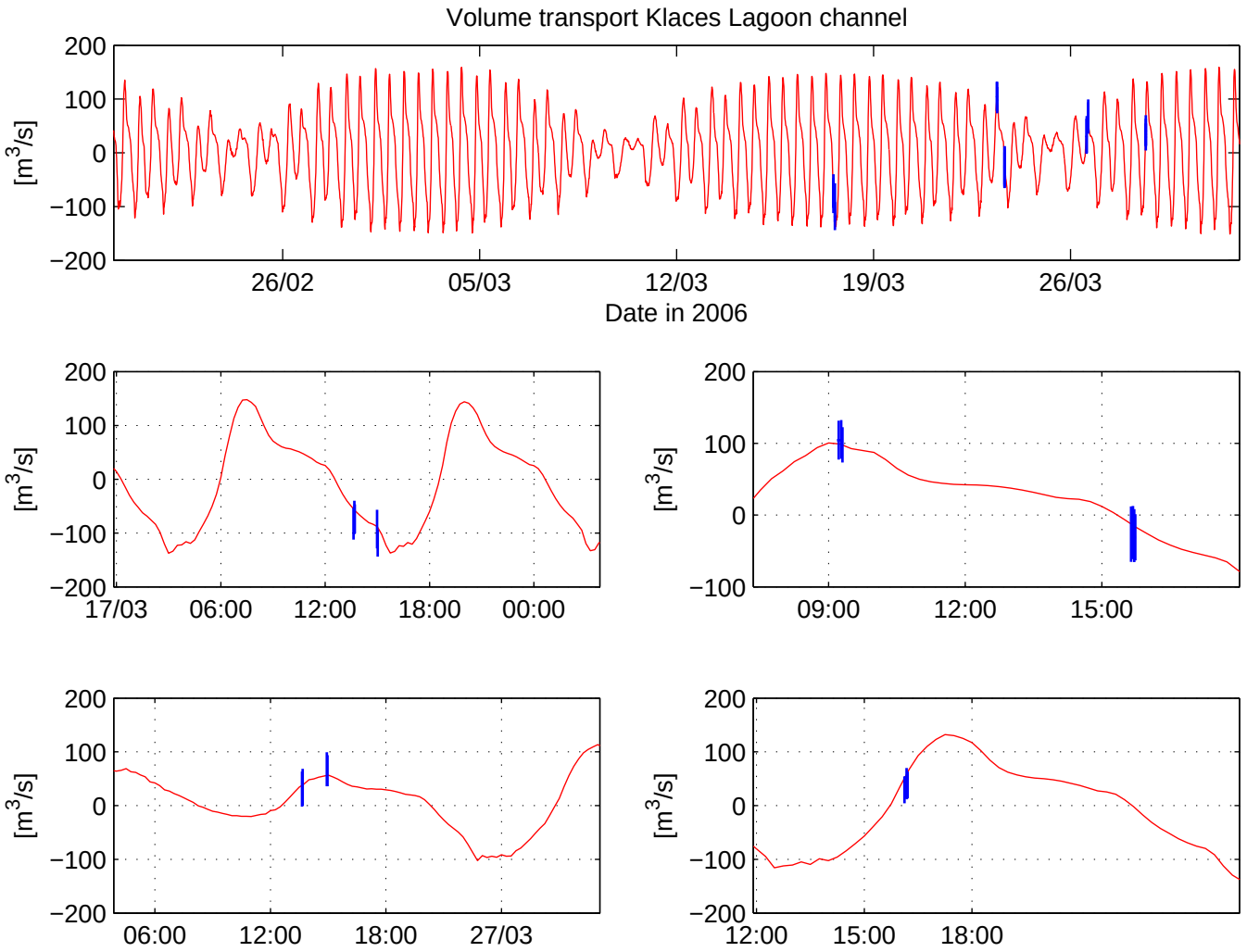

Figure 6.11: Klaces Lagoon channel measured (blue) and computed discharge (red).

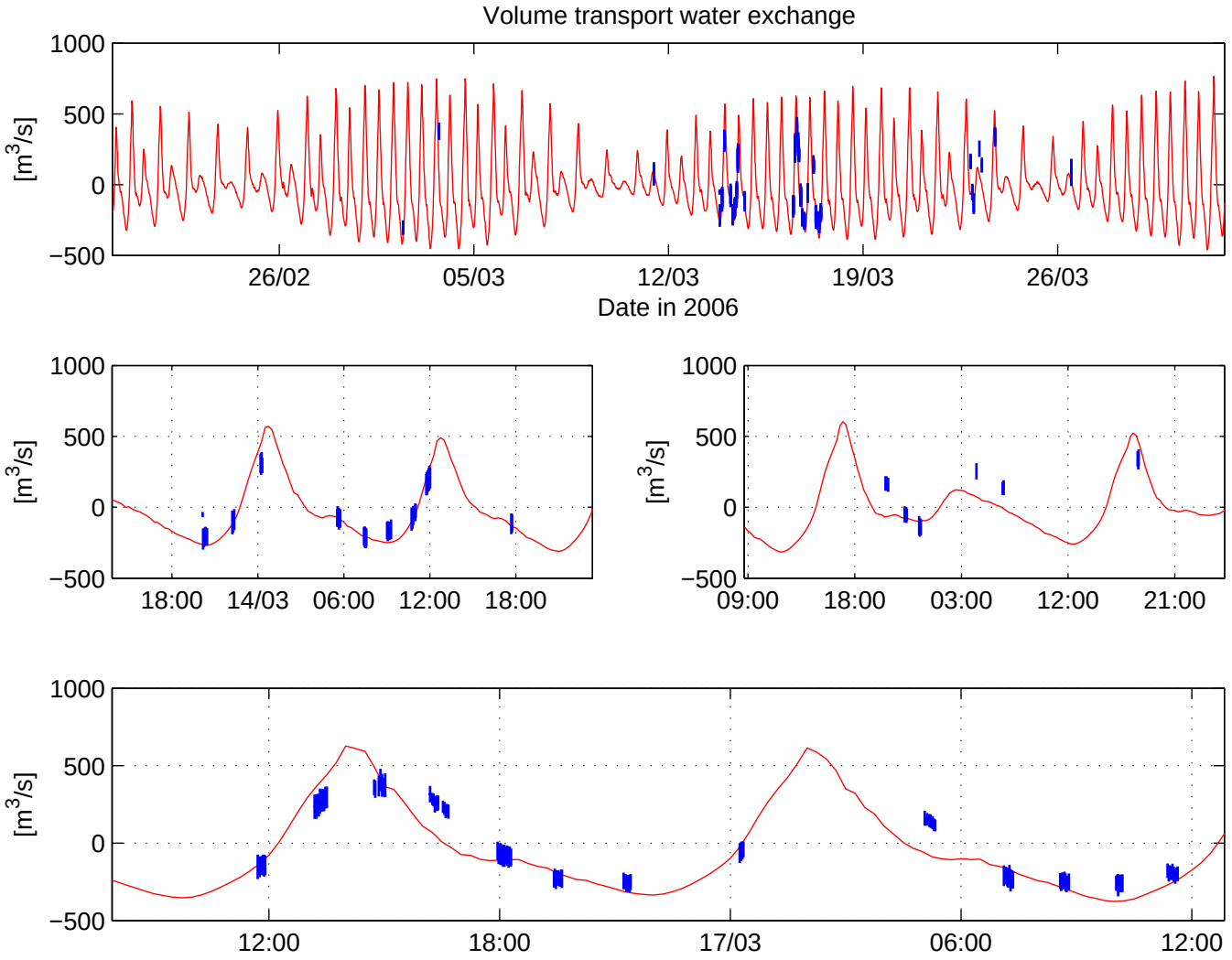

Figure 6.12: Water Exchange measured (blue) and computed discharge (red).

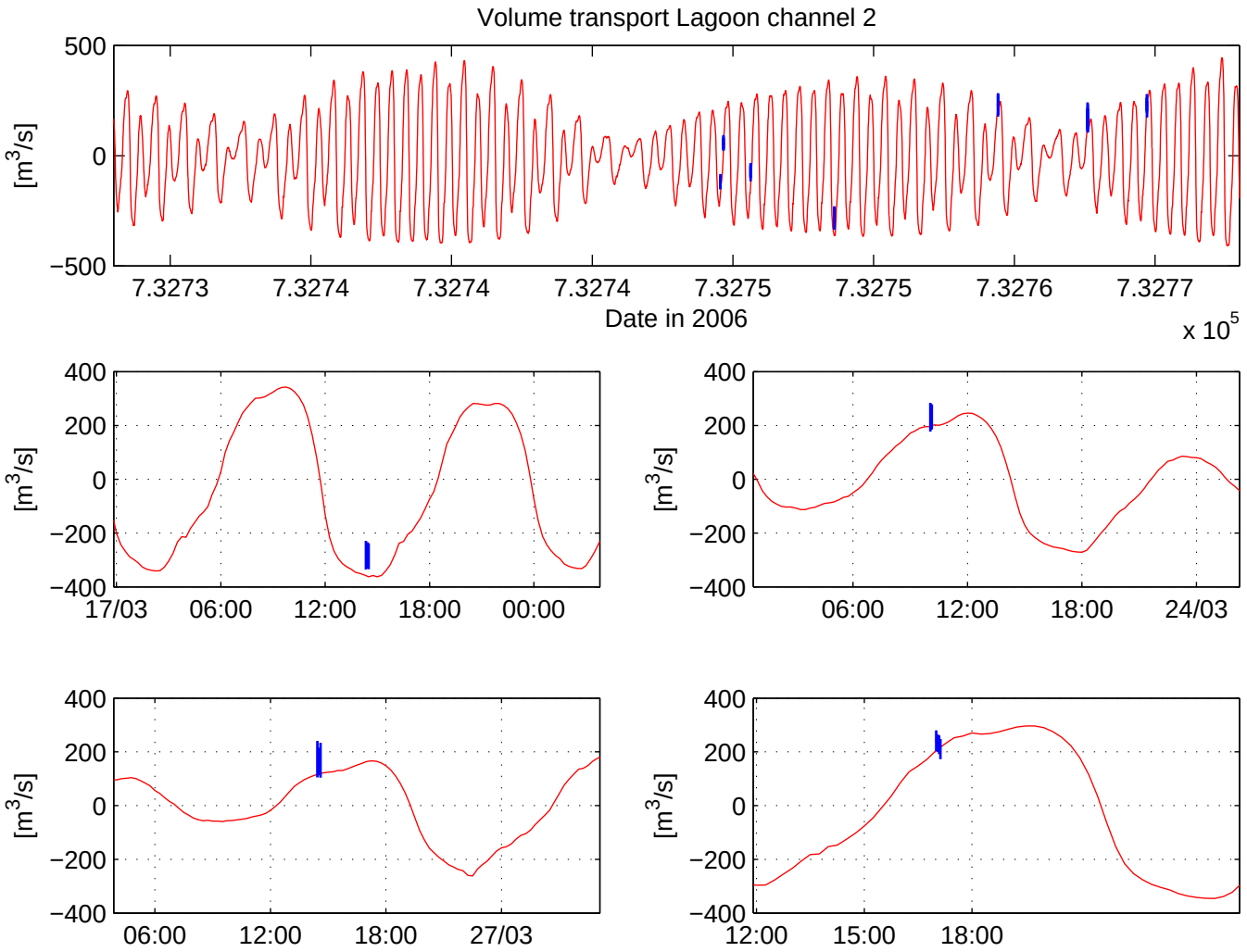

Figure 6.13: Lagoon Channel 2 measured (blue) and computed discharge (red).

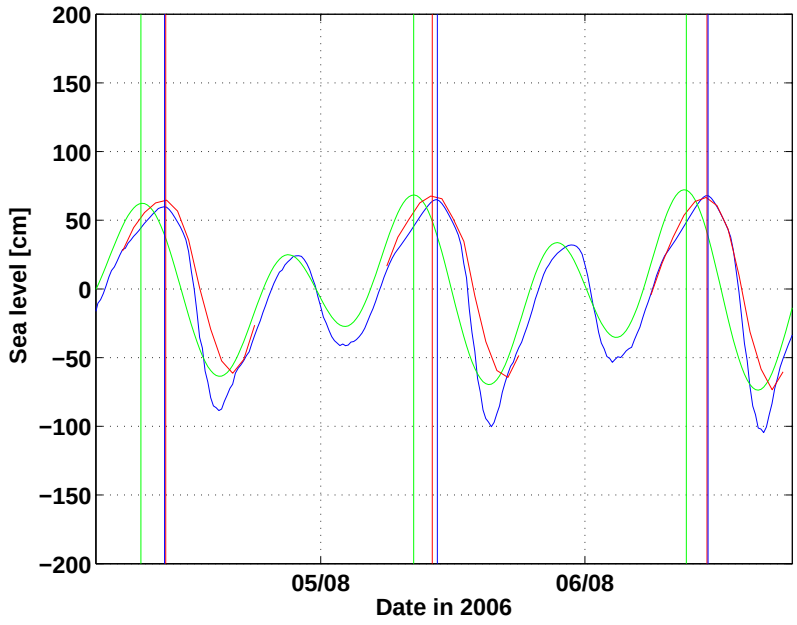

Figure 6.14: Example of the tidal delay in Motean. Green: forcing tide at the outlets; blue: sea level computed with GETM; red: measured sea level. The tidal delay of table 6.2 is an average of the time difference between the highest amplitude at the outlets (green vertical line) and the red (measured delay) respectively blue (GETM computed delay) vertical line.

Station	time delay (measured) [hh:mm]	time delay (GETM) [hh:mm]
Seleko 2005	00:18±00:24	00:22±00:15
Seleko 2006	00:24±00:27	00:31±00:09
Klaces 2006	01:11±00:30	01:10±00:14
Motean 2005	01:32±00:35	01:22±00:49

Table 6.2: Average delay of the highest daily sea level recorded at the tide gauges and the sea level at the outlets. The right column shows the delay computed with GETM. See also figure 6.14.

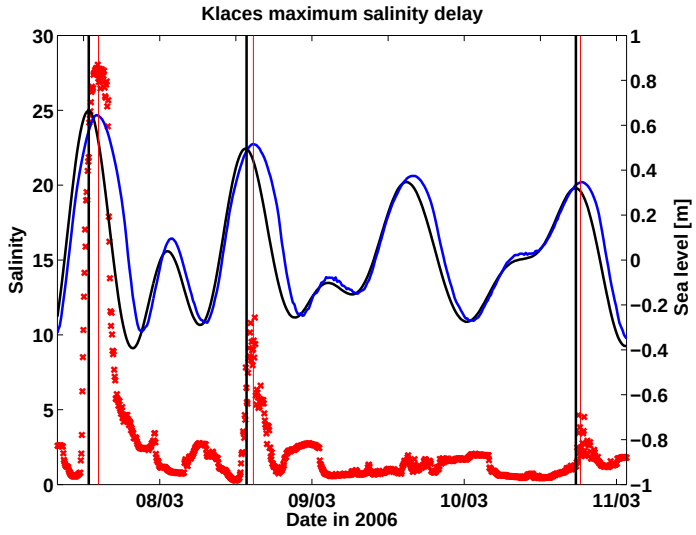

(a) neap tide

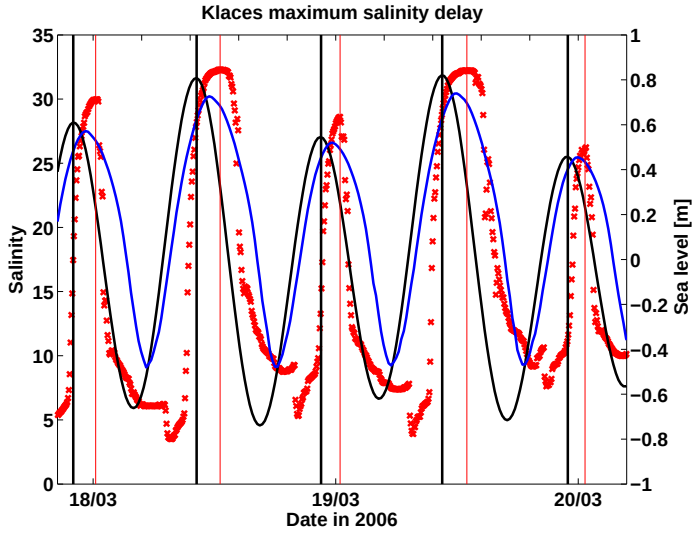

(b) spring tide

Figure 6.15: The time delay between high tide at the outlets and highest salinity in Klaces is $01:47 \pm 00:42$ [hh:mm]. Black line: sea level at the outlets; blue line: sea level in Klaces (model); vertical black lines: highest tidal level of the day, following vertical red line: highest salinity in Klaces.

not much affected. The maximum tidal delay seems to be in the northern part of the central lagoon and the channel west to Motean with approximately 110 minutes.

6.4.3. Tidal lag between the outlets and similarity of sea level at Seleko and the Indian Oceans tide

The in situ data has a big lack, the external ocean tide entering Segara Anakan was not recorded during the field trips (section 4.3). This is compensated with tidal constituents calculated for Cilacap and the western outlet. Comparison of the sea level calculated with *Egbert and Erofeeva* [2002] at the eastern outlet and the GETM computed sea level in Seleko shows a small modulation of the incoming tidal wave due to the bathymetry (figure 6.17). Also the comparison of the computed tide and measured tide in Seleko indicates a good correlation. The average of the difference between the computed tide and the measured tide is 10 cm but can reach up to 50 cm (March 16.,2006) and is during neap tide less than 5 cm. Having the manual tide gauge readings and measuring conditions in mind, the result is satisfying and authorises us to take the tidal constituents of *Egbert and Erofeeva* [2002] as the forcing.

White et al. [1989] report a phase lag of 1-2 hours between the western and eastern outlets. This is in contrast to the computed phase lag of 3 minutes between west and east. Without in situ measurements of the ocean tide at the outlets these disagreements cannot be resolved. But the above mentioned similarity of the measured tide in Seleko and the computed tide level indicate the correct prediction of *Egbert and Erofeeva* [2002]. Furthermore the timings of the measured sea level in Klaces in the western part correlate with the computed timings of the model (figure 6.25) computed with synchronous sea-levels at the outlets. This strengthens the assumption of a tidal lag in the range of minutes rather than of hours.

6.5. Precipitation, Citanduy discharge and salinity in Klaces

The Salinity in Klaces is dominated by the saline Indian Oceans water plume and the Citanduy freshwater. Tide and corresponding maximum salinity delay due to ocean water is discussed in section 6.4.1. Figure 6.20 plots long time salinity measurements in Klaces and the ocean sea level. It shows two different salinity trends in neap tide situations: Between the Mar. 9.,2006 and Mar. 11.,2006 the water is brackish to fresh. But one neap tide cycle later, from Mar. 24.,2006 until Mar. 27.,2006 significant salinity peaks were recorded. A possible reason could be the Citanduy discharge. The discharge measurements on Mar. 4.,2006 show an discharge of about 200-300 m^3/s decreasing to 100 m^3/s on Mar. 12. to 13.,2006. The missing salinity peaks between the Mar. 9 to 11.,2006 are accompanied with a Citanduy discharge of about 200 m^3/s. In contrast the discharge of 70 m^3/s between the Mar. 28.,2006 and the Mar. 29.,2006 corresponds with the salinity peaks at neap tide between Mar. 24.

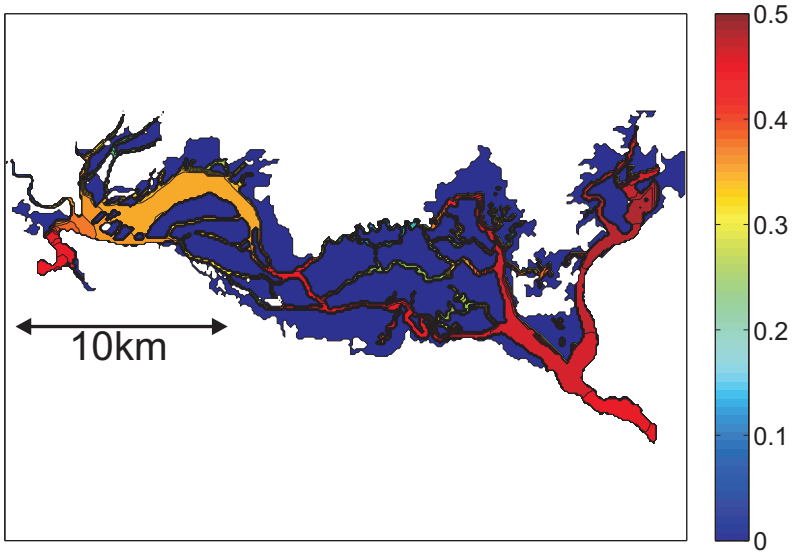

(a) M_2 amplitude

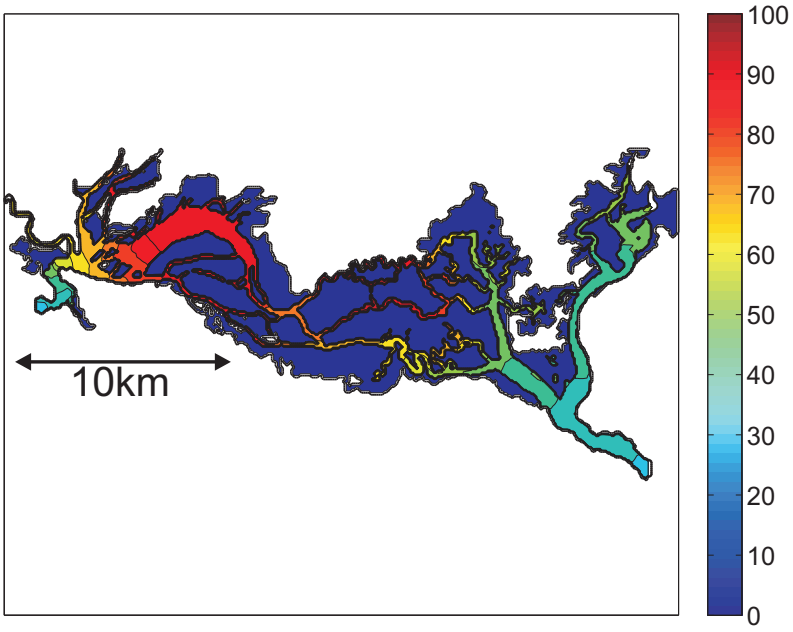

(b) M_2 phase

Figure 6.16: Upper panel: M_2 amplitude in meter computed with GETM sea-levels. Lower panel: M_2 phase in degrees. Computed with GETM sea-levels; isolines are in 5 degrees distance. This is approx. 10 minutes time difference.

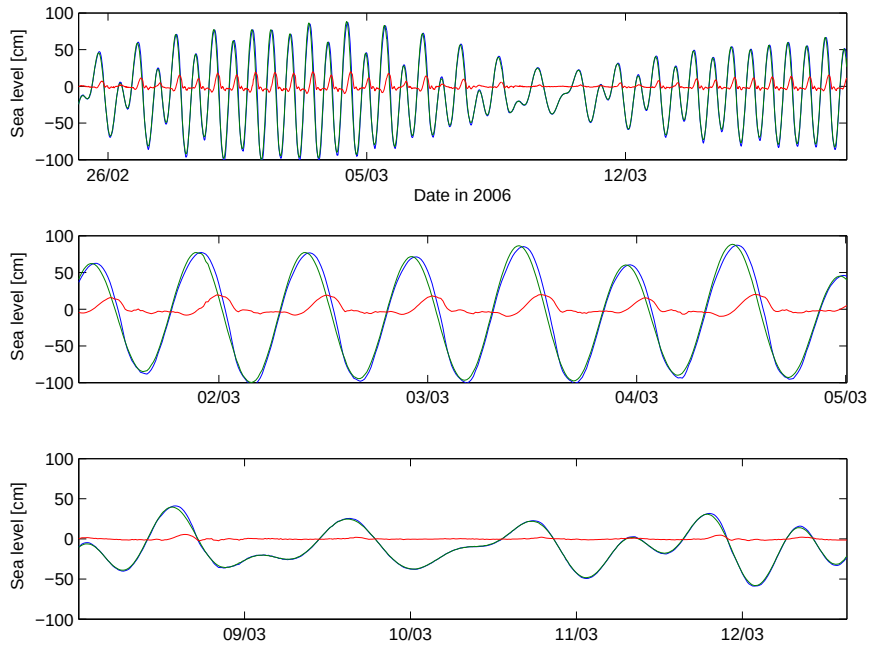

Figure 6.17: Comparison of the boundary sea level derived from *Egbert and Erofeeva* [2002] with the Seleko sea level, computed with GETM. Blue line: Seleko sea level, green: boundary sea level, red: difference between boundary and Seleko sea level; upper panel: overview, middle and lower panel: detailed view of a spring and neap tide cycle.

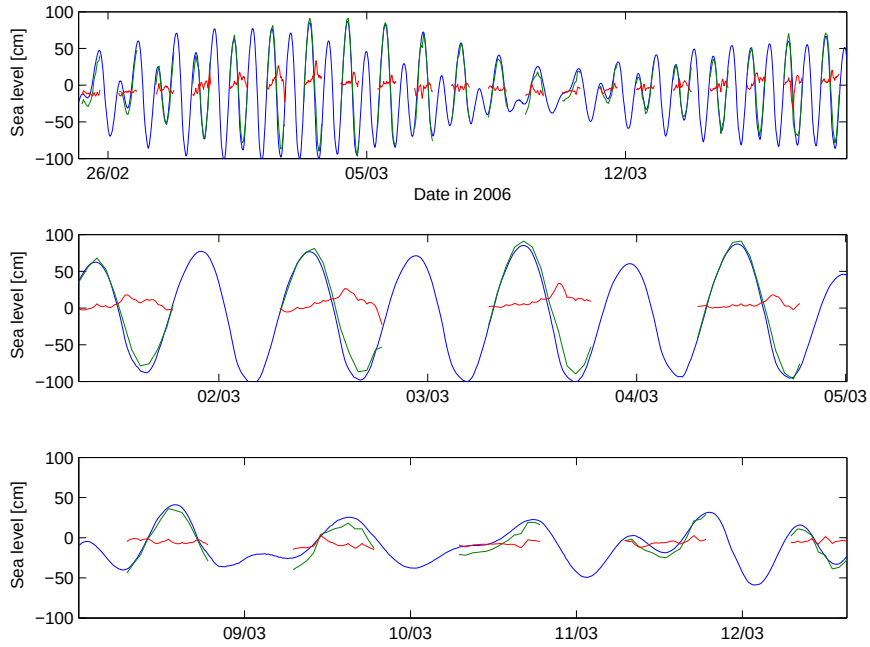

Figure 6.18: Comparison of the computed with the measured sea level in Seleko. Blue line: computed sea level, green: measured sea level, red: difference between computed and measured sea level; upper panel: overview, middle and lower panel: detailed view of a spring and neap tide cycle.

to 27.,2006. There seems to exist a correlation between the neap tide salinity intrusion through Plawangan and the Citanduy discharge. A discharge with a magnitude greater 200 m^3/s prevents the intrusion of salt water, in contrast to a discharge of about 100 m^3/s, which cannot stop the ocean water to enter Segara Anakan through Plawangan. These conclusions are assisted by the model results calculated with a constant discharge of 300 m^3/s for the 2006 field trip and 100 m^3/s discharge for the 2005 field trip (see Klaces salinity in figure 6.21).

To confirm the assumption of a relation between neap tide salinity peaks in Klaces and Citanduy discharge the model results can be used. Figure 6.22 shows the sea level and salinity and in Klaces with details in Figures 6.23, 6.24. Green lines are the GETM computations, the blue lines are the measurements. GETM overestimates the tidal range but with an accurate timing. The salinity peaks with the correct timing are well represented, but are again overestimated. This is probably due to the overestimated tidal range. Figure 6.24 shows details of the second neap tide cycle with freshwater quantities in the model and the mentioned measured peaks for the Mar. 26.,2006. In figure 6.21 the salinity's for 2005 and 2006 are plotted with the mean salinity in red. There is a clear indication of salinity peaks with 100 m^3/s and the absence with a discharge of 300 m^3/s. The discharge measurements in Plawangan are another hint: The lower right panel in figure 6.9 shows an overestimated outflow and a too small inflow into the lagoon compared with the measurements on Mar. 27.,2006. This is the result of the too high predefined Citanduy discharge. Another

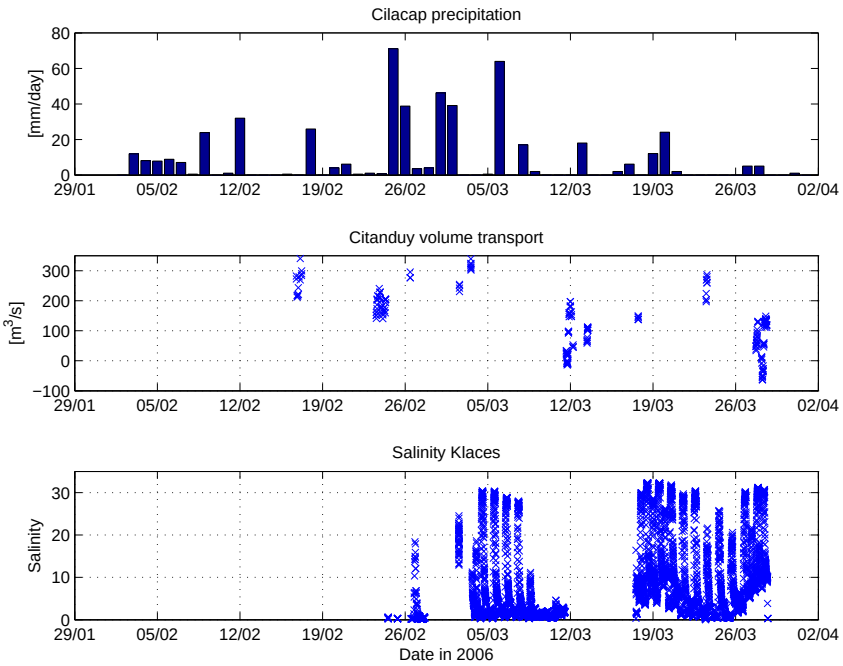

Figure 6.19: Upper panel: Precipitation in Cilacap; middle panel: Measured discharge of the Citanduy; lower panel: Salinity in Klaces.

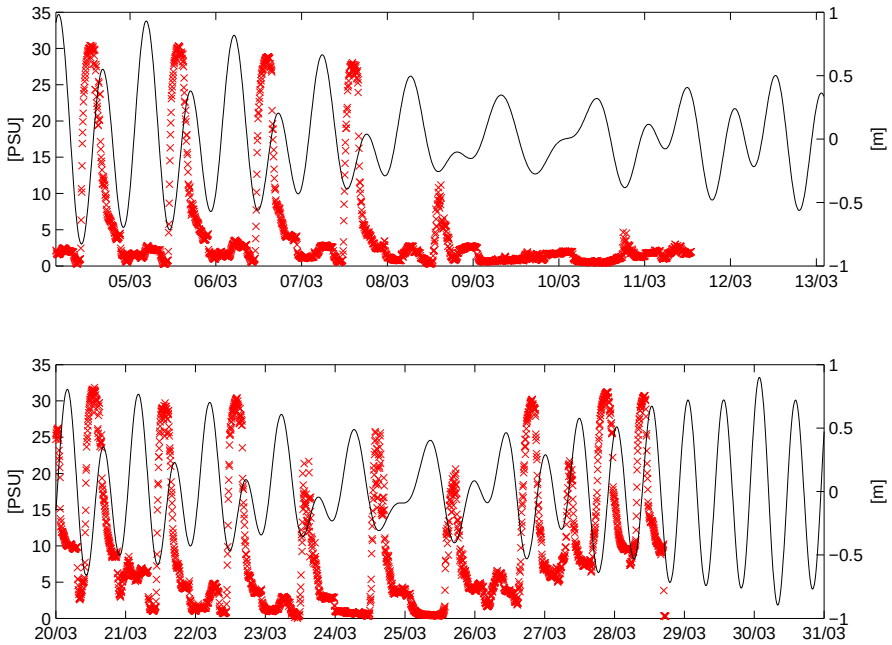

Figure 6.20: Salinity peaks in Klaces due to the incoming Indian Ocean water. Red salinity measurements, black Indian Oceans sea level. The upper panel shows a neap tide cycle without salinity peaks in contrast to the lower panel with salinity peaks.

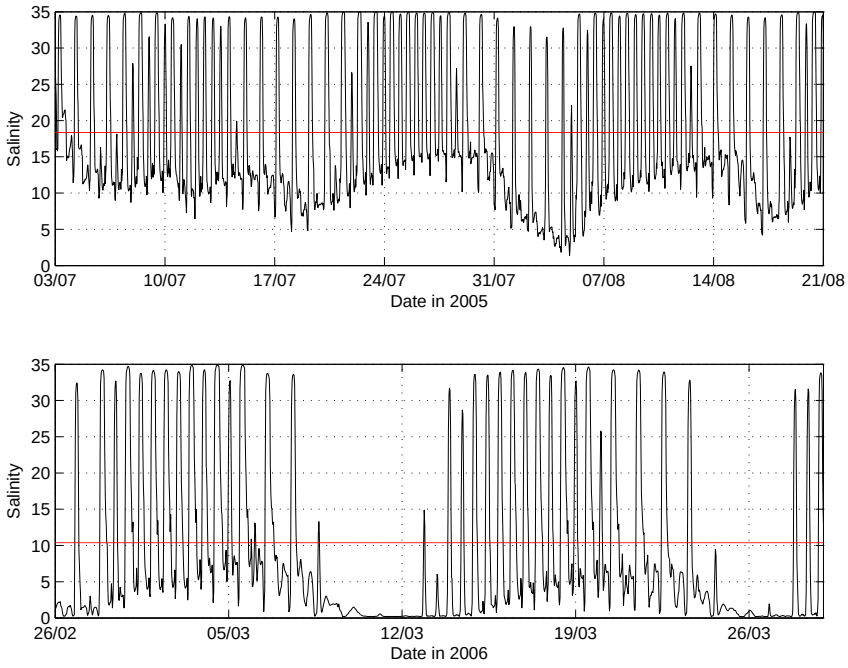

Figure 6.21: Changes of salinities in Klaces between the seasons computed with constant Citanduy discharges of 100 m^3/s for 2005 and 300 m^3/s for 2006. Note the Salinity peaks during neap tide in 2005 and the absence in 2006. Red: mean salinity.

strengthening option could be the increase of the mean sea level recorded in end of March 2006 (sea level in figure 6.24 in contrast to the sea levels in figure 6.24). A higher sea level will strengthen the intrusion of saline water even at low tide.

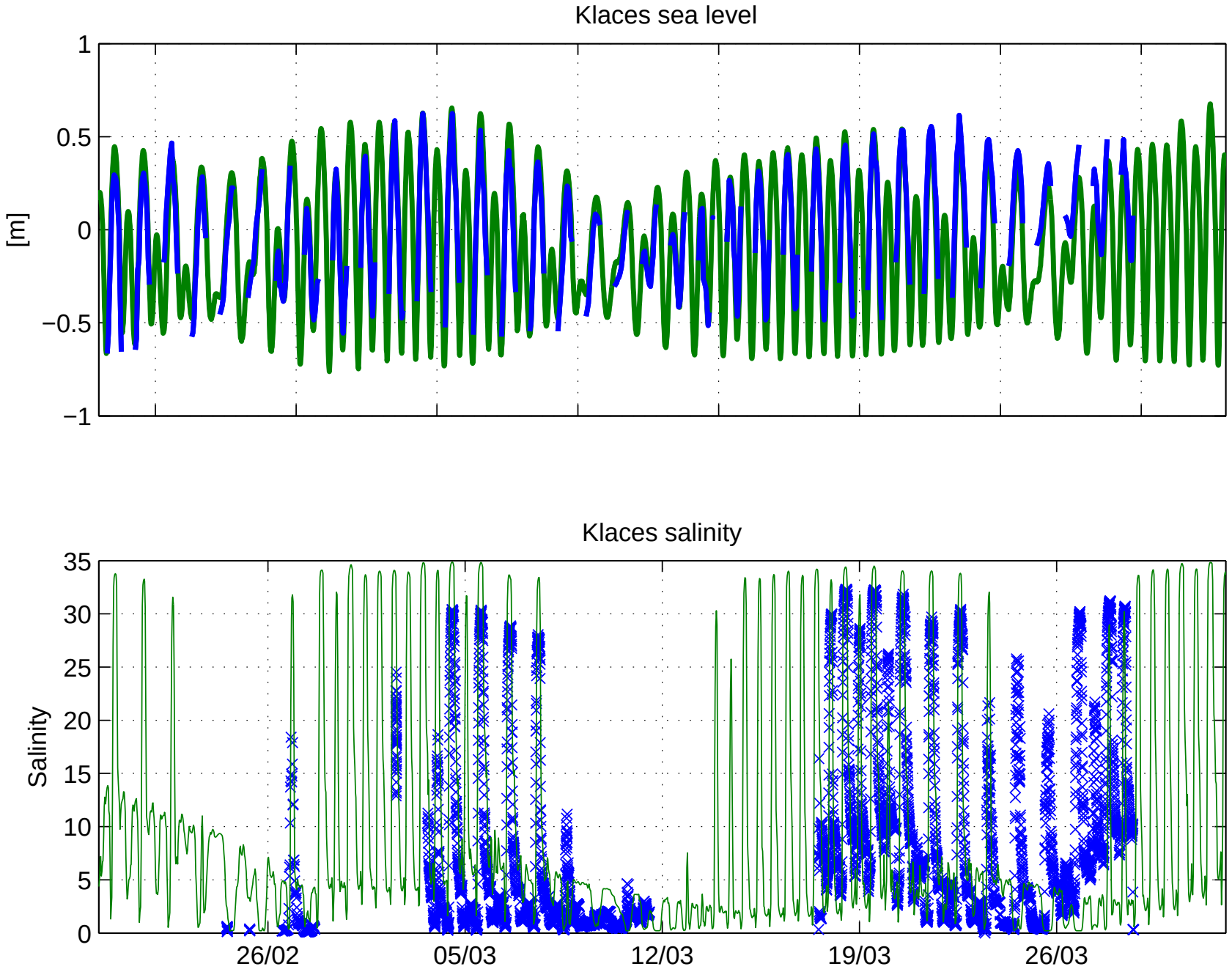

Figure 6.22: Overview of computed (green) and measured (blue) sea level and salinity in Klaces Feb.- Mar. 2006.

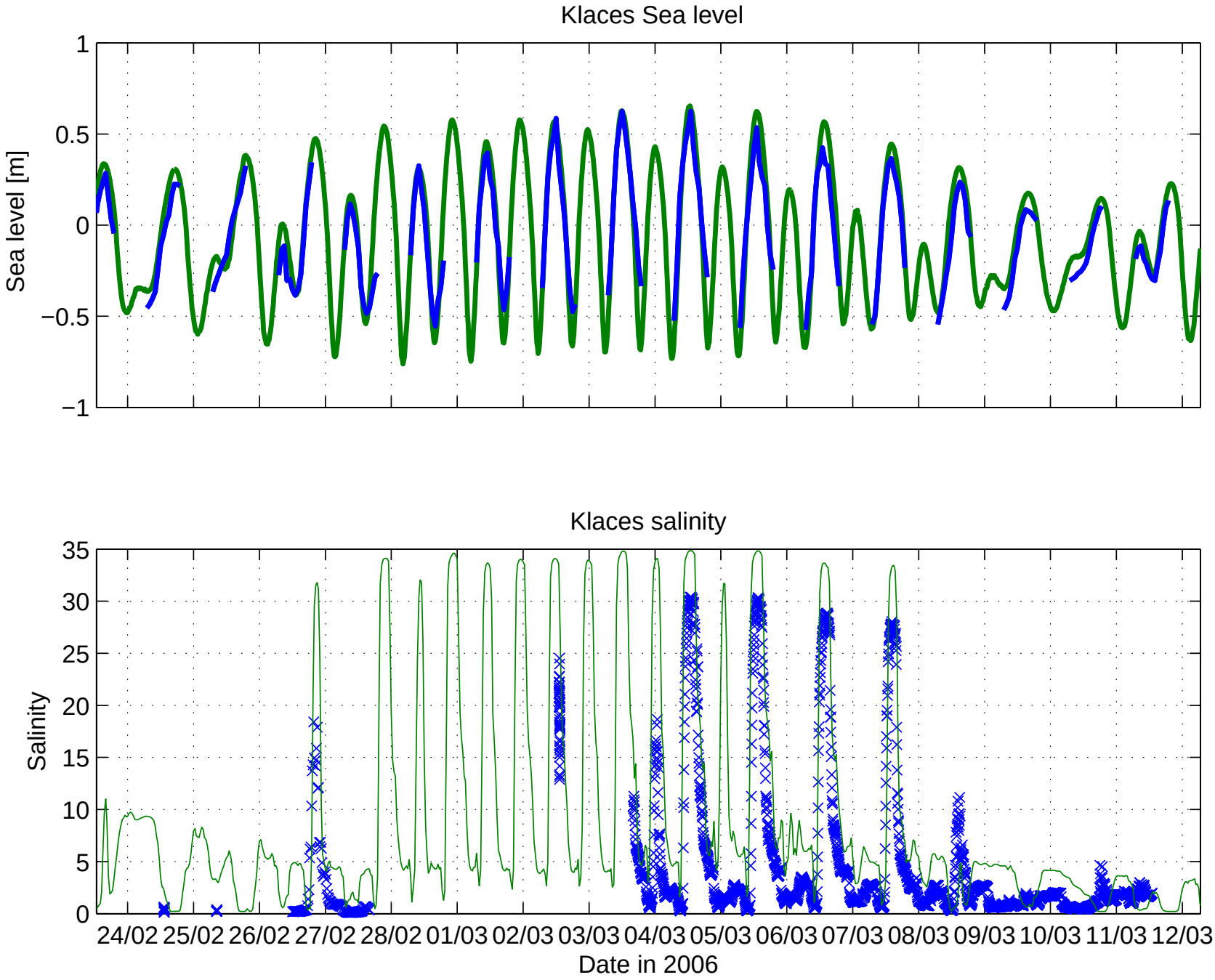

Figure 6.23: Detail view of computed (green) and measured (blue) sea level and salinity in Klaces 2006.

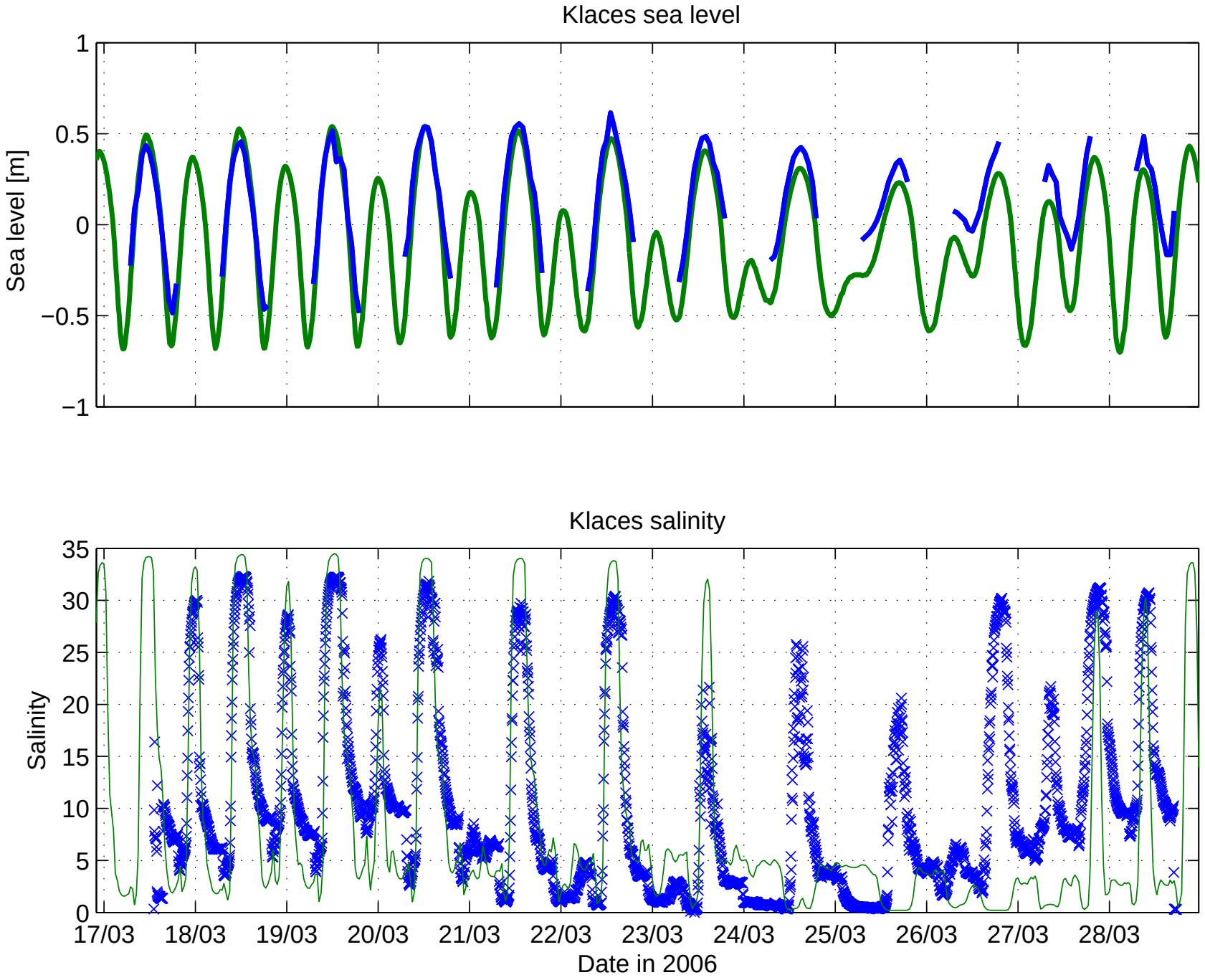

Figure 6.24: Detail-view of computed (green) and measured (blue) sea level and salinity in Klaces 2006.

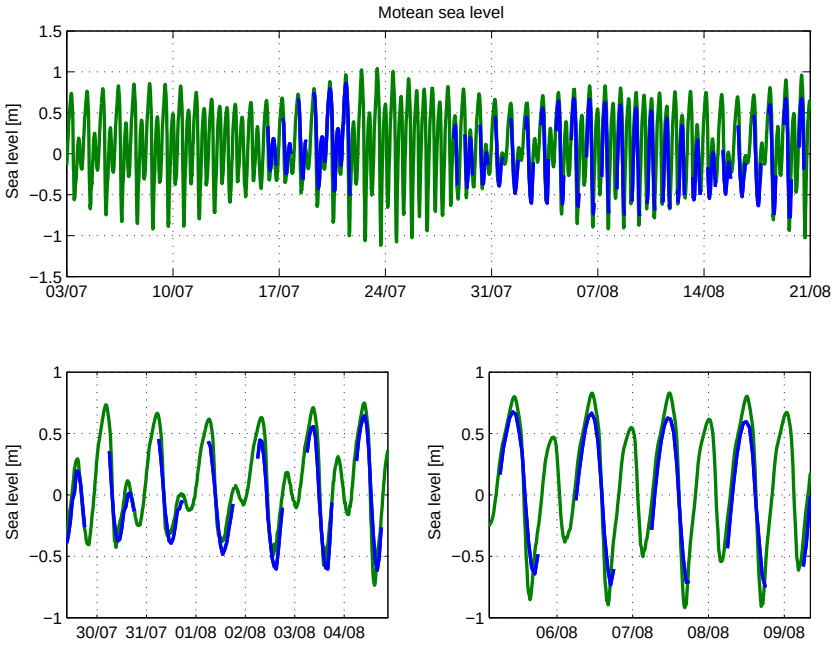

Figure 6.25: GETM (green) and recorded (blue) sea level in Motean 2005. GETM overestimates the amplitude during spring tide but with correct timing.

6.6. Salinity in Motean and Water Exchange

No long term measurements are available for Motean and the water exchange channel. However, good tidal data for 2005 together with the location in the center of Segara Anakan make the places interesting. Figure 6.25 shows GETM and recorded sea levels for the 2005 field trip. The timing is accurate but the amplitude is overestimated. The salinities in 2006 are plotted in figure 6.27. The maximum salinity timing is correct, but overestimated. It seems that the water in Motean is more influenced by saline water as the model estimates. This can have manifold reasons. A potential possibility is the unknown bathymetry in the west of Motean and the unresolved fine channels running northwards to the central part of Segara Anakan (figure 4.11). Figure 6.28 displays the sea level and the measured vs. computed salinities in the Water exchange channel. The order of magnitude is correct and some measurements are well represented. In general the changes between spring and neap tide could end up in a faster salinity changes (measured salinity in the end of the neap tide cycle on the 13th March 2006 is higher but becomes more correct in the middle of the spring tide on the 16th March 2006 and is overestimated when the sea level range becomes smaller at the beginning of the 23th March 2006 neap tide cycle). As the salinity is mainly affected by the eastern outlet this could mean a stronger and more direct influence of the oceans water plume at spring tide in the middle of Segara Anakan. The model seems to underestimate this influence.

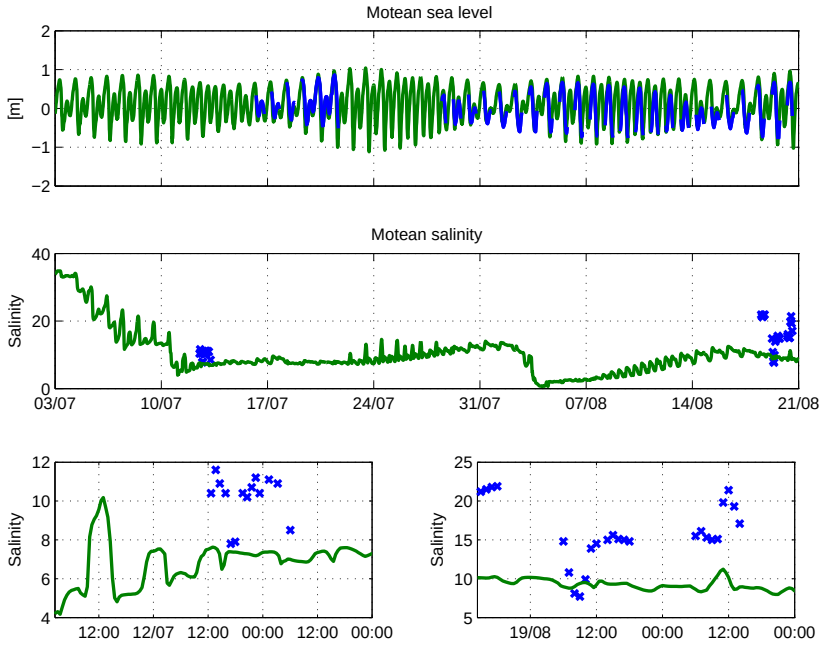

Figure 6.26: Motean 2005; upper panel: sea level: green computed, blue measured; middle panel: salinity: green computed, blue measured;lower panel: detailed view of the measurements.

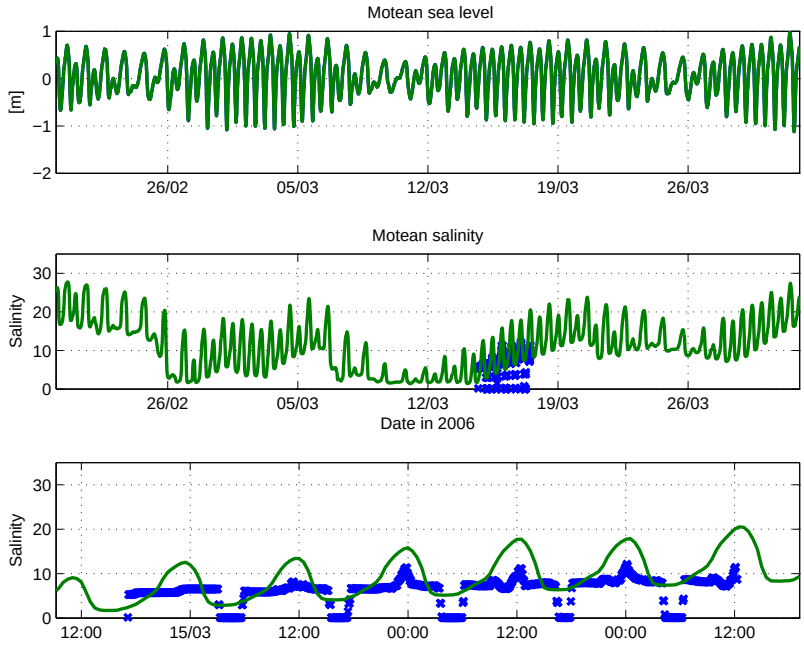

Figure 6.27: Motean 2006; upper panel: sea level: green computed, blue measured; middle panel: salinity: green computed, blue measured; lower panel: detailed view of the measurements, zero salinity is due to dry falling of the SBE16 sensor.

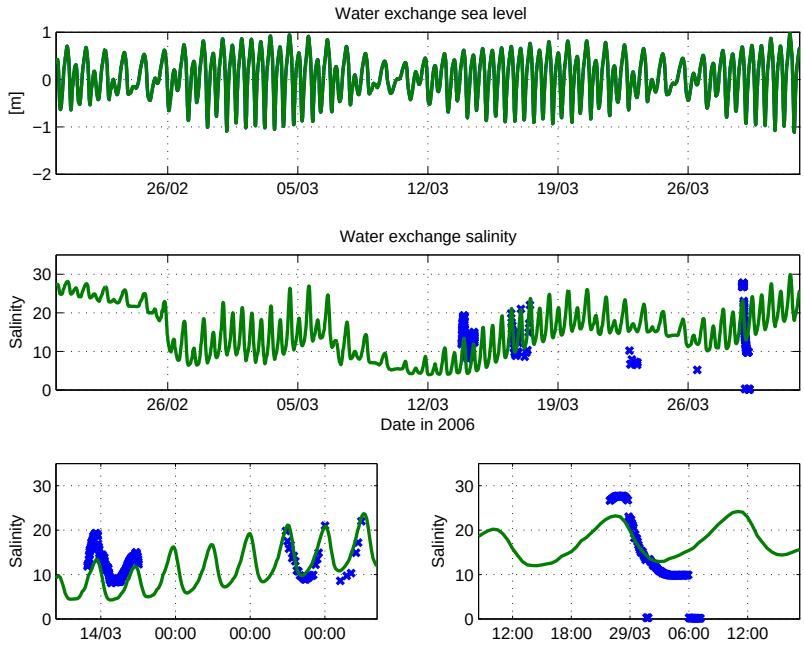

Figure 6.28: Water exchange channel 2006; upper panel: sea level: green computed, blue measured; middle panel: salinity: green computed, blue measured; lower panel: detailed view of the measurements, zero salinity is due to dry falling of the SBE16 sensor.

6.7. Changes during the monsoon seasons

The mean salinity in Segara Anakan varies between the rainy and dry season. Freshwater input into the lagoon is at least doubled between the seasons. Two effects amplify lower salinity: more freshwater volume and a higher pressure of the Citanduy water preventing the tide to enter the lagoon. The following discussion will be based upon the model results since the salinity samples in time and space are too coarse. Figure 6.29 shows the salinity in the center of Segara Anakan and in Klaces for the dry season 2005 and the rainy season 2006. Figure 6.30 plots the mean for the whole lagoon. Both figures mark the expected salinity increase during the dry season caused by a reduced freshwater input. The over the lagoon averaged salinity is 8 for 2005 and 13 for 2006. Due to the five times bigger water flux through the eastern outlet and smaller incoming rivers (Donan) the mean salinity of the eastern part is higher than the western part with the Citanduy. The Citanduy water plume is most likely the reason for the salinity changes. A high discharge can completely hinder the intrusion of ocean water during neap tide and small tidal ranges. This happens in the rainy season. While in dry season the ocean water still enters the lagoon and causes the higher salinity (figure 6.31). Figure 6.30 shows a slight north-south gradient in the central part. This is due to the river plume of the Citanduy, which is pushed northwards by the oceans tide. Hence it enters the lagoon through the lagoon channel (channel number 3 on figure 6.2) and the shallow channel north to channel 3. The northern bound low saline water of the Citanduy mixes with the incoming water of the Cikando river and creates a lower saline environment on the northern part of the central lagoon.

Higher Citanduy freshwater runoff means a pressure gradient between the western and the eastern part. The 24 hour measurements in 2005 and 2006 may indicate a net eastward transport in 2006 (rainy season figure 6.12) and a zero or slightly westward transport in 2005 (dry season with figure 6.8). Since the model discharge in the water exchange channel does not represent the measurements, model data cannot be used for validation and more in situ discharge measurements are needed.

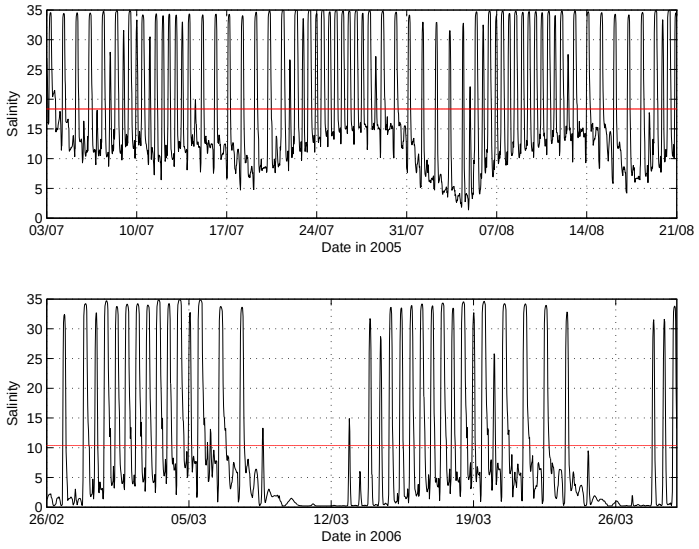

(a) Klaces

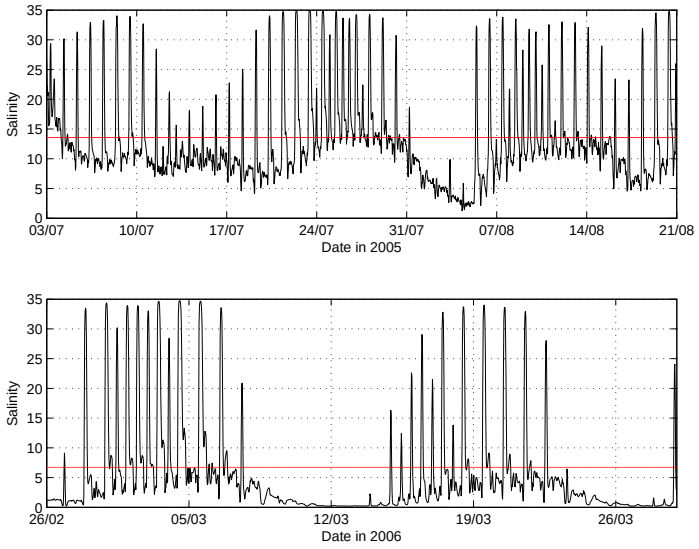

(b) Lagoon

Figure 6.29: Changes of salinities in Klaces and the lagoon between dry season (2005) and rainy season (2006). (a):Klaces (b):Lagoon; red line: mean salinities.

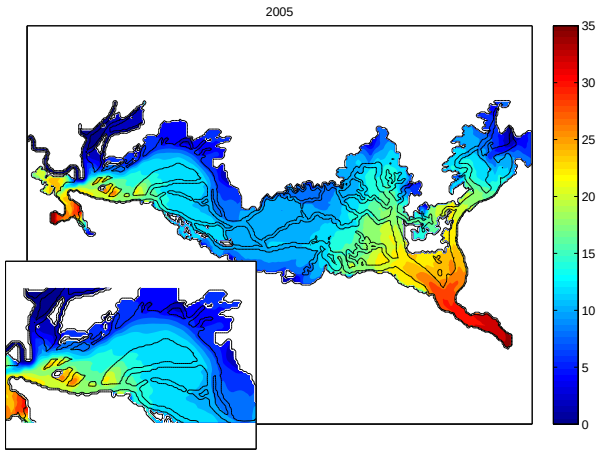

(a)

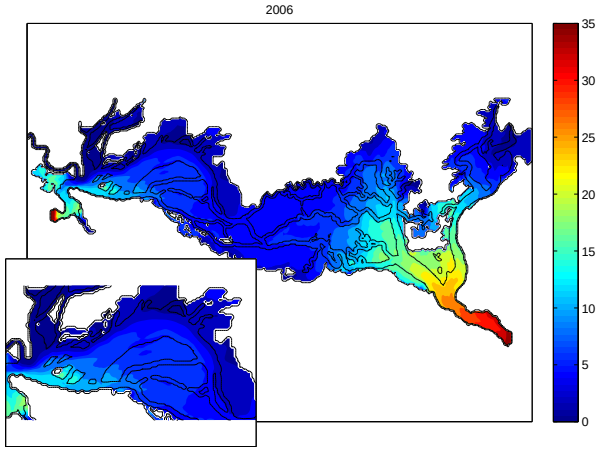

(b)

Figure 6.30: Computed mean salinity for the dry season 2005 (panel a) and the rainy season 2006 (panel b). The black lines are the borders between mangroves and water. The spatial averaged mean salinity is 13 for 2005 and 8 for 2006.

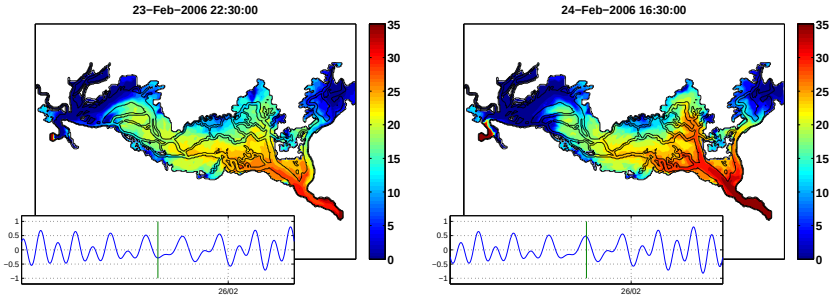

(a) Rainy season neap tide low. (b) Rainy season neap tide high.

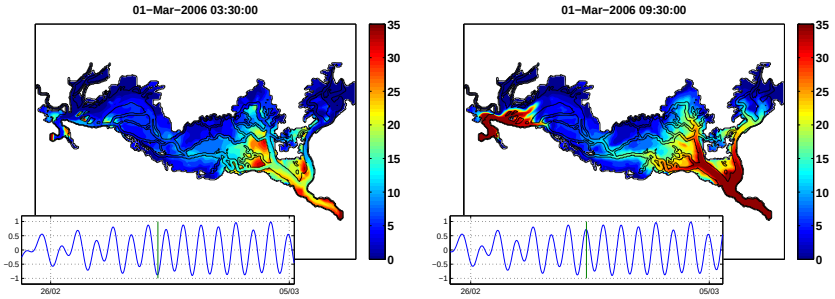

(c) Rainy season spring tide low. (d) Rainy season spring tide high.

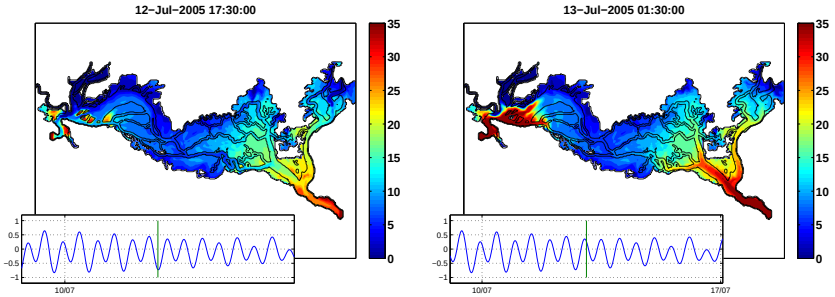

(e) Dry season neap tide low. (f) Dry season neap tide high.

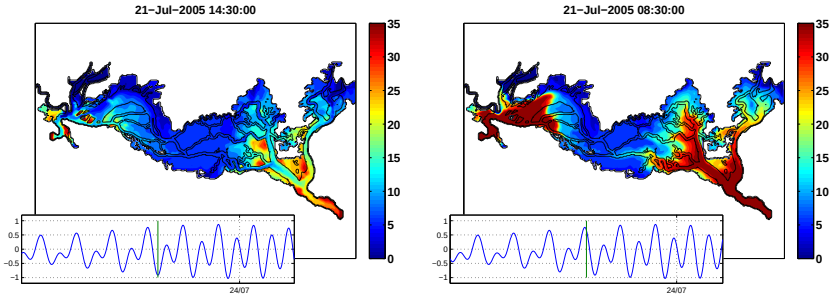

(g) Dry season spring tide low. (h) Dry season spring tide high.

Figure 6.31: Salinity distribution during different tide cycles in dry season 2005 and rainy season 2006.

6.8. Stratification

Large vertical salinity gradients cause a stratification and can block the exchange of more dense high saline deep water with the less dense surface water. *White et al.* [1989] report well mixed conditions in the central lagoon and a stratification in the Citanduy estuary. Stratification of 1.5 on the surface vs. 8.8 bottom salinity are reported approx. 4 km upstream the Citanduy. Since no vertical salinity measurements were taken we do not know much about stratification. An indication for a stratified water column are the ADCP velocity profiles of the Citanduy river (figure 6.32). It shows two water masses with different velocities and an increased back-scatter signal on the boundary layer between the water masses. The back-scatter signal is a typical halocline effect. GETM results do not show stratification inside the Citanduy river. As discussed in section 6.3.1 the too short river path of this GETM setup has a limited water volume. It is not possible to simulate an accumulation of freshwater during high tide thus the volume flux variations in tidal time scales are underestimated (see chapter 6.3.1 and figure 6.3). Furthermore the too small Citanduy water volume hinders a stratification. Model results show stratified areas in the central part of Segara Anakan and around the Citanduy estuary. But stratified conditions never last longer than one tidal cycle. This complies with 24h ADCP measurements in the Citanduy river, showing stratification at high tide but well mixed conditions at low tide.

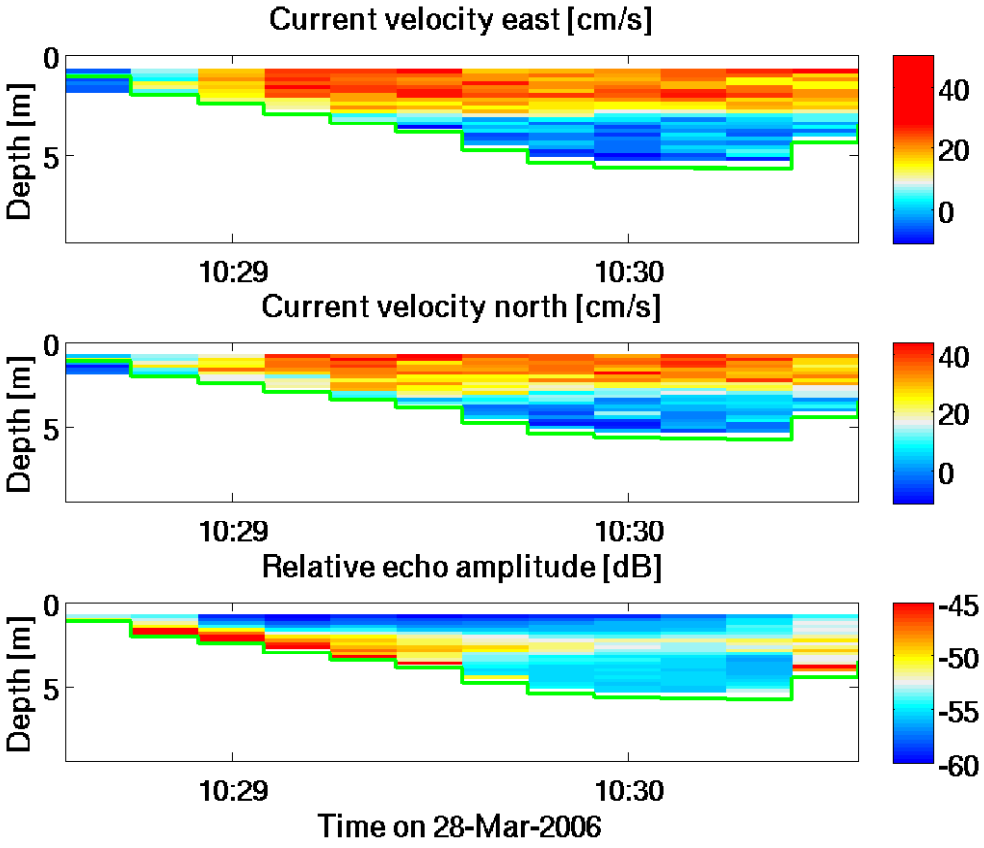

Figure 6.32: Velocity and back-scatter profile of a Citanduy transect. The vertical profile is divided into a fast flowing 2.5 m thick surface layer and a standing bottom layer. The back-scatter signal between the layers is increased. This is a typical effect of a halocline.

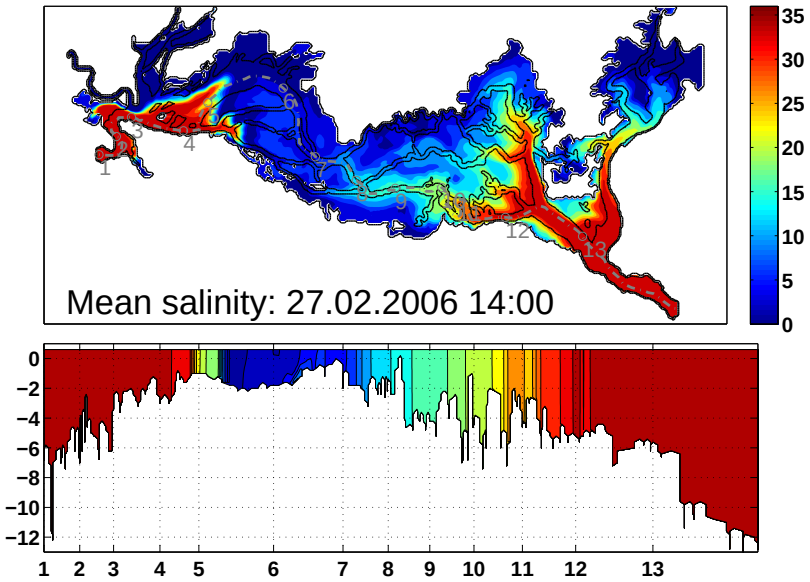

(a)

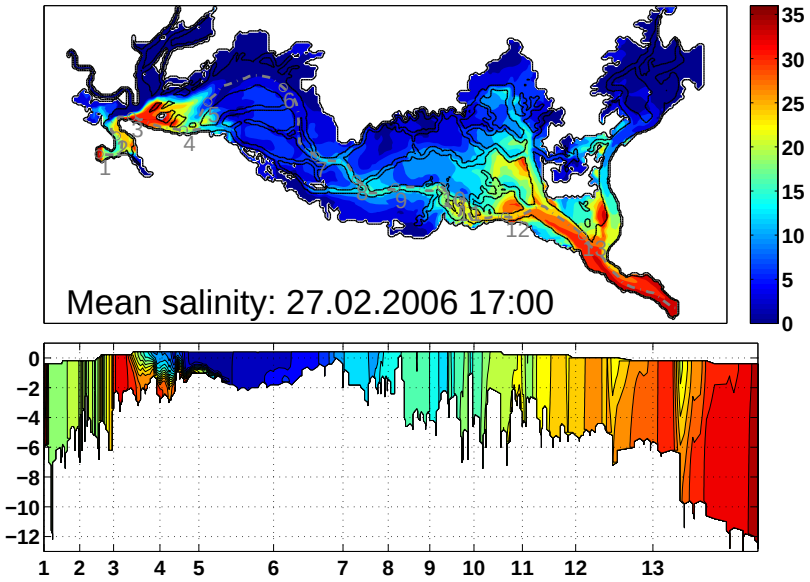

(b)

Figure 6.33: Snapshot of the mean salinity and a vertical transect through the lagoon (grey line in the upper panel with stations). Salinity isolines in the lower panel are in the distance of 2 ppt. Panel (a) with a well mixed water columns except a slight stratification between stations 7 and 8. Panel (b) shows stratification inside the northern part of the central lagoon and between stations 4 and 5 due to the leaving fresh water. The duration of stratification usually lasts not longer than one tidal cycle.

6.9. Flushing time and seawater age

The basic definition of the flushing time T is the time to exchange a solute mass M as measured at high tide in an estuary, at a rate equal to that solutes inflow I into the the estuary

$$T = \frac{M}{I}. \tag{6.1}$$

This is the ratio of the water volume and the flux through the boundaries (*Dick and Schönfeld* [1996]).

The turnover time T_e is the time necessary to reduce the water volume to a fraction e^{-1} of the original volume. The determination of the turnover time is complicated. A parameterization was done by *Ridderinkhof* [1990] by comparing three tidal basins. They obtained following equation:

$$T_e = \frac{V_{hightide}}{\beta \Delta V}, \tag{6.2}$$

where $V_{hightide}$ is the volume at high tide, the constant β determined at $\beta = 0.12$ and ΔV the tidal prism. This is valid for estuaries flushed by tide only. The tidal flux through the outlets is approx. 10 times higher than the freshwater input. Hence the method can be used as a first approach to calculate the flushing time. Referred to table 2.1 the tidal prism of Segara Anakan is at neap tide: $(0.113 + 0.006 - 0.0995)$ km^3=0.0195 km^3
and at spring tide: $(0.130 + 0.048 - 0.082)$ km^3=0.0960 km^3. Thus the flushing time is in the range of

$$T_e^{neap} = \frac{0.113 + 0.006}{\beta\ 0.0195} = 51\ t_{tide}$$

and

$$T_e^{spring} = \frac{0.130 + 0.048}{\beta\ 0.0960} = 16\ t_{tide}$$

tidal cycles. With t_{tide} the length of one tidal cycle which is due to the semidiurnal tide 6 hours.

If the boundary conditions of the age tracer defined in chapter 3.4 are set in a way that incoming water has the age zero, the seawater age can be interpreted as the residence time of water inside the lagoon. Fresh incoming water gets older inside the model area and leaves the lagoon with the time it spent.

The initial age conditions are zero everywhere. The biggest water exchanges are the outlets and the incoming river. Areas far away from these influences should age linear with time, since no influence and mixing with "young" water is expected. After a time which can be considered as the initial time, the age of the water should reach an average age. The spring tide flushes more "young" water into the model and we expect a lower age during this time. Hence the age will not be a constant but fluctuate with spring and neap tide cycles as well as precipitation and river input around the average age. Figure 6.34 shows the seawater age evolution in the Klaces and Motean villages. Spring and neap tide cycles and precipitation (e.g. Feb. 26.,2006) influences can be seen. Figures 6.35 and 6.36 plot the average seawater age in the whole lagoon for dry and

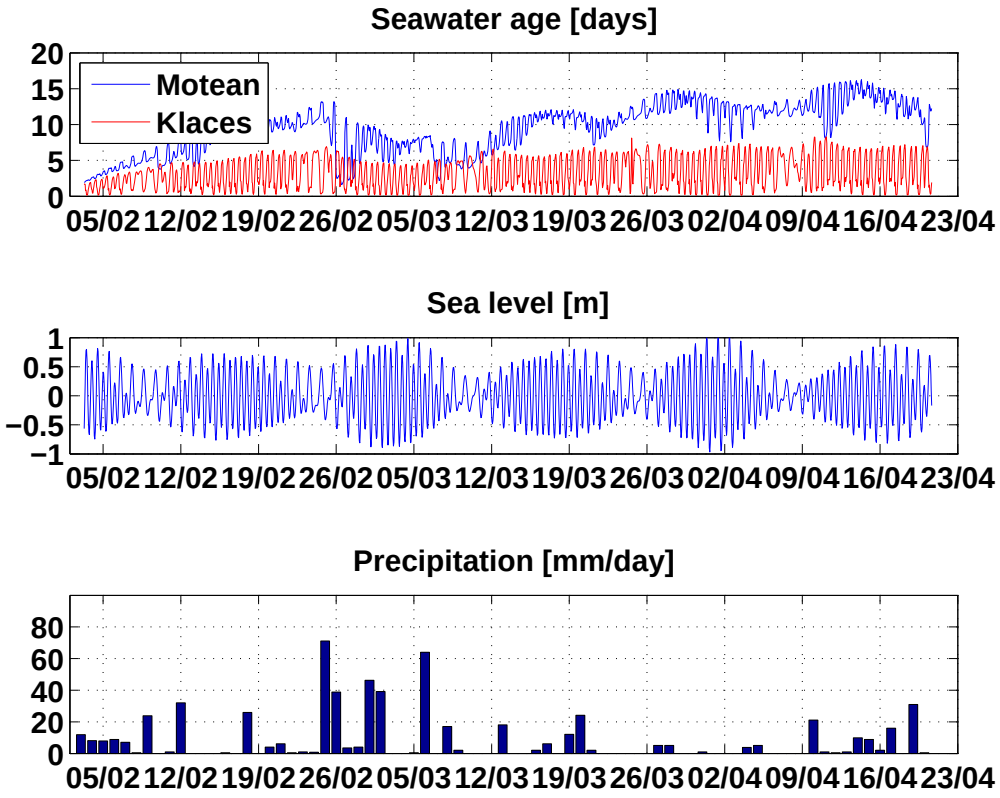

Figure 6.34: Seawater age in Klaces and Motean villages. After the initial zero the age grows to the mean age. Depending on freshwater input and tide the age fluctuates around the mean age.

rainy season. The age increases with a growing distance to freshwater sources. As expected the highest water age can be found in the center of Segara Anakan. Similar to the salinity a north south gradient develops in the central part. The old water from the center of the lagoon discharges through the south side of the central part and the channel at Klaces while the younger Citanduy water enters through the northern part. In general the seawater resides longer during the dry season. This is due to less fresh water input. Remarkable is the long residence time in the northern east part during dry season. The timescales of the turnover times and the computed residence time agree.

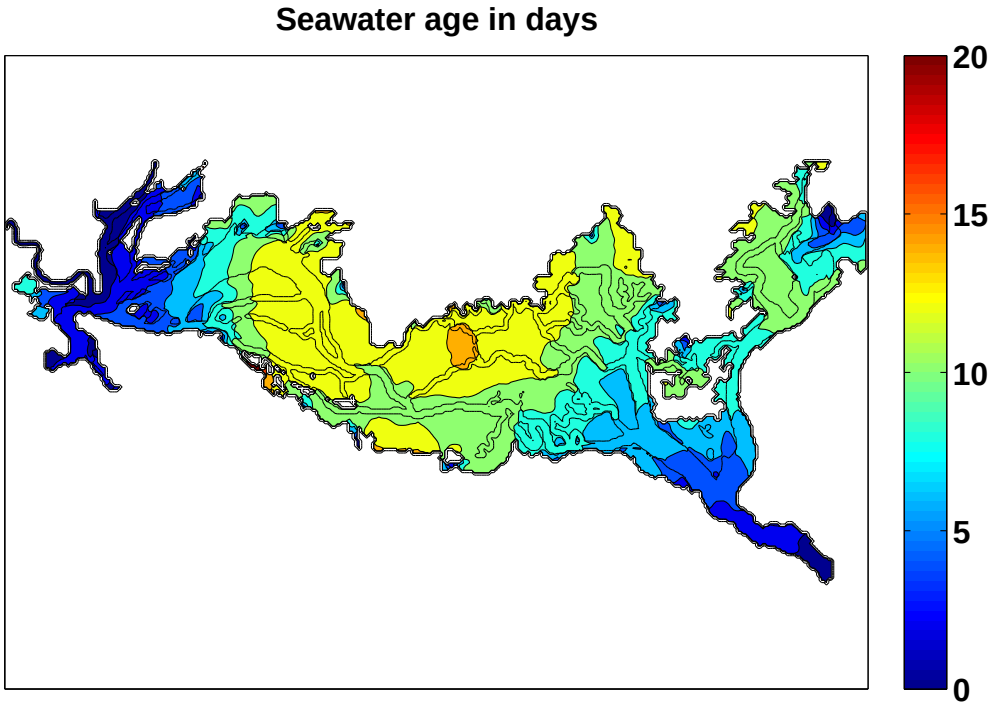

Figure 6.35: Average of the seawater age in Segara Anakan 2005 during dry season. Isoline are two days difference.

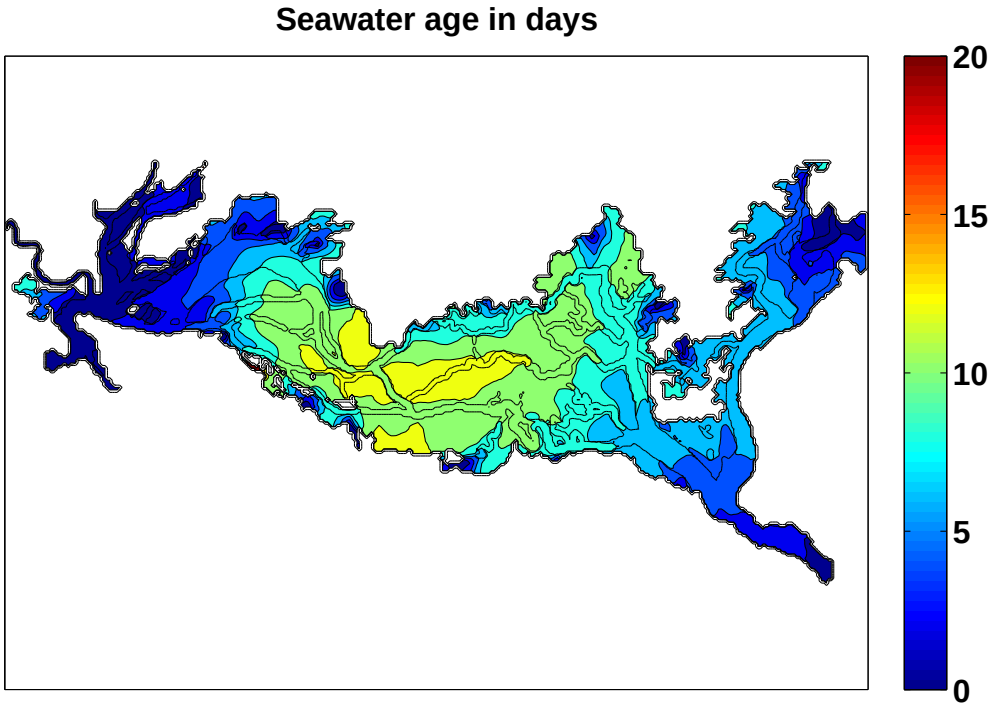

Figure 6.36: Average of the seawater age in Segara Anakan 2006 during rainy season. Isoline are two days difference.

7. Outlook

The present work sets a frame to improve the model by adding parameters playing an important role like the suspended matter. As mentioned in the preceding chapters, more time is needed for the finetuning and better prescription of the boundary conditions. This will likely require more in situ measurements. Main features of the lagoon were sucessfully reconstructed with the GETM model and available boundary conditions. But the setup is by no means complete. Some assumptions are too simple and a number of effects typical for mangrove estuaries are not included. The bathymetry should be revised including more depth soundings in the eastern part. The freshwater input is a crucial parameter for the hydrodynamics. Small rivers with less than a tenth of the Citanduy input can change the average salinity in the center of Segara Anakan. The tidal scale volume flux range of the Citanduy can be improved by inserting a longer river bed.

Figure 2.2 shows the high sediment load of the Citanduy river. A logical step is the implementation of a suspended sediment tracer. This helps to understand and quantify the spatial distribution and accumulation of sediment. It may be possible that the hydrodynamics may change due to the sediment, since the density of the Citanduy water will increase. The water exchange between the eastern and western part is responsible for a salinity increase inside the central lagoon. The model does not well describe the quantities of the volume fluxes and more in situ measurements and a fine tuning of the model setup is needed. A part of the plume leaving Segara Anakan through the outlets will reenter the area within the next tidal cycle. This effect is not modelled here and corresponding measurements have to be done. Modelling a part of the Indian Ocean or prescription of the reentering water due to boundary conditions are necessary to quantifiy the exchanges.

Since the tide is prescribed by tidal constituents the mean sea level is zero. Non tidal sea level changes are not resolved within these boundary conditions. An increasing or decreasing sea level due to wind events can significantly change the mean salinities inside Segara Anakan. To measure if those sea level changes occur a long time tide gauge has to be installed on the coast to the Indian Ocean.

The long time measurements in Klaces helped a lot to understand the hydrodynamics in tidal time scales. Similar stations in the central and eastern part of Segara Anakan would be beneficial.

The water residence time in Segara Anakan computed with the age tracer shows a spatial distribution with residence times of up to 15 days in the central lagoon. The changes of the residence time and salinitiy due to a changing Citanduy river discharge will be investigated in a following study.

8. Acknowledgements

Numerous people helped me and I like to say thanks to them.

- my parents
- my brothers Christoph, Sebastian, Hannes, Daniel for being my brothers
- Süne for the numerous LaTeX tips
- Tim Jennerjahn for the planning and realisation of the work and all the time he spent to answer my questions and ideas
- Hans Burchard for the efforts to supervise my work and all the ideas he had to help me out, especially when another GETM run crashed due to the really "hard core" bathymetry
- Iwan Tejakusuma
- Allo for helping and translating almost 4 months
- Andrew with his boat Miund for driving me around in the lagoon and the patience and time to realize my ideas. As well as the waking hours in the night to measure discharge transects.

(a) Research vessel Miund passing research vessel Sonne.

(b) Me helping to row a logboat with a wood plank.

Bibliography

American Embassy Jakarta, Petroleum product consumption and refining, 2000.

Ardli, E. R., and M. Wolff, Quantifying habitat and resource use changes in the Segara Anakan lagoon (Cilacap, Indonesia) over the past 25 years (1978-2004), *Asian Journal of Water, Environment and Pollution*, accepted.

Barber, C. B., D. P. Dobkin, and H. T. Huhdanpaa, The quickhull algorithm for convex hulls, *ACM Transactions on Mathematical Software*, *22, No. 4*, 469–483, 1996.

Blake, R. A., The dependence of wind stress on wave height and wind speed, *Journal of Geophysical Research*, *96*, 20,531–20,545, 1991.

Burchard, H., and K. Bolding, GETM – a general estuarine transport model. Scientific documentation, *Tech. Rep. EUR 20253 EN*, European Commission, 2002.

Burchard, H., G. Flöser, J. V. Staneva, T. H. Badewien, and R. Riethmüller, Impact of density gradients on net sediment transport into the Wadden Sea, *J. Phys. Oceanogr.*, 2007, submitted.

Deleersnijder, E., J.-M. Campin, and Eric J.M. Delhez, The concept of age in marine modelling i. theory and preliminary results, *Journal of marine systems*, *28*, 229–267, 2001.

Dick, S., and W. Schönfeld, Water transport and mixing times in the north frisian wadden sea results of numerical investigations, *Deutsche Hydrographische Zeitschrift*, *48*, 27–48, 1996.

Egbert, and Erofeeva, Efficient inverse modeling of barotropic ocean tides, *Journal of Atmospheric and Oceanic Technolgy*, *19,N2*, 183–204, 2002.

Gordon, R. L., Acoustic measurement of river discharge, *Journal of Hydraulic Engineering*, *115*, 925–936, 1989.

GRASS Development Team, *Geographic Resources Analysis Support System (GRASS GIS) Software*, ITC-irst, Trento, Italy, 2007.

Hatayama T. T. Awaji, and K. Akimoto, Tidal currents in the Indonesian Seas and their effect on transports and mixing, *Geophys. Res.*, *101*, 12,353–12,373, 1996.

Hogarth, P. J., *The Biology of Mangroves*, Oxford University Press, Oxford, 1999.

Hydrographic Office, U., Cilacap and approaches, Sea chart 1:15000, 1994.

Jerlov, N. G., *Optical oceanography*, Elsevier, 1968.

Kondo, J., Air-sea bulk transfer coefficients in diabatic conditions, *Bound. Layer Meteor.*, *9*, 91–112, 1975.

Mazda, Y., E. Wolanski, B. King, A. Sase, D. Ohtsuka, and M. Magi, Drag force due to vegetation on mangrove swamps, *Mangroves and Salt marshes*, *1*, 193–199, 1997.

Monismith, S., An experimental study of the upwelling response of stratified reservoirs to surface stress, *J. Fluid Mech.*, *171*, 407–439, 1986.

Paulson, C. A., and J. J. Simpson, Irradiance measurements in the upper ocean, *J. Phys. Oceanogr.*, *7*, 952–956, 1977.

Pohlenga, I., Närstoffkreisläufe in Mangrovensedimenten der Segara Anakan Lagune (Java), 2007.

RD Instruments, Workhorse installation guide, 2002a.

RD Instruments, Broadband primer, 2002b.

Ridderinkhof, H., Tidal exchange between the north sea and dutch wadden sea and mixing time scales of the tidal basins, *Neth. J. Sea Res.*, *25(3)*, 331–350, 1990.

Simpson, M., and R. N. Oltmann, An acoustic doppler discharge measurement system, *Proceedings of the 1990 National Conference on Hydraulic Engineering*, *2*, 903–908, 1990.

Stanev, E. V., G. Flöser, and J.-O. Wolff, Dynamical control on water exchanges between tidal basins and the open sea. A case study for the East Frisian Wadden Sea, *Ocean Dynamics*, *53*, 146–165, 2003.

Stieglitz, T., Hydrodynamic processes in tropical mangroves, Ph.D. thesis, Universität Trier, 2002.

Umlauf, L., H. Burchard, and K. Bolding, General Ocean Turbulence Model. Source code documentation, *Tech. Rep. 63*, Baltic Sea Research Institute Warnemünde, Warnemünde, Germany, 2005.

Wang, Y., Windgetriebene Strömungen in einem Rechteckbecken und im Bodensee, Ph.D. thesis, Technische Hochshule Darmstadt, 1995.

White, A. T., P. Martosubroto, and M. Sadorra, The coastal environmental profile of Segara Anakan-Cilacap, South Java, Indonesia, *Association of Southeast Asian Nations / United States Coastal Resources Management Project, Technical Publications*, *Series 4, 522*, 1–82, 1989.

Wolanski, E., and Gardiner, Flushing of salt from mangrove swamps, *Australian Journal for Marine and Freshwater Research*, *32*, 681–683, 1981.

www.citypopulation.de, June 5.,2007.

Yuwono, E., T. Jennerjahn, I. Nordhaus, E. A. Riyanto, M. H. Sastranegara, and R. Pribadi, Ecological status of Segara Anakan, Java, Indonesia, a mangrove-fringed lagoon affected by human activities, *Asian Journal of Water, Environment and Pollution*, *4*, 61–70, 2007.

A. Tidal constituents for the Indonesian Seas derived from TOPEX/POSEIDON altimeter data

The TOPEX/POSEIDON satellite altimeter was launched 1992 to measure the sea surface elevation until end of 2005. It measures the elevation with an accuracy of 5 cm and reaches a spot every 10th day. This sampling frequency is not high enough for a direct determination of the tidal constituents, but the data can be used to tune a tidal model. The Indonesian Seas tide is of high amplitude and spatially complex. The large tidal currents can affect ship navigation and there are evidences that the tide is an important factor in the interchange process between the Pacific and the Indian Ocean. It is greatly influenced by the complex topography and makes it difficult to model it with a purely hydrodynamic model. *Egbert and Erofeeva* [2002] used TOPEX/POSEIDON sea surface altimeter data as the input for a generalized inverse (GI) model. The data is assimilated into a global barotropic tidal model by minimizing a penalty function to the linearized shallow water equations and the data. The forcing of the linearized shallow water equations are the tidal coefficients of the $M_2, S_2, K_1, O_1, N_2, P_1, K_2, Q_1$ tides.

As an example of the GI advantages *Egbert and Erofeeva* [2002] use the GI approach for the TOPEX/POSEIDON altimeter data of the Indonesian Seas. The solutions produced are compared to pure hydrodynamic models (e.g. *Hatayama T. T. Awaji and Akimoto* [1996]). It shows up that the RMS with the GI approach are especially in shallow waters lower. Therefore, the freely available tidal constituents calculated with the GI method is the best choice for the tidal forcing of Segara Anakan.

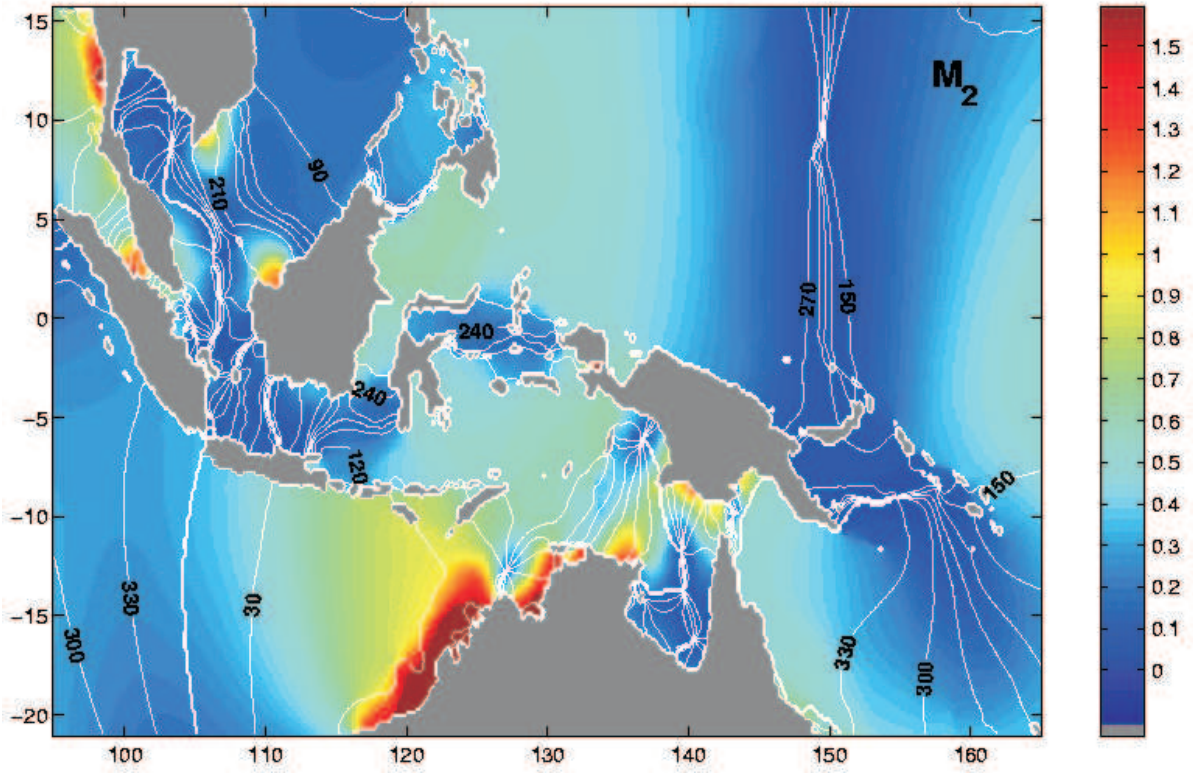

Figure A.1: M_2 Tide of the Indonesian Seas calculated using an inverse tidal solution. The isolines are the phases, the colors are the amplitudes in meters (http://www.coas.oregonstate.edu/research/po/research/tide/ind.html).

B. ADCP Setups

The data measured by the ADCP has to be stored somewhere. The used ADCP has an internal memory of 32 MByte respectively 64 MByte in February 2006. This is enough for a half day measurement. If the data is stored into the internal memory, the ADCP has to be programmed once. After the measurements are finished it can be read out in a safe environment. This is a suitable solution for long time or under water moorings, wet conditions and conditions in general where a computer cannot be used for online data reading from the ADCP. If a computer is available, the ADCP can be connected via a serial connection to the computer. The data is transfered directly to the computer and can be observed in real time. This immediately allows to recognize bad measurements and to change the setup. The used WinRiver Software is capable of merging GPS position data into the ADCP data file. This is very handy for bathymetry measurements.

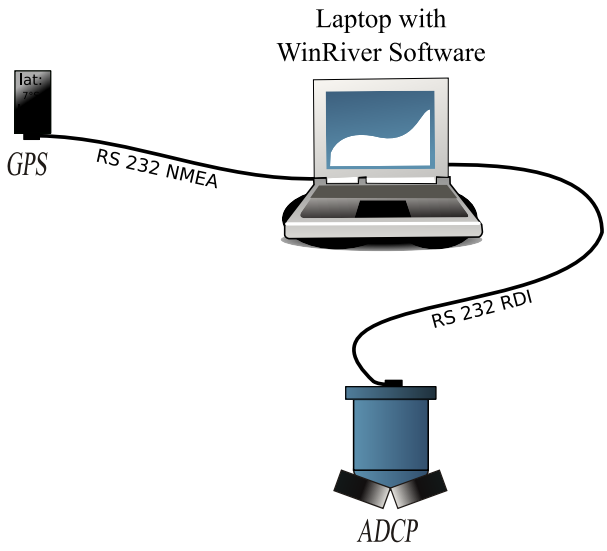

Figure B.1: ADCP Setup with GPS and serial connection to a laptop.

C. Changes of the GETM source code for the Segara Anakan setup

GETM version 1.5.1 was customized. The changes in the original modules are listed below:

- sealevel.F90 emergency break
- rivers.F90 added precipitation
- salinity.F90 NaN and zero test, to break computing
- depth_update.F90 a more restrictive way to calculate α (minimum depth of d(i) and d(i+1) is taken)
- short_wave_radiation.F90 With a Cartesian setup the module short_wave_radiation has a bug and sets the lat and lon values to -9999 and hence the radiation is zero. lat and lon where hard coded to proper values
- m2d.F90 variable bottom roughness of the mangroves and water areas
- output.F90 numbered restart files for easier restart at a desired time step

The seawater age module is a copy of the salinity.F90 module with a source term of one.